NTNU – Trondheim
Norwegian University of
Science and Technology

Design of Beam Ends with Copes

Hågen Urseth

Civil and Environmental Engineering
Submission date: June 2013
Supervisor: Arne Aalberg, KT
Co-supervisor: Per Kristian Larsen, KT

Norwegian University of Science and Technology
Department of Structural Engineering

NTNU

Master Thesis

Design of Beam Ends with Copes

Written by:
Hågen Urseth

Supervisor:
Arne Aalberg

Faculty of Engineering Science and Technology
Department of Structural Engineering

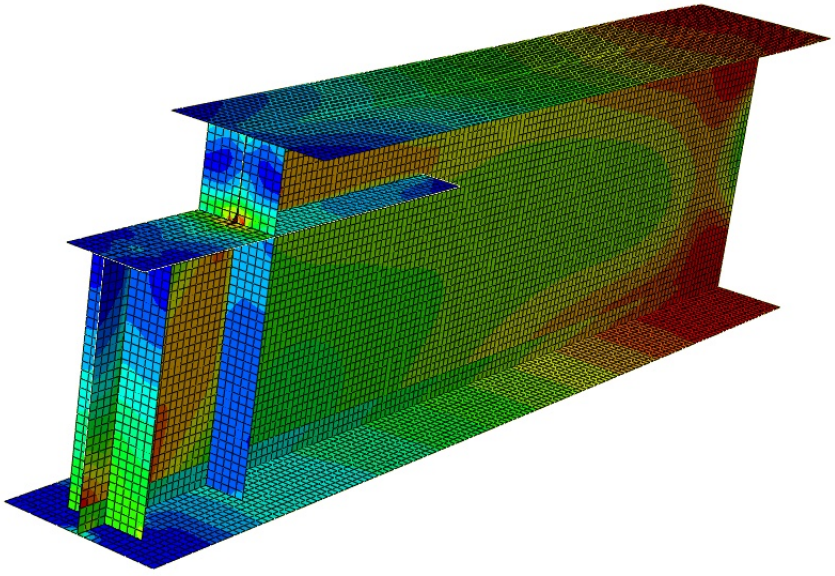

NTNU
Det skapende universitet

Declaration of Authorship

I, Hågen Urseth, declare that this thesis titled, 'Design of Beam Ends with Copes' and the work presented in it are my own. I confirm that:

- This work was done wholly or mainly while in candidature for a research degree at this University.
- Where any part of this thesis has previously been submitted for a degree or any other qualification at this University or any other institution, this has been clearly stated.
- Where I have consulted the published work of others, this is always clearly attributed.
- Where I have quoted from the work of others, the source is always given. With the exception of such quotations, this thesis is entirely my own work.
- I have acknowledged all main sources of help.
- Where the thesis is based on work done by myself jointly with others, I have made clear exactly what was done by others and what I have contributed myself.

Signed: _____

Date: _____

Abstract

Coping of beams is usually done in order to allow for clearance at connections, but doing so reduces the beams strength and makes it susceptible to local web buckling at the coped section. Due to this reduction of the beam's strength, it was of interest to reinforce the web at the coped end. Previous researchers have proposed several design recommendations for reinforcement of coped beams. Possible measures involves welding on endplates or use of bolted connections at the coped end, and provision of stiffeners at the coped region.

In this thesis a numerical study on the coped beam's strength and behaviour is presented. Nonlinear finite element analyses have been conducted to predict the structural behaviour and capacities of coped beams with varying cope dimensions. The beam was strengthened by either restraining the coped end from lateral translation or by provision of stiffeners at the coped region.

The effect of restraining the coped end depended on the cope dimensions. For cope length-to-reduced beam hight ratios lesser than 1 ($c/h_0 < 1$), restrainment of the coped end would successfully increase the beams capacity. For ratios equal to or more than one ($c/h_0 \geq 1$), the effect was negligible.

Reinforcement in longitudinal direction only did not prevent the occurence of local web buckling, so that the recommended reinforcement details of the coped beam included a combination of stiffeners in both vertical and longitudinal direction for which the beam was able to develop the plastic moment capacity of the full beam section without any significant sideways rigid body movement of the longitudinal stiffeners. The proposed design recommendations considers the webs slenderness and coped dimensions.

For coped beams with web depth-to-thickness ratios (h_w/t_w) less than or equal to 58 and cope length-to-reduced web hight ratios (c/h_0) less than one, longitudinal and vertical stiffeners were required while double vertical stiffeners were required for cope ratios equal to or more than 1. For coped beams with web depth-to-thickness ratio more than 58 and less than or equal to 67 and cope ratios less than or equal to 0.5 vertical and longitudinal stiffeners were required, while double vertical stiffeners were required for cope ratios of more than 0.5.

Sammendrag

Utkapp og tilpasninger må av og til lages for at bjelken skal passe til de konstruksjonsdelen den skal festes til. Som en følge reduseres bjelkens kapasitet og gjør den sårbar for knekking av stegplaten. Det er derfor av interesse å forsterke steget ved bjelkens utkappete ende. Gjennom tidligere studier har det blitt foreslått flere måter å forsterke slike utkappede bjelker på. Mulige tiltak vil være å stive av bjelkeenden med påsveiste endplater og med bolteforbindelser, eller ved bruk av stivere i langsgående og/eller tversgående retning.

I denne oppgaven presenteres et numerisk studium på kapasitet og oppførsel til utkappete bjelker gjennom ikke-lineære element analyser i ABAQUS/CAE. Bjelken er forsøkt forsterket ved enten fastholding av enden mot forskyvning ut av planet og/eller rotasjon om vertikalaksen, eller ved avstivning av den utkappede enden.

Effekten av å fastholde bjelkeenden var svært avhengig av utkappets størrelse. Fastholdingen økte bjelkens kapasitet når forholdet mellom utkappslengden og den reduserte bjelkehøyden var mindre enn 1 ($c/h_0 < 1$). Effekten var derimot utbetydelig når dette forholdet var lik eller overskred 1 ($c/h_0 \geq 1$).

Avstivning av bjelkens utkappede ende i kun langsgående retning forhindret ikke knekking av steget, uavhengig av stivernes lengde og dimensjoner. Dermed var det ønskelig å anvende avstivningsløsninger med både langsgående og tversgående stivere. For slike avstivningsløsninger var det mulig å forhindre knekking av steget, som gjorde det mulig å nå bjelkens plastiske momentkapasitet av bjelkens fulle høyde uten nevneverdig sideveis forskyvning av de langsgående stiverne.

For forhold av høyden og tykkelsen til steget (h_w/t_w) mindre eller lik 58 og for forholdet mellom utkappslengde og den reduserte bjelkehøyden (c/h_0) mindre enn 1 var det nødvendig med både langsgående og ett sett med tversgående stivere. For utkappsforhold større eller lik 1 var det nødvendig med langsgående i tillegg til doble sett med tversgående stivere. For forhold steghøyde og tykkelse lik eller større enn 58 men mindre enn 67 og utkappsforhold mindre enn eller lik 0.5, var det nødvendig med både langsgående og ett sett med tversgående stivere. For utkappsforhold større enn 0.5 var det påkrevd langsgående og doble sett med tverrsgående stivere.

Acknowledgements

This thesis is the final work concluding my Civil and Environmental Engineering study at the Norwegian University of Science and Technology, NTNU. A major part of the thesis is numerical analyses carried out with the finite element program ABAQUS/CAE. The work has been conducted at the Department of Structural Engineering.

I thank my supervisor Arne Aalberg for all the help and support during this final semester. The informal correspondance and meetings have been essential for my master thesis.

Contents

List of Figures

List of Tables

Symbols

A_c, $A_{c,eff}$	Compressional areas	mm^2
N_{cr}	Critical buckling load	N
K_t, K_m, K_g	Stiffness properties	N/mm
N_x, N_y, N_{xy}	Membrane forces	N/mm
E	Young's modulus	N/mm^2
G	Shear modulus	N/mm^2
t_w	Web thickness	mm
t_f	Flange thickness	mm
b	Beam width	mm
h	Beam hight	mm
h_0	Reduced beam hight	mm
h_w	Web hight	mm
$h_{w,red}$	Reduced web hight	mm
k, k_σ, k_τ	Plate buckling coefficient	
f	Adjustment factor	
c	Cope length	mm
d_c	Cope depth	mm
f_y, f_{yw}, f_{yf}	Yield stress	N/mm^2
L	Beam length	mm
R_{max}	Maximum reaction force	N
$F_{max,BUCKLE}$, $F_{max,BONKERUD}$	Maximum applied force	N
$R_{T15,0}$, $R_{T15,TF2}$, $R_{T2,0}$, $R_{T2,TF2}$	Maximum support force	N
$R_{M,pl}$, $R_{V,pl\&pl}$, $R_{M,el}$	Moment and shear capacity full beam section	kN
$R_{M,pl,red}$, $R_{V,pl\&pl,red}$, $R_{M,el,red}$	Moment and shear capacity reduced beam section	kN
L_x	Longitudinal stiffener length	mm
L_{y1}, L_{y2}	Vertical stiffener length	mm
e_x	Longitudinal stiffener extension length	mm
t_x	Longitudinal stiffener thickness	mm
b_x	Longitudinal stiffener width	mm

t_{y1}, t_{y2}	Vertical stiffener thickness	mm
b_{y1}, b_{y2}	Vertical stiffener width	mm
l_y, l_e	Effective load length	mm
m_1, m_2	Parameters	
$\sigma_{x,cr}$	Critical buckling stress	N/mm^2
$\tau_{xy,cr}$	Critical shear stress	N/mm^2
τ_{max}	Max. shear stress	N/mm^2
ν	Poisson's ratio	
ϵ_L, ϵ_E, ϵ_G, ϵ_A, ϵ_{pL}	Strain measures	
σ_T, σ_E	Stress measures	N/mm^2
λ_j	Eigenvalue	
φ_j	Eigenvector	
λ_F	Relative slenderness	
χ_F	Reduction factor	

Chapter 1

Introduction

In steel constructions secondary beams are usually connected to the main girders in a way that elevates the top flanges at the same hight, which is usefull in design of floor slab constructions. To construct such a connection and to provide clearance for the supports, the secondary beams must be coped at the end, as shown in figure 1.1. The cope can be at the top, at the bottom or at both flanges.

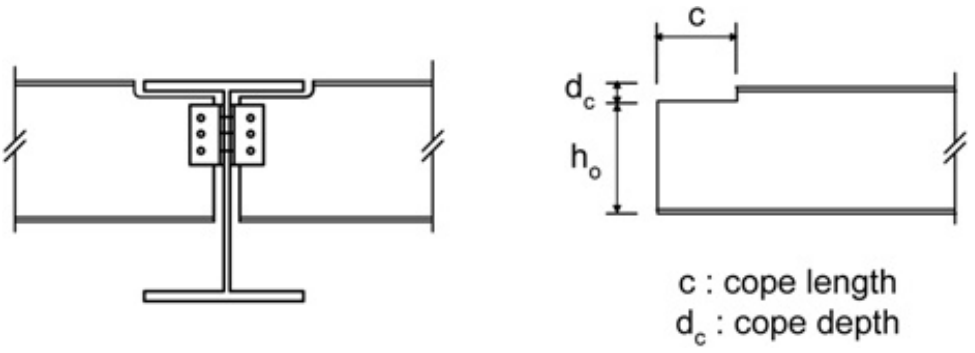

FIGURE 1.1: Top flange coped I-beam.

As a consequence of coping the end, the strength of the beam can be reduced significantly. Thus, the coped beam may fail in local web buckling, shear yielding, flexural yielding or block shear failure. Coping will also affect the beam's lateral torsional buckling capacity, hence the beam can also fail in lateral torsional buckling if not properly braced [7]. The coped beams strength and behaviour have been investigated by a number of researchers, both worldwide and at the Department of Structural Engineering, NTNU. From numerical and experimental studies, several design recommendations have been provided for the coped beam's capacity against the most common failure modes.

Due to the beams reduced strength, it may be necessary to reinforce the web at the coped end. Cheng and Yura (1986) proposed a set of reinforcement details, shown in figure 2.4.

These recommendations were based on a numerical study only, so that later Yam et al. (2007) conducted a series of laboratory tests on the stiffened coped beam's strength and behaviour in order to assess those recommendations [8]. Based on this study, certain modifications to the reinforcement details were proposed, as seen in figure 2.5. The experimental study was followed by a more comprehensive numerical study in order to increase the proposed reinforcement details applicability [9].
Another measure to increase the coped beam's capacity is to restrain the coped end in some way. This can be done with a welded-on endplate or with a bolted connection to adjacent construction. In his master thesis, Carlsen (2008) studied the effect an endplate and its connection properties would have on the coped beam's capacity [10]. The capacity was seen to increase with increasing endplate thickness.

In this thesis, the coped beam's strength and behaviour in both an unreinforced and reinforced state was investigated for a series of cope details. No experimental testing was conducted, hence the study relied solely on results from the finite element analyses. The coped beam was reinforced with the following measures

- Restrainment of the web at coped end
- Reinforcing the coped region with stiffeners in horizontal and/or vertical direction

The main objective was to examine the proposed reinforcement measures effect on the coped beam's capacity, and for which cope dimensions reinforcement of the coped end would be less efficient. The results were compared to the design recommendations presented in the litterature to check their applicability.

Chapter 2

Teoretical Background

2.1 Plate Buckling Theory

2.1.1 General

Slender structures, such as plates or columns exposed to compressive loading are vulnerable to buckling, refered to a state where a very small increase of the loading causes the structure to deflect in a very large manner. The expression is used somewhat imprecise about two phenomenons, namely *elastic instability* and *inelastic failure*. When loaded with a critical load (N_{cr}) the structure looses its state of equilibrium, i.e. it becomes unstable [1].
More specifically, buckling occurs when the structures stiffness is dramatically reduced, i.e. the following expression drops to zero

$$[K_t] = [K_m] + [K_g] = 0$$

where K_t is the resultant tangent stiffness, composed of the elastic (material) stiffness K_m and the stress (geometrical) stiffness K_g. In ABAQUS/CAE, the elastic stiffness depends on the material properties, while the stress stiffness depends on the state of stress. Thus, tensile stresses will increase the stiffness while compressive stresses will decrease it [4].
In terms of energy considerations, buckling occurs when the membrane (axial) strain energy is converted into bending strain energy with no change of externally applied load. In slender columns and thin plates or shells, the membrane stiffness is much greather than the bending stiffness. Thus, large deformations will occur when the convertion takes place.
In design of plates one differs between two cases: *elastic plate buckling* and *over-critical plate buckling behaviour*.

2.1.2 Elastic Plate Buckling

The web in a steel I-beam will act as a plate loaded with membrane actions. If those membrane actions exceeds the webs critical buckling capacity the web becomes unstable and buckles. Coped beams are particularly vulnerable, as the web in the coped section has lost its support by one or both of the flanges.
The critical membrane actions are determined based on the plates differential equation derived from equilibrium considerations of an infinitesimal deformed element. Thus, for an isotropic material the plate's differential equation reads [11]

$$\nabla^4 w = \frac{1}{D}(N_x \frac{\partial^2 w}{\partial x^2} + N_y \frac{\partial^2 w}{\partial y^2} + N_{xy} \frac{\partial^2 w}{\partial x \partial y}) \tag{2.1}$$

The equation is solved with respect to the boundary conditions and type of loading, in order to assess the following expression for critical buckling load for plates loaded in axial compression and moment

$$\sigma_{x,cr} = k_\sigma \frac{\pi^2 E}{12(1-\nu^2)} \left(\frac{t}{b}\right)^2 \tag{2.2}$$

where the plate buckling factor k_σ includes the plates boundary conditions and the distribution of externally applied forces.
For plates loaded in shear, the buckling shape is inclined at an angle. The critical shear stress is given by the following expression

$$\tau_{xy,cr} = k_\tau \frac{\pi^2 E}{12(1-\nu^2)} \left(\frac{t}{b}\right)^2 \tag{2.3}$$

where k_τ is the plate buckling factor for shear.
Longitudinal and vertical stiffeners are commonly used to increase the plates capacity [1]. When the plate buckles, it will buckle in a number of sinuswaves in the longitudinal and vertical direction. Use of stiffeners will alter this buckling pattern.

2.1.3 Capacity of Plates

Unlike columns which will collaps during buckling, there will for plates be possible to exceed the external load over the critical buckling load, due to a redistribution of the internal stresses. This over-critical capacity can be significant and usefull in design.
Design recommendations for plates are found in the Eurocode 3 [12]. For plates loaded by axial forces and moment the capacity is based on the plates effective area in the compressional zone. This effective area is defined by the expression $A_{c,eff} = \rho A_c$, where A_C is the plates compressional area and ρ is a reduction factor. The reduction factor (ρ) depends on the plate

slenderness (λ_p), given by the following expression

$$\lambda_p = \sqrt{\frac{f_y}{\sigma_{cr}}} \tag{2.4}$$

where σ_{cr} is the elastic critical buckling stress. Thus, the plates capacity reads as follows

$$N_x = \rho f_y A_c = f_y A_{c,eff} \tag{2.5}$$

For plates loaded with transverse forces, the following design recommendations are provided by the Eurocode 3 [12]. The plate's load capacity depends on the plate's slenderness, defined the plate hight-to-thickness ratio (h_w/t_w). Regarding the plate's slenderness, three failure modes are identified, as seen in figure 2.1.

- For small values of h_w/t_w the web near the loaded position will be subject to plastification
- For intermediate values of h_w/t_w the beam fails in global buckling of the web
- For large values of h_w/t_w the web cripples directly below the loaded position, while the rest of the web stays nearly undistorted

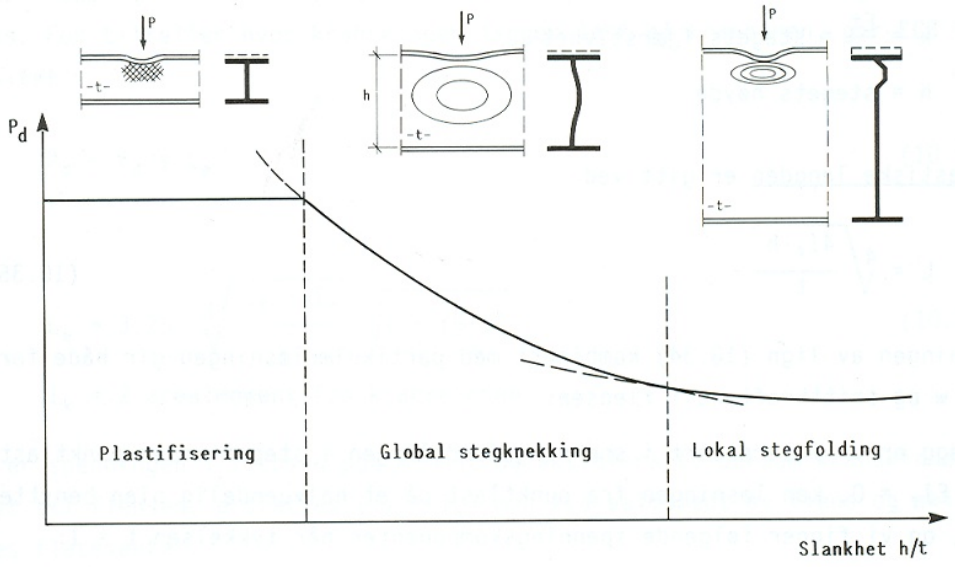

FIGURE 2.1: Failure modes for beam loaded with transverse forces [1].

The design recommendations are based on the design model developed by Lagerqvist [13], which covered all the failure modes in figure 2.1.
The capacity is determined based on the assumption that the vertical stresses in the web below the loading are distributed equally over a section with length L_{eff}, thus the beam's capacity reads

$$F_{Ed} \leq F_{Rd} = \frac{f_{yw} L_{eff} t_w}{\gamma_{M1}} \tag{2.6}$$

where

$$L_{eff} = \chi_F l_y \tag{2.7}$$

The reduction factor χ_F is expressed by the formula

$$\chi_F = \frac{0.5}{\lambda_F} \qquad \chi_F \leq 1.0 \tag{2.8}$$

where the plates relative slenderness is defined by

$$\lambda_F = \sqrt{\frac{f_{yw} t_w l_y}{F_{cr}}} \tag{2.9}$$

and

$$F_{cr} = 0.9 k_F E \frac{t_w^3}{h_w}$$
$$k_F = 2 + \frac{6(s_s + c_s)}{h_w} \leq 6$$

l_y is defined by the following formulas

$$l_y = min \begin{cases} l_e + t_f \sqrt{\frac{m_1}{2} + (\frac{l_e}{t_f})^2 + m_2} \\ l_e + t_f \sqrt{m_1 + m_2} \end{cases}$$

where

$$l_e = \frac{k_F E t_w^2}{2 f_{yw} h_w} \leq s_s + s_c \tag{2.11}$$

and

$$m_1 = \frac{f_{yf} b_f}{f_{yw} t_w}$$
$$m_2 = 0.02(\frac{h_w}{t_f})^2 \qquad \text{for} \qquad \lambda_F > 0.5$$
$$m_2 = 0 \qquad \text{for} \qquad \lambda_F \leq 0.5$$

2.2 Relevant Scientific Papers

2.2.1 Cheng and Yura (1986)

In their scientific paper *Local web buckling of coped beams* [14] Cheng and Yura presented a method for design of coped beams against local web buckling. Due to the discontinuity of the web and flange at the coped corner a stress concentration may occur at this point, making regular calculations for bending and shear stresses unable to describe the actual stress distribution at the coped region. If the stress concentration is high enough the material will yield at the coped corner, causes the beam to fail due to inelastic local web buckling. For slender webs, failure can occur by elastic local web buckling at the coped region.

Cheng and Yuras study included both experimental testing in the laboratory and numerical simulations with use of a finite element program. For practical reasons, only beams with cope lengths less than twice the beam depth ($c < 2h$) and with cope depth less than half the beam depth ($d_c < h/2$) where considered. The difference between the testdata and numerical solutions were quite small, ranging from $2 - 5$ %. They then came up with a design model. To make it simple for design purposes, they descided to start up with a regular plate buckling model and then adding factors representing the complex nature of the buckling problem.
Figure 2.2 shows the plate model of the coped section, consisting of a plate simply supported on three edges and free on the last with a linear stress distribution over the edges.

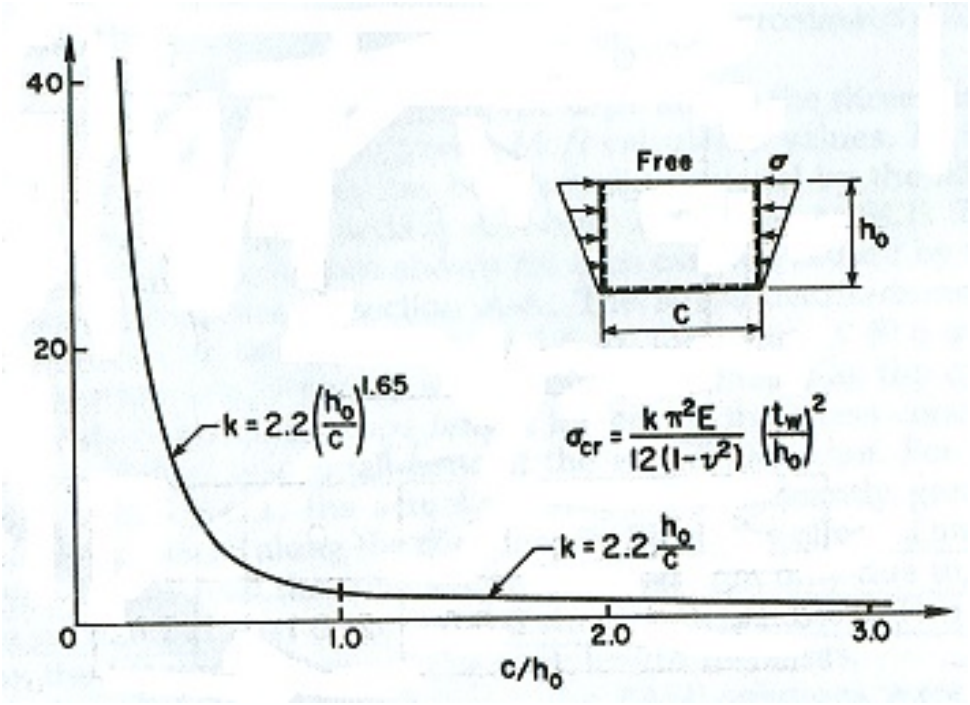

FIGURE 2.2: Plate model for design.

The plate buckling capacity where set to

$$\sigma_{cr} = f k_\sigma \frac{\pi^2 E}{12(1-\nu^2)} \left(\frac{t_w}{h_0}\right)^2 \tag{2.12}$$

where

$$k_{cr} = 2.2\left(\frac{h_0}{c}\right)^{1.65} \qquad \text{for} \quad \frac{c}{h_0} \leq 1.0$$
$$k_{cr} = 2.2\left(\frac{h_0}{c}\right) \qquad \text{for} \quad \frac{c}{h_0} \geq 1.0$$

and

$$f = 2\left(\frac{c}{h}\right) \qquad \text{for} \quad \frac{c}{h} \leq 1.0$$
$$f = 1 + \left(\frac{c}{h}\right) \qquad \text{for} \quad \frac{c}{h} > 1.0$$

The plate buckling coefficient (k_{cr}) considers the cope dimensions and was obtained from excisting litterature and by curve fitting techniques. The adjustment factor (f) considers the stress concentrations, shear stresses, cope depths and moment variations over the coped end. Observe that this factor increases with an increasing cope length, which again increases the beams buckling capacity. This is an effect of the stress consentration at the coped corner. For short cope length the stress consentration at the coped corner will make the actual stresses significantly higher than the regular bending stresses along the cope length. As the cope length increases, this stress consentration will be restricted to a small area at the end of the cope.

In their concluding remarks they stated that localized yielding due to stress concentration would not affect the coped beams buckling capacity in any significant manner. Also, regular bending and shear stresses causing yielding of the coped region would provide a conserative approach for checking inelastic local web buckling for coped beams.
For elastic local buckling of the web of top flange coped beams, the proposed design model gave a good estimate.

2.2.2 Yam et al. (2003)

In their report *Local web buckling strength of coped steel I-beams* [15] Yam et al. continued the work done by Cheng and Yura [14] on the behaviour of coped steel I-beams and their capacities against local web buckling. They stated that the previously obtained design formulas underestimated the beams capacity, specially for a small cope depth-to-beam hight ratio (d_c/h).

Thus, a more accurate expression was desired.

Both full-scale testing in the laboratory and numerical simulations were conducted. From the results they observed that the buckling line inclined at an angle for short cope lengths. It was belived that shear stresses dominated the buckling behaviour for cope length-to-reduced beam hight ratios (c/h_0) lesser than 1.5.

Based on the shear stress distribution over the coped beam, they suggested a modified plate model, as seen in figure 2.3

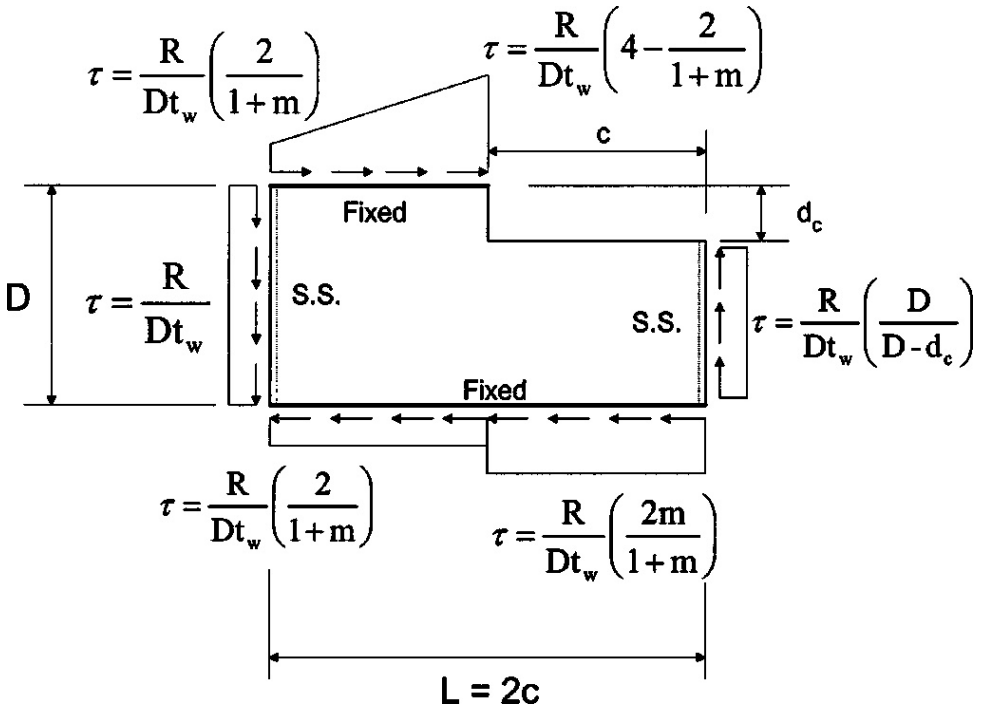

FIGURE 2.3: Platemodel with shear stress distribution.

The shear stresses at the coped T-section exceeded those of the I-section, due to the discontinuity at the cope. Also, to maintain equilibrium the shear stresses at the junction between the compressional flange and the web became larger than in theory. Moment was not considered, as its influence was neglected for small cope depth-to-hight ratios. To minimize the effect of the boundary conditions, they increased the plate model's length from $2c$ to h_0 for cope lengths less than half the cope depth.

Following design formulas were developed

$$\tau_{cr} = k_s \frac{\pi^2 E}{12(1-\nu^2)} \left(\frac{t_w}{h_0}\right)^2 \qquad \text{for} \qquad \tau_{cr} \leq \tau_{max} = \frac{f_y}{\sqrt{3}} \tag{2.13}$$

where

$$k_s = a\left(\frac{h_0}{c}\right)^b \tag{2.14}$$

and

$$a = 1.38 - 1.79\frac{d_c}{h}$$
$$b = 3.64\left(\frac{d_c}{h}\right)^2 - 3.36\left(\frac{d_c}{h}\right) + 1.55$$

The value of the shear buckling coefficient (k_s) was found by rearranging τ_{cr} and implement the critical shear stress obtained from the numercial solutions.
They concluded that the results from the proposed design formula compared well with the test results, with test-to-predicted ratios from 0.92 to 1.06.

2.2.3 Yam et al. (2007)

In their report *The Local Web Buckling Strength of Stiffened Coped Steel I-Beams* [2] Yam et al. studied the effect of reinforcing the coped region with stiffeners in order to improve the coped beam's capacity. Reinforcement of the coped region was originally investigated by Cheng and Yura [7], where stiffeners were provided to improve the local web buckling strength of coped beams. They recommended three reinforcing details, as shown in figure 2.4

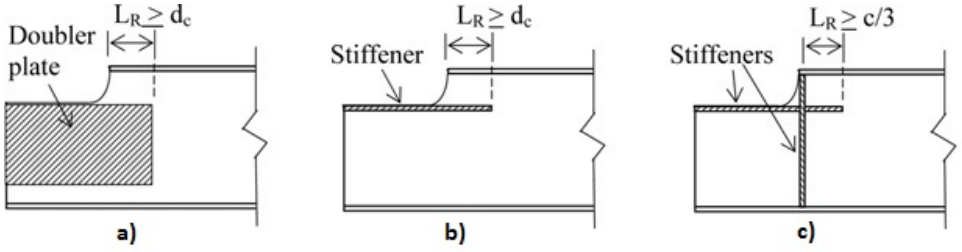

FIGURE 2.4: Web reinforcement details for coped beams [2].

Through numerical simulations in the program *BASP* they were able to determine the beam's buckling loads with varying reinforcement dimensions. For thin web members ($d/t_w > 60.0$) they recommended use of type b) reinforcing detail with $L_k \geq c/3$, while for rolled sections type a) and c) reinforcing details with $L_k \geq d_c$ was recommended.
However, no experimental evidence was provided, making it impossible to validate the design recommendations.
Therefore, in order to verify the reinforcing details recommended for strengthening of the coped region, Yam et al. conducted an experimental and numerical study of coped steel I-beams.
In the experimental study, three full-scale tests were carried out. They showed that web distortion occured at the coped section even when horizontal stiffeners were provided.
In the numerical study, the effect of horizontal stiffeners were investigated for stiffener type

B. However, extending the horizontal stiffeners length did not increase the local web buckling capacity efficiently. Thus, a minimum length of vertical stiffeners were provided in addition to the horizonal stiffeners. The stiffener arrangements are shown in figure 2.5. Provision of vertical stiffeners were also belived to prevent sideways movement of the coped end, but as seen in figure 2.6 the horizontal stiffeners still experienced severe sideways movement.

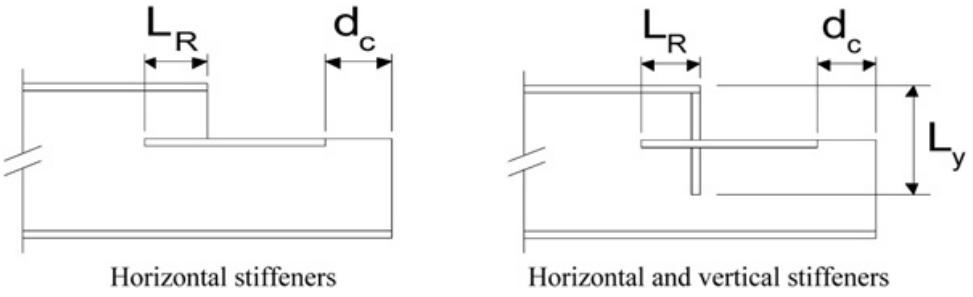

FIGURE 2.5: Different types of stiffeners at the cope region [2].

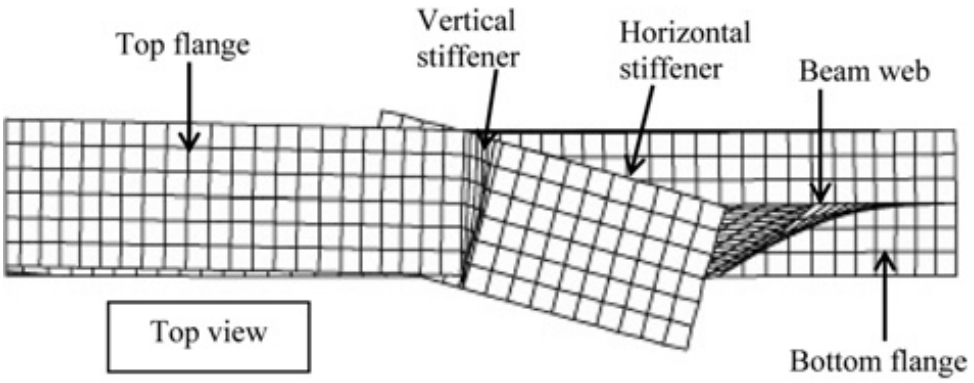

FIGURE 2.6: Buckled mode shape of coped beam with stiffeners in both horizonatal and vertical direction [2].

Provision of stiffeners in both direction did improve the coped beams capacity, but it was still lower than the reaction force corresponding to the yield moment and the shear yielding resistance of the coped web. Also, extending the vertical stiffener length over the whole beam's depth had little effect in improving the coped sections local web buckling capacity.
In their concluding remarks they proposed the following design recommendations for reinforcement of coped beams:

- For beams where $c/D > 1$, both the extension length of the horizontal stiffeners, L_R and the length of the vertical stiffener, L_y should not be less than $2d_c$
- For beams where $c/D < 1$, both the extension length of the horizontal stiffeners, L_R and the length of the vertical stiffener, L_y should not be less than d_c

2.3 Previous Student Work

2.3.1 Bonkerud (2007)

In his master thesis *Capacity of coped beams* [3] Bonkerud investigated the behaviour of coped steel I-beams and proposed a set of design recommendations for such. The following design criterias where checked:

A. Elastic moment and shear capacity, and the interaction of both

B. Plastic moment and shear capacity, and the interaction of both

C. Local web buckling

He assumed, after recommendations from Cheng and Yura [14], that for webs with $\frac{h}{t_w} < 42$ and $\frac{c}{h} < 2.0$ there would not be necessary to check for buckling and that yielding would determine the beams capacity. For an IPE300 beam however $\frac{h}{t_w} \approx 42$, buckling had to be considered. Comparison of elastic and plastic interaction between moment and shear with numerical solutions, showed that all three could be critical depending on the cope dimension. However, it was concluded that the coped beam's stress distribution is of such complexibility that regular capacity checks may prove inaccurate.
The coped beam's behaviour was investigated in a numerical study in the finite element program ABAQUS/CAE. Several cope dimensions were analyzed and compared with experimental data obtained in a previous study by Petterson and Røe [16].
Bonkerud presented two design formulas for design of coped beams. One based on a previously derived formula and the other based on a plate model.

Design formula 1: Continuation of developed formula

The following formula was presented in [17] and [16]

$$R_{coped} = R_{uncoped}\left(1 - B\frac{c}{h_0}\right) \tag{2.15}$$

where the factor B equals 0.32 for steel and 0.4 for aluminimum. From the numerical results and through curve fitting techniques in Excel the following design formula was presented

$$R_{coped} = R_{uncoped}\left(1 - B\frac{c}{h_0}\right) \tag{2.16}$$

where

$$B = 0.36 + \frac{1}{470}\frac{d}{t_s} - 0.09\frac{E}{E_{steel}} \tag{2.17}$$

and $R_{uncoped}$ are obtained from Eurocode 3 [12].
It was concluded that the formula provided valid results, but that more testing would be necessary to reveal possible flaws.

Design formula 2: Plate model

Figure 2.7 shows the plate model developed by Bonkerud. As seen from the figure the plate model represent a rectangular plate simply supported on three edges set askew, due to the similarities of deformation pattern between the coped beam and the three-sided simply supported plate.

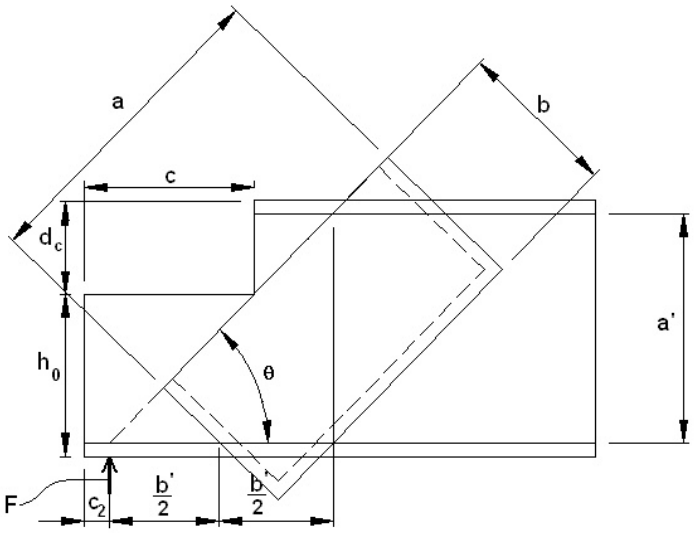

FIGURE 2.7: Plate model developed by Bonkerud [3].

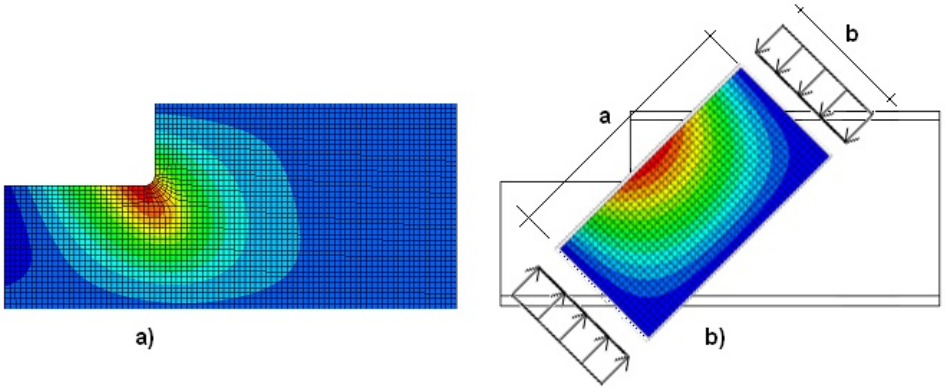

FIGURE 2.8: Deformation pattern for a) Coped beam and b) Simply supported plate on three edges [3].

The following formula was presented

$$F_d = f_d \chi t_s b \sin(\theta) \tag{2.18}$$

The formula showed unphysical behaviour when the cope dimension was either very small or very large. It shows the difficulty of developing general design recommendations for all types of cope dimensions, since the behaviour of a small cope differs from that of a large cope.

2.4 Finite Element Method

2.4.1 General

The finite element method simply shortened FEM, is a tool for obtaining numerical solutions of field problems, in this case stress analysis. A field problem is described by differential equations or by an integral expression, both used to formulate finite elements. In each finite element a field quantity can have only a simple spatial variation, which can be described by polynominal terms up to x^2, xy or y^2 [5]. Obviously FEM provides approximate solutions only, as the actual variation is almost certainly more complex.
In order to investigate the coped beam's behaviour during loading, numerical simulations with use of a finite element program is a valuable tool. In this instace ABAQUS/CAE was chosen. The solutions obtained from such simulations can supplement or replace real testing in the laboratory and will make it possible to produce data for a large number of specimens at a small cost. The test specimens are also not restricted to practical purposes, meaning that any shape, dimension and type of loading can be tested. However, care must be taken when evaluating the results as several errors might occur. Such errors might be possible to identify within the model itself through energy checks, but often the model has to be validated through external data checks. Such validation include comparison of test results from laboratory experiments, comparison with analytical solutions and results from other numerical simulations.

2.4.2 Linear Buckling Analysis

In ABAQUS/CAE linear buckling analyses are performed through the step BUCKLE, providing the critical buckling load of the structure. As earlier mentioned buckling refers to a state where a slender structure, in this case the web plate, experience a dramatic loss of its structural stiffness and becomes unstable. In other words, the stiffness of the structure drops to zero, i.e. becomes singular. Thus, the buckling analysis is represented by solving the following eigenvalueproblem [4]

$$\big([K_m] + \lambda_j [K_g]\big)\{\varphi\}_j = \{0\} \tag{2.19}$$

Where λ_j denotes the eigenvalues and $\{\varphi\}_j$ denotes the eigenvectors representing the corresponding buckling shapes. The buckling load P_j is provided by the product of the eigenvalue and the applied load: $P_j = \lambda_j P$.
The buckling load will however differ from the real capacity of the structure, due to imperfections and other nonlinearities.

2.4.3 Nonlinear Analysis

Nonlinear FEA differs from linear FEA in that the stiffness and loads become functions of displacement or deformation. Thus, as the structural equations for linear analysis reads $[K]D = R$, for nonlinear FEA the expression becomes $[K(D)]D = R(D)$, where $[K]$ and R defines respectivily the stiffness matrix and load vector. The nonlinear structural equation cannot be solved directly, thus an iterative process is required. Also, the principle of superposition is not applicable to the nonlinear equations so that each different load case requires a seperate analysis.
Compared to linear FEA, nonlinear FEA is much more computationally costly and requires substantially more effort from the analyst due to the difficulty of describing nonlinear problems with realistic mathematical and numerical models and solving of the following nonlinear equations. So why choose nonlinear FEA instead of a linear approach?
As linear FEA provides satisfactory approximations for many problems, substantial departure from linearity is quite common. Nonlinear behaviour on the other hand allows for a wide varity of phenomena. In structural analysis nonlinear FEA makes it possible to investigate the structures stability as well as the global strength. The overall behaviour of the structure is graphically represented by the equilibrium path, shown in figure 2.9 for the linear and nonlinear response. The linear structure is able to undergo any load and deformation, while the nonlinear is restricted by a critical point where the structures maximum capacity is reached.

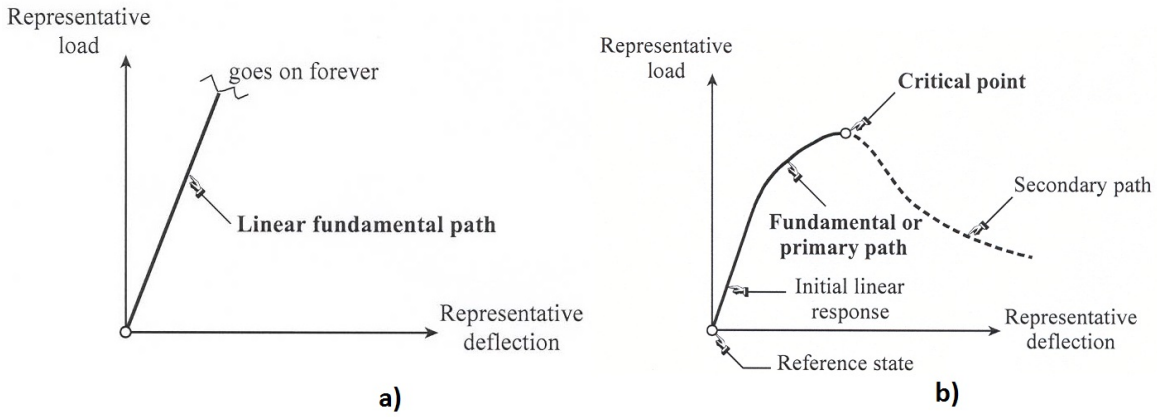

FIGURE 2.9: Equilibrium path for a) linear structure and b) nonlinear structure [4].

The nonlinear equlibrium equations can be solved with use of the numerical technique Newton's method, shown graphically in figure 2.10. This method is prefered to other solution techniques primarily in terms of convergence rate. The equations are solved by an iterative procedure as follows. After an iteration i an estimate for the displacement u_i^M to the solution is obtained. This estimate is not exact, where c_{i+1}^M defines the difference between this solution and the exact solution. Thus,

$$F^N\left(u_i^M + c_{i+1}^M\right) = 0$$

The left-hand side of the equation is expanded in a Taylor series about the estimated solution u_i^M, where all but the first two terms are neglected as the magnitude of each c_{i+1}^M will be small. Thus, obtain a linear system of equations

$$K_i^{NP} c_{i+1}^P = -F_i^M \tag{2.20}$$

where

$$K_i^{NP} = \frac{\partial F^N}{\partial u^P}(u_i^M) \qquad \text{and} \qquad F_i^N = F^N(u_i^M)$$

The next approximation to the solution is then

$$u_{i+1}^M = u_i^M + c_{i+1}^M$$

The iteration continues until convergence, where all entries in F_i^N and c_{i+1}^N are sufficiently small [18].

2.4.4 Material Behaviour

In ABAQUS/CAE the models elastic material properties are implemented by Young's modulus (E) and Poisson's ratio (ν), while the plastic material properties are implemented as the stress-strain relation. ABAQUS/CAE uses true strain and stresses, hence material data which originally are given by the engineering values must be converted into such.

Strain Measures

There exist several different strain measures, such as Green strain (ϵ_G), Almansi strain (ϵ_A), true strain (ϵ_L) and conventional strain (ϵ_e). Common to all of them is that they have to satisfy the constraints of finite strain measures. To fulfill those criterias the finite strain measures have to be able to predict zero strain for rigid-body motion and reduce to infinitesimal strains if

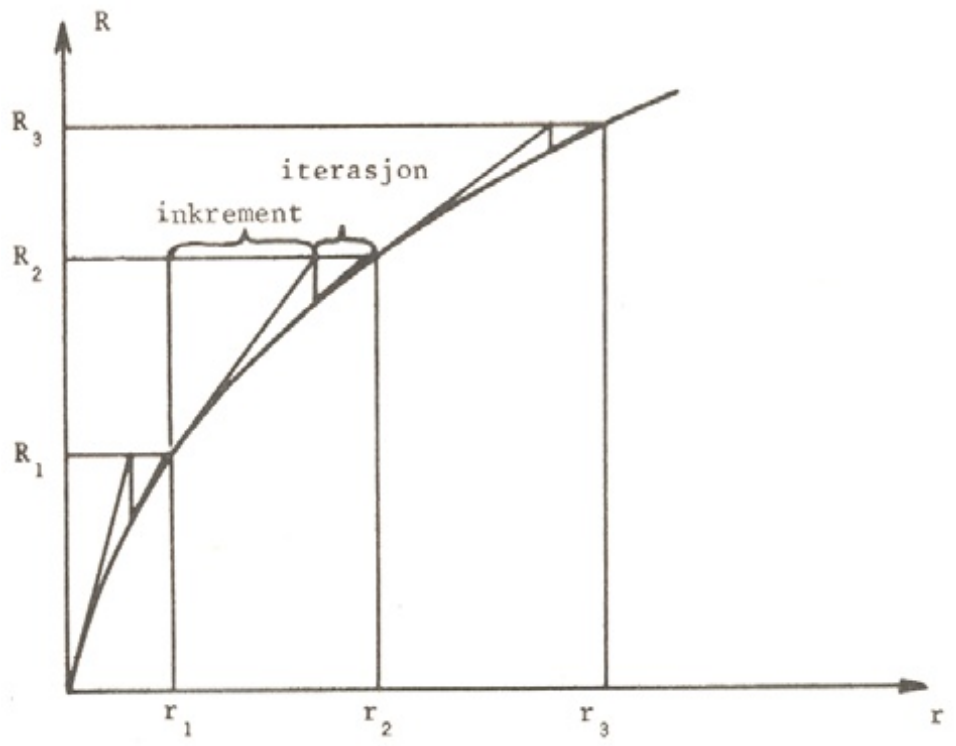

FIGURE 2.10: Iterations t convergence [4].

nonlinear terms are neglected. Additionally the strain measures should be able to predict finite strain in a realistic manner, i.e. for full compression it should diverge to an infinite negative strain ($\epsilon \to -\infty$ as $L \to 0$), and for infinite elongation it should diverge to an infinite positive strain ($\epsilon \to \infty$ as $L \to \infty$) [4]. See from figure 2.11 that the only strain measure that fulfilling those criterias is the true (logarithmic) strain (ϵ_L).

Unlike conventional (engineering) strain (ϵ_E), true strain accounts for the geometrical changes the specimen undergoes during deformation. Thus, the strain increment is defined with respect to the current gauge length (L)

$$d\epsilon_l(t) = \frac{du_L(t)}{L} \tag{2.21}$$

Integration of the strain increment over the deformation length yields the expression for true strain

$$\epsilon_l = ln\Big(\frac{L}{L_0}\Big) = ln(1 + \epsilon_e) \tag{2.22}$$

with the plastic strain given by

$$\epsilon_{pl} = \epsilon_l - \epsilon_e l = ln(1 + \epsilon_e) - \sigma_t/E \tag{2.23}$$

Stress Measures

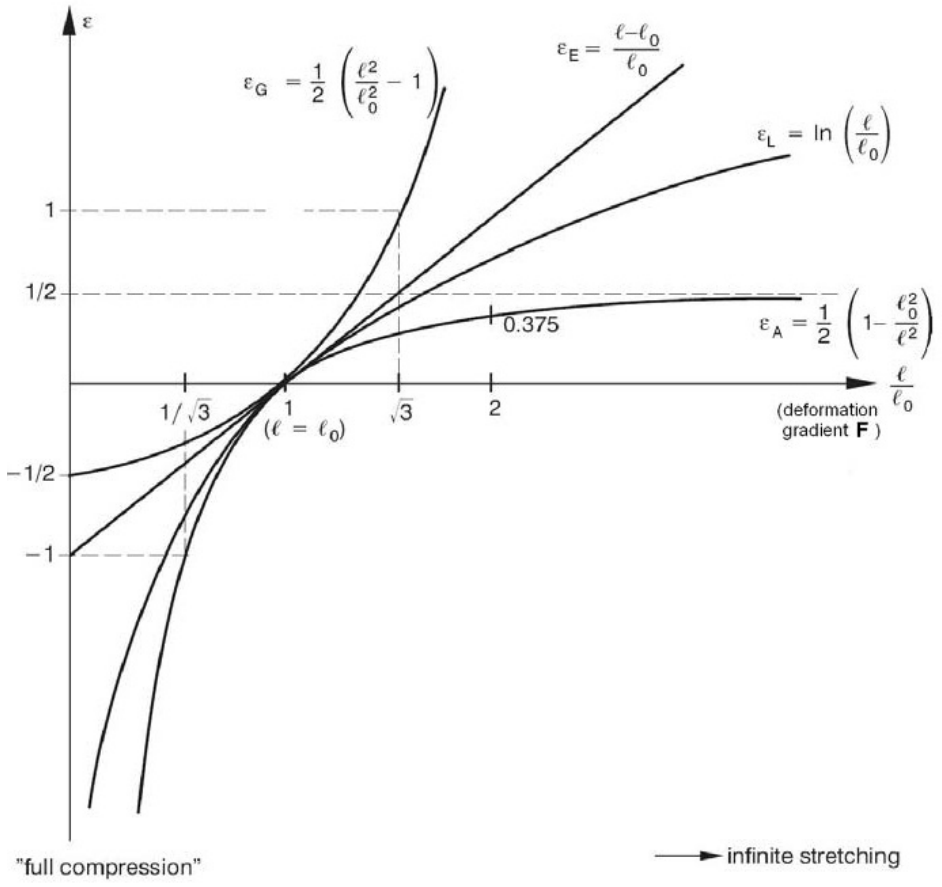

FIGURE 2.11: Finite strain measures [4].

Work conjugate to true strain is the true stress (σ_t) which refers to the current cross sectional area. The expression for the stress measure make use of the fact that the strains in metals remain small and that plastic deformation is incompressible [19], giving

$$A_0 L_0 = AL \tag{2.24}$$

Implementing this term yields the following expression for the true stress

$$\sigma_t = \sigma_e \exp(\epsilon_l) = \sigma_e(1 + \epsilon_e) \tag{2.25}$$

Chapter 3

Development of Numerical Model

The coped beam's behaviour in both stiffened and unstiffened mode was analyzed with use of the finite element program ABAQUS/CAE. The obtained results were compared to similar numerical solutions on the topic.

3.1 Procedure

Geometry

The models cross section was that of an IPE300 steel beam with dimensions corresponding to the standard europian values [20]. The beam's length was set to 1000 mm, restrained from translation in all directions at one end and the free end resting on a rigid block. The contact surface between the underside of the flange and the block was simulated through a contact algorithm. The block was chosen as the master surface and the underside of the flange acts as the slave surface. The beam was loaded by moving the block in the vertical direction.
Considering the beams symmetric behaviour about the restrained end, the beam's behaviour was similar to that of a simply supported beam with a total length of 2000 mm.
A series of cope details were tested, where the coped corners were given a rounded shape with a radius of 12 mm, according to the design recommendations in the American steel manual [21]. Figure 3.1 show the coped beam's dimensions, with the copes dimensions as shown in table 3.1

Material

The beam and stiffeners are given similar material behaviour corresponding to that of S355 construction steel [22]. The material properties implemented in ABAQUS/CAE are presented in table 3.2. The max. stress and strain on the stress-strain curve are respectivily given as 612 N/mm^2 and 0.179. The analyses are however not expected to reach that far on the stress-strain curve.

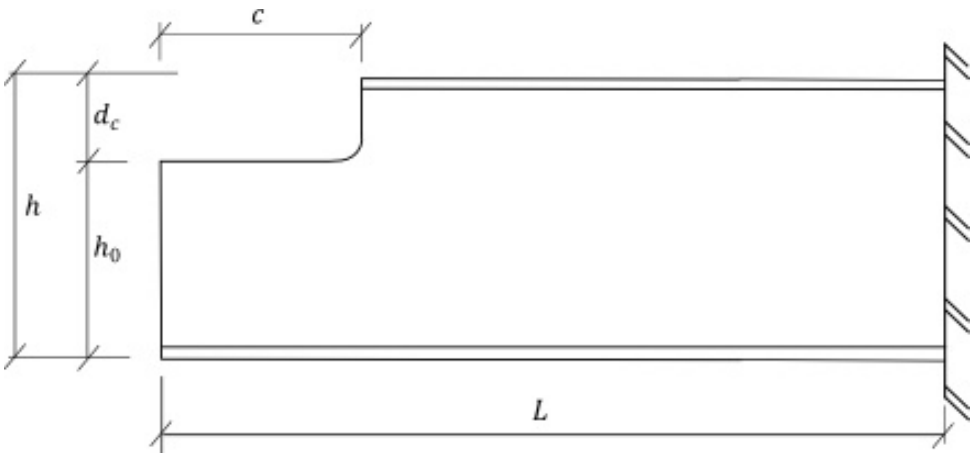

FIGURE 3.1: Dimensions of coped beam.

Cope length c	Cope depth d_c [mm]	Cope ratio c/h_0
0	0	0
100	70	0.43
100	110	0.53
100	150	0.67
200	70	0.87
200	110	1.05
300	70	1.30
200	150	1.33
300	110	1.58
300	150	2.00

TABLE 3.1: Dimensions of coped region.

True stress σ_T $[N/mm^2]$	Logarithmic plastic strain ϵ_{pL}
355.6	0
378	0.047
612	0.179

Young's modulus E $[N/mm^2]$	Shear modulus G $[N/mm^2]$	Poissons ratio ν
210 000	81 000	0.3

TABLE 3.2: Material properties for S355 steel.

Elements - Shell Elements S4 and S4R

The shell elements stress resultant have parts in both bending (out-of plane) and membrane (in-plane). For plane elements there are no coupling between the membrane and bending action, thus the stiffness matrix can be established by superimposing the membrane and plate stiffness relations [4].
The shell elements ability to describe stress distribution through the thickness is restricted, where the solid elements will give more accurate results. However, for slender structures shell elements will provide accurate results, which makes them preferable to the more computationally costly solid elements.
There exist several different shell elements. The S4 element is a plane 4-node fully integrated general purpose element type with 6 degrees of freedom in each node, able to describe large strain behaviour [23]. Figure 3.2 shows the graphical representation of this element compared to the 8-node solid element

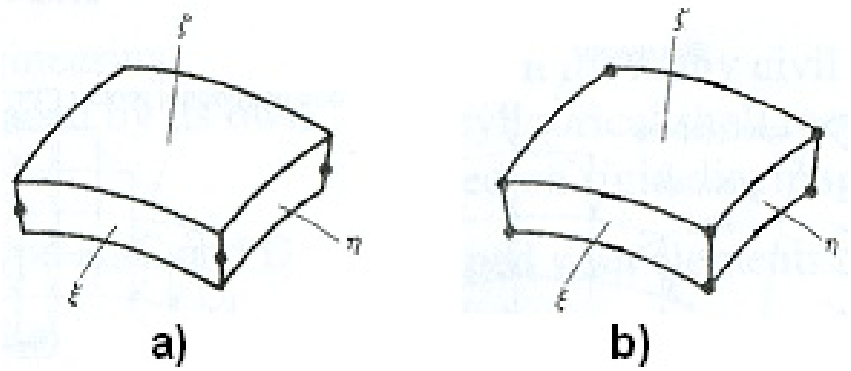

FIGURE 3.2: Type of elements, a) 4-node shell element, b) 8-node solid element.

The S4 element does not have hourglass modes, thus hourglass controll is not required. The S4R element is the S4 element with reduced integration. For undistorted elements reduced integration usually provides more accurate results compared to full integration, because it softens the behaviour of the element [24]. It is also preferable in that reduced integration significantly reduces the computational time. The downside is that hourglass modes may occur, so that hourglass controll is required. Hourglass modes are also known as spurious modes or zero-energy deformation modes, and are deformation modes that are not rigid body motions were the strain energy will integrate to zero. An element who exhibit a spurious mode has no resistance to nodal loads that tend to activate the mode [5]. Figure 3.3 shows the independent displacement modes of a 4-node plane element, where the hourglass modes are represented by modes 7 and 8.

Hourglass control applies constraints to prevent hourglass modes. The energy used to prevent hourglass modes is represented by the artificial energy, which should be very small compared to the strain energy. If not, a refined mesh or use of fully integrated S4 elements is required.

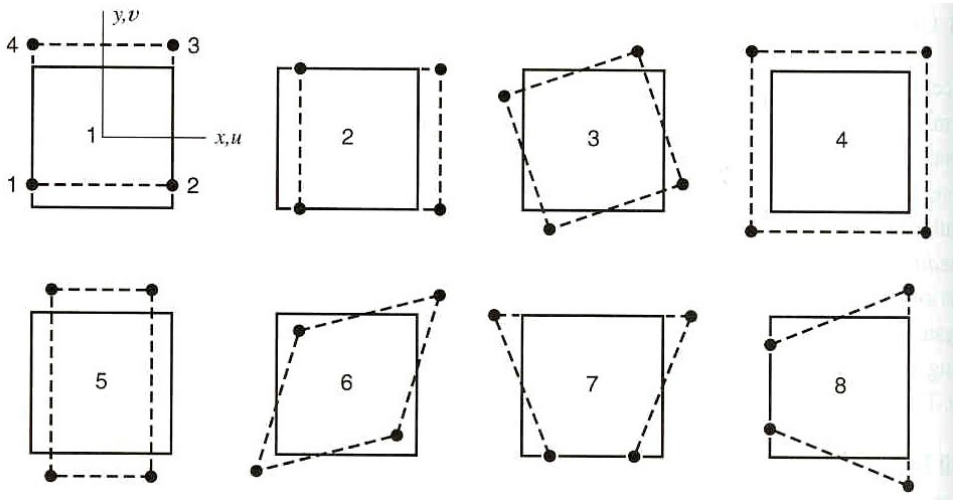

FIGURE 3.3: Independent displacement modes of a 4-node plane element [5].

Chose S4R elements in modeling of the coped beam due to its advantages mentioned above. Since shell elements does not have a volume, it's not possible to model the web's rounded shape at the intersection between the web and flanges in an exact manner, as seen in figure 3.4

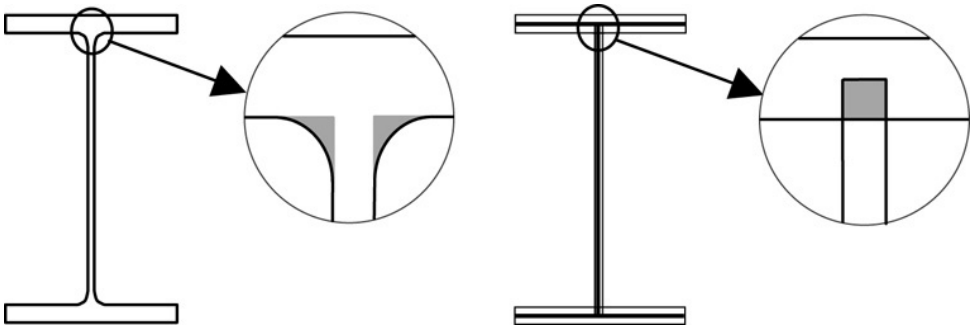

FIGURE 3.4: Real section (left hand) and model with shell elements (right hand) [6].

Compared to the real section the element model will have different cross-sectional properties, particularly significant for the torsional constant which can up to 30 % [6]. In order to model the beam's cross section in a more proper manner, elements in the web near the intersection of the web and flanges were assigned a larger thickness than the rest of the web. In his study, Bonkerud solved this by assigning the external three elements in the web at the intersection between the web and flanges an increased thickness. He proposed that a doubling of the element thickness was sufficient [3]. This would add extra material to the flanges, but of such a small amount that the effect was assumed to be negligible. Thus, the same procedure for modelling of the beam's cross section was contucted in this study.

Mesh - Element Size and Mesh

The element size is important for the element models accuracy, which will improve with refined mesh. A refined mesh also lowers the appearance of hourglass modes in the model. However, the gain in accuracy comes with the cost of severely increased computational time [4]. In his study, Bonkerud investigated the effect of redused element size on his model's accuracy. He concluded that a element size of 10 mm or less provided accurate results, hence for further studies he chose a mesh size of 7 mm [3]. In this thesis, an element size of 7 mm was also prefered. The model was meshed as shown in figure 3.5

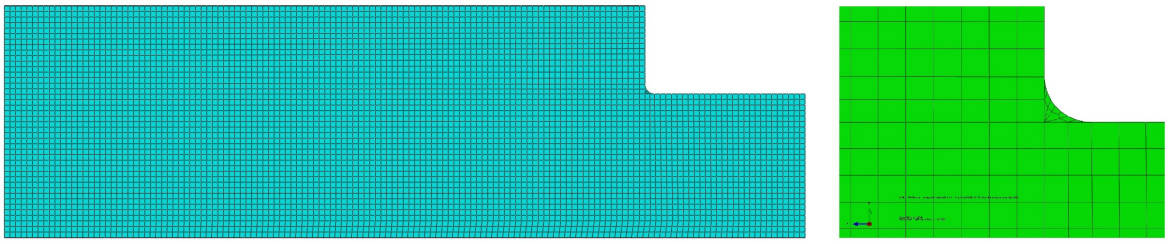

FIGURE 3.5: Coped beam meshed in 7 mm sized elements.

Type of Analysis

The model was analyzed in a static manner through the general static analysis step with non-linear effects taken into account, as the long-term response of the coped beam was of interest. A static analysis was also prefered to a dynamic analysis in that it is much less computationally costly.

Contact

The contact between the underside of the flange and the rigid block was modeled with a master/slave formulation, where the nodes of the slave surface cannot penetrate the master surface segments. The nodes of master surface on the other hand are free to penetrate the slave surface segments [4]. In the model, the rigid block was chosed to act as the master surface, while the lower flange's underside was chosed to act as the slave surface.

Imperfections

All structures and components are postponed to geometrical imperfections. It is therefor necessary to implement such in the numerical model. In ABAQUS/CAE there are several methods for implementation of imperfections. In this study, only two methods are considered. The first one is to use buckling shapes from the linear buckling analysis. The buckling shape corresponding to the lowest eigenvalue was choosen and assigned a suitable scaling factor. The other way was to manually implement sinus half waves by changing the node coordinates in the input file with use of the formula

$$w = w_0 \cos\left(\frac{n\pi y}{h}\right) \sin\left(\frac{m\pi z}{L}\right) \tag{3.1}$$

where w_0 is the amplitude, L the beam length and h the beam hight. m denotes the number of sinus half waves in the longitudinal direction, while n is the number of sinus half waves in the vertical direction, in this instance always equal to 1.
To determine which type of imperfection to implement in the model, the unreinforced coped beams capacity was evaluated through a nonlinear analysis. The objective was to find the most conservative type, providing the lowest capacity. A selection of cope details was selected and evaluated for the following imperfections

1. **Buckle** - Buckled shape corresponding to lowest Eigenvalue from Linear elastic buckling analysis
2. **Sinus 1** - 1 sinus half wave in longitudinal direction, 1 sinus half wave in vertical direction
3. **Sinus 2** - 2 sinus half wave in longitudinal direction, 1 sinus half wave in vertical direction
4. **Sinus 3** - 3 sinus half wave in longitudinal direction, 1 sinus half wave in vertical direction

The element model developed in chapter 3 was used for the analyses. The beam was restrained from translation in every direction at one end and loaded by moving a rigid block in the vertical direction at the other end. The coped region was assigned dimensions as listed in table 3.1. The model's setup is shown in figure 3.6.

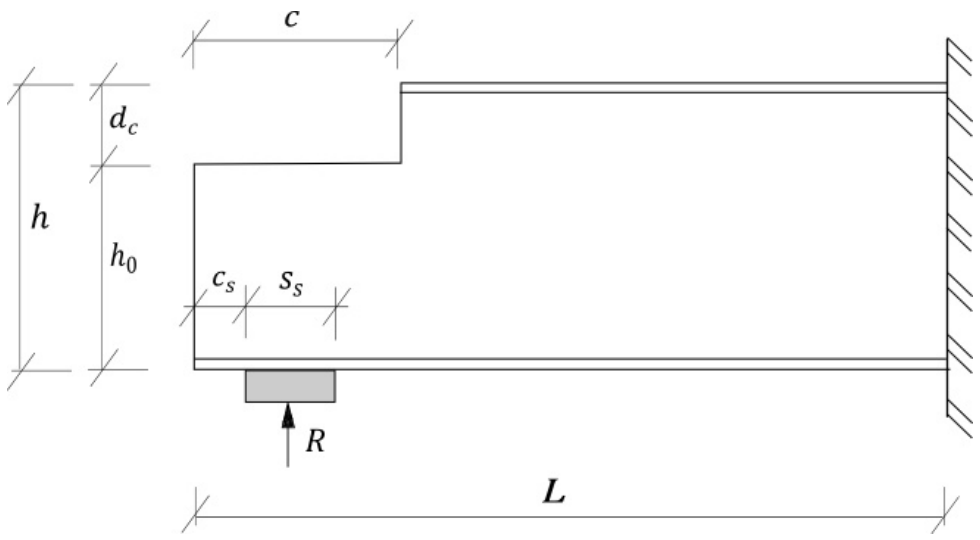

FIGURE 3.6: Loaded coped beam.

The element size was set to 7 mm and arranged in the mesh shown in figure 3.5. All of the imperfections were scaled with a factor of 0.3.
The results from the nonlinear analyses were presented in terms of the beam's maximum capacity for the different cope details, represented by the cope ratio (c/h_0) as shown in figure 3.7 and table 3.3.

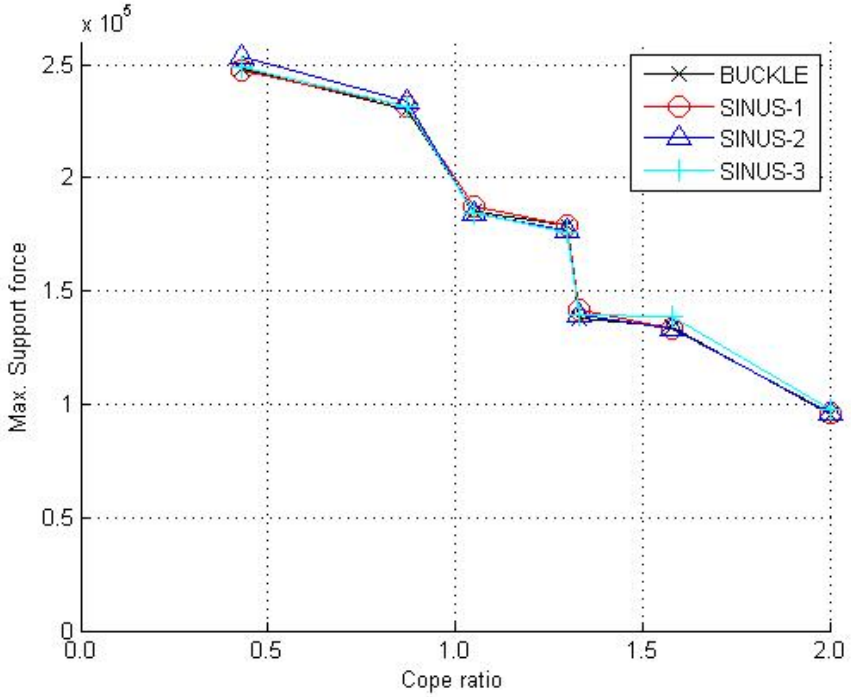

FIGURE 3.7: Max. Support force for different types of imperfections.

Cope length c	Cope depth d_c [mm]	Cope ratio c/h_0	BUCKLE R_{max} [N]	SINUS-1 R_{max} [N]	SINUS-2 R_{max} [N]	SINUS-3 R_{max} [N]
100	70	0.43	248 063	247 522	253 366	248 944
200	70	0.87	230 344	231 628	233 429	231 792
200	110	1.05	185 086	187 325	184 651	184 094
300	70	1.30	179 129	178 668	176 621	176 045
200	150	1.33	138 337	141 737	139 598	139 153
300	110	1.58	134 210	133 785	133 178	138 607
300	150	2.00	95 636	96 548	96 200	97 618

TABLE 3.3: Max. Support force for different types of imperfections.

Observe that the difference in maximum support force was quite small for all of the tested cope details regarding type of imperfection implemented in the element model. The difference between the lowest and highest value varies from 2 % for cope ratio $c/d_c = 2.00$ to 4 % for cope ratio $c/d_c = 1.58$. Which type of imperfection to choose was not obvious, as all of them for a certain cope detail came up with the lowest maximum capacity. It was also not easy to spot a pattern regarding the different cope dimensions. For the beams with cope length of 300 mm, it was expected that SINUS-3 would provide the critical value, as the amplitude of one of the sinus waves was located near the coped corner where the stress concentrations are the largest. This is the case for cope ratio of 1.30, but not for the other details with cope length 300 mm. Figure 3.8 shows the lateral deformed pattern for this cope detail at the point where it has reached it's maximum capacity, for each type of imperfection.

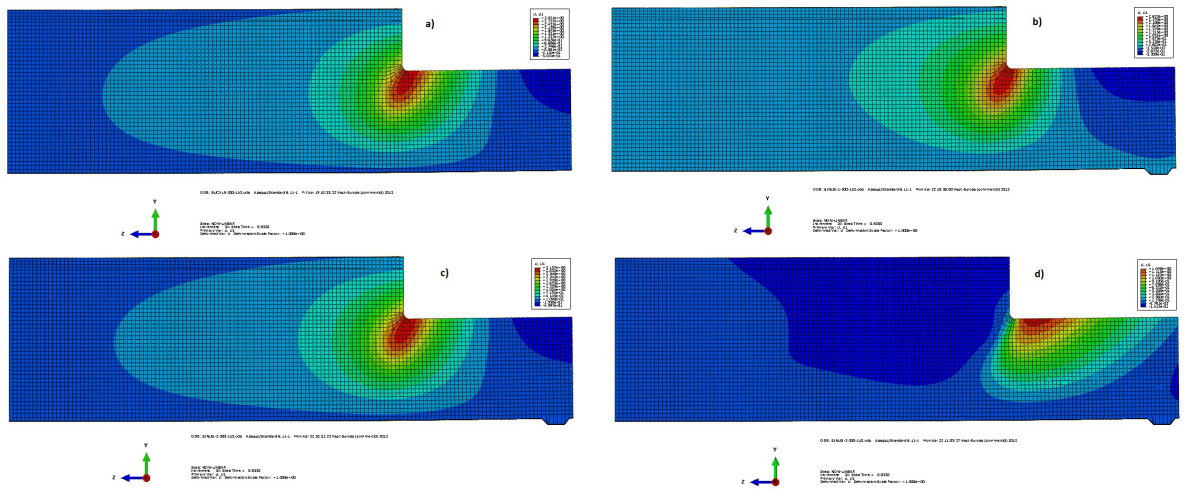

FIGURE 3.8: Lateral displacement U1 at max.support force, where a) BUCKLE, b) SINUS-1, c) SINUS-2 and d) SINUS-3

As seen from the figure, the largest lateral displacements were located at the coped corner. However, with three sinus waves in the longitudinal direction (SINUS-3) the deformed geometry was somewhat different. Here the largest lateral displacement did not occur at the coped corner, but close to it.

The type BUCKLE provided the critical value most often and was a simpler and more reliable way of implementing imperfections in the model, as changing the node coordinates manually in the input file was both time consuming and a possible sorce of error. Thus, chose BUCKLE as the default.

Validation of the Numerical Model

In order to determine the developed numerical model's accuracy, the results from the nonlinear analyses were compared to a similar finite element model. The model chosen was the one developed by Bonkerud [3]. For comparison, this model was well suited as it had many of the same features. The beam's length was however shorter, and had slightly different material properties and cross sectional dimensions. Thus, this model should provide higher capacities, however it was expected that this model should be more resistant to the applied forces.

The unstiffened coped beam was tested in a nonlinear manner, both for the uncoped beam and the coped beams. Imperfections were implemented in both models as the buckling shape from a linear elastic buckling analysis corresponding to the lowest Eigenvalue and scaled with a factor of 0.3. The beams capacity was measured in terms of the maximum applied force caused by contact with the rigid block and the beam.

Table 3.4 show the comparison of max. support force for the element model to the corresponding results from Bonkerud's study, defined respectivily $F_{max,BUCKLE}$ and $F_{max,BONKERUD}$.

c	d_c [mm]	c/h_0	$F_{max,BUCKLE}$ [N]	$F_{max,BONKERUD}$ [N]	$\left(\frac{F_{max,BUCKLE}}{F_{max,BONKERUD}}\right)$
0	0	0.00	249 356	288 270	0.87
100	70	0.43	248 050	275 490	0.90
100	110	0.53	248 274	261 670	0.95
100	150	0.67	213 951	218 830	0.98
200	70	0.87	230 208	230 480	1.00
200	110	1.05	185 423	186 380	0.99
300	70	1.30	138 686	141 100	0.98
200	150	1.33	179 202	172 870	1.04
300	110	1.58	134 393	135 330	0.99
300	150	2.00	95 878	98 150	0.98

TABLE 3.4: FEA results of max. support force.

Observe that the two models solutions corresponded well with each other. Similar to Bonkerud's model, the coped beam failed for all cope dimensions at the coped section, despite its increased length. As expected, for nearly all cope details Bonkeruds model reached a slightly higher maximum support force.

Chapter 4

Numerical Analysis: Coped Beam with End Restrictions

4.1 Effect of Doubling the Flanges Thickness at the Fixed End

Bonkerud developed an element model for his master thesis [3] which was made to simulate a simply supported IPE300 beam with length 1200 mm, loaded with a concentrated force at the midspan. But, to reduce the model's size and computational time only half the beam was modeled. Considering the beam's symmetry about the midspan, the deflection pattern would be the same. Hence, the beam was modeled with a length of 600 mm, with the end restrained from lateral movement in all three directions.
The model was compared to a series of lab experiments together with results from a selection of hand calculation methods, and from these comparisons it was concluded that the element model gave valid results. However, there were some shortcomings to this model. By going through the results for each simulation in terms of the force-displacement plots, distribution of stresses and the deformation pattern, a change of behaviour was spotted when the web thickness was increased to one and a half or two times the original value, respectivily 10.35 mm and 13.8 mm. Figures 4.1 show the stress distribution for an uncoped beam with web thickness of 13.8 mm for an uncoped beam and a coped beam with cope length-to-reduced beam hight ratio of 0.53.

What happened was that the increased web thickness raised the webs buckling capacity, so that a larger rection force was required to make the web buckle. For the uncoped beam and for the coped beams with small cope dimensions, the increased buckling capacity was large enough that yielding occured at the beam's fixed end as a consequence of the increased bending stresses, followed by buckling of the compressional flange. Thus, it was desired to change the model to make it coincide more with the models with lower web thicknesses. Two improvements were proposed. The first included reduction of the bending stresses at the fixed end by lowering

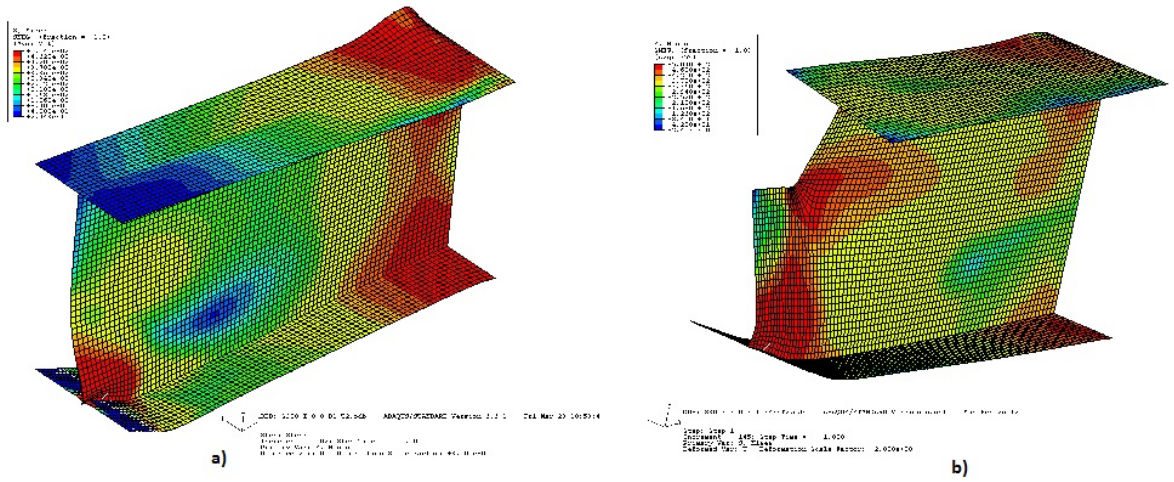

FIGURE 4.1: Stress distribution for a) uncoped beam and b) coped bema 100-110 with web thickness of 13.8 mm.

the applied loads level arm. For that purpose the nodes accross the upper and lower flange was restrained against movement in the vertical direction, reducing the moment to zero at this point.

Considering the regular expression for bending stresses, $\sigma = \frac{M}{I}y$, an increase of the flanges cross-sectional area would increase the beams moment capacity at the fixed end. For that purpose, the thickness of the upper and lower flange was doubled over a section 20 elements spanning from the fixed end. A few models were analyzed for each case, and it was concluded that the second method gave the best results. Thus, all of the cope details for the models with web thicknesses of 10.35 mm and 13.8 mm where analyzed.

4.1.1 Results and Discussion

In figure 4.2 and in table 4.1 the capacities for the uncoped and coped beams with doubled flange thicknesses at the fixed end were compared to the original solutions presented by Bonkerud. The original model's capacity with web thickness one-and a half and two times the original value, denotes respectivily $R_{T15,0}$ and $R_{T2,0}$, while the beam's capacity with doubled flange thickness at the fixed end denotes respectivily $R_{T15,TF2}$ and $R_{T2,TF2}$.

See that the max. capacity of the coped beams stays nearly unaltered for the increased flange thickness. The max. gain in strength is 6% for the uncoped beam with doubled web-thickness, while for most of the coped beams the gain in strength is negligible. Thus, the effect of doubling the flanges thickness at the fixed end seems insignificant. However, considerig the stress distribution over the deformed beams, the beams behaviour are clearly improved. As mentioned earlier, the uncoped beam and the coped beam with cope lenght-to-reduced web hight of 0.53

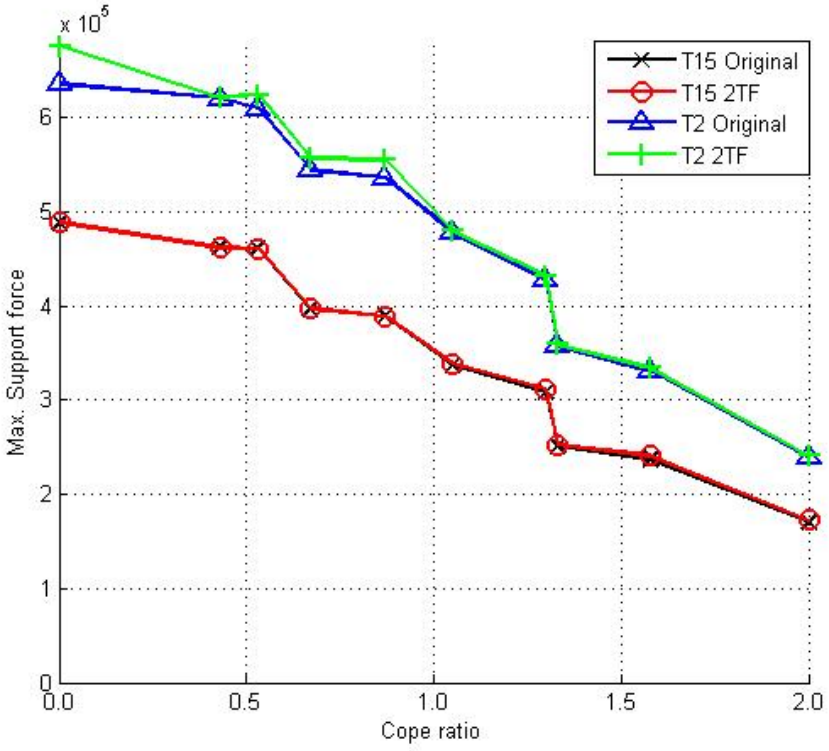

FIGURE 4.2: Max. support force vs cope ratio.

Cope ratio	Max. support force					
	Web thickness $1.5t_w$			Web thickness $2.0t_w$		
c/h_0	$R_{T15,0}$ [N]	$R_{T15,TF2}$ [N]	$\frac{R_{T15,TF2}}{R_{T15,0}}$	$R_{T2,0}$ [N]	$R_{T2,TF2}$ [N]	$\frac{R_{T2,TF2}}{R_{T2,0}}$
0.00	487 268	488 936	1.00	635 318	676 110	1.06
0.43	461 794	461 556	1.00	620 673	620 847	1.00
0.53	460 266	461 027	1.00	609 301	623 762	1.02
0.67	395 928	396 928	1.00	544 262	556 719	1.02
0.87	388 566	388 713	1.00	535 785	554 783	1.04
1.05	337 139	338 401	1.00	477 723	479 666	1.00
1.30	251 282	252 647	1.00	357 707	358 850	1.00
1.33	308 432	311 478	1.01	427 096	431 695	1.01
1.58	237 431	241 224	1.02	330 958	333 836	1.01
2.00	170 848	172 675	1.01	238 973	240 679	1.01

TABLE 4.1: Max. support force for beam with doble flange thickness at fixed end.

experienced buckling of the flanges at the fixed end. With the increased flange thickness however, the beams moment capacity were increased to prevent such behaviour. Figure 4.3 show the stress distribution for the improved models for the uncoped beam and the coped beam. See that for the uncoped beam the increased moment capacity at the fixed end prevents formation of large stresses there, hence the beam is forced to fail in local web buckling at the loaded position.

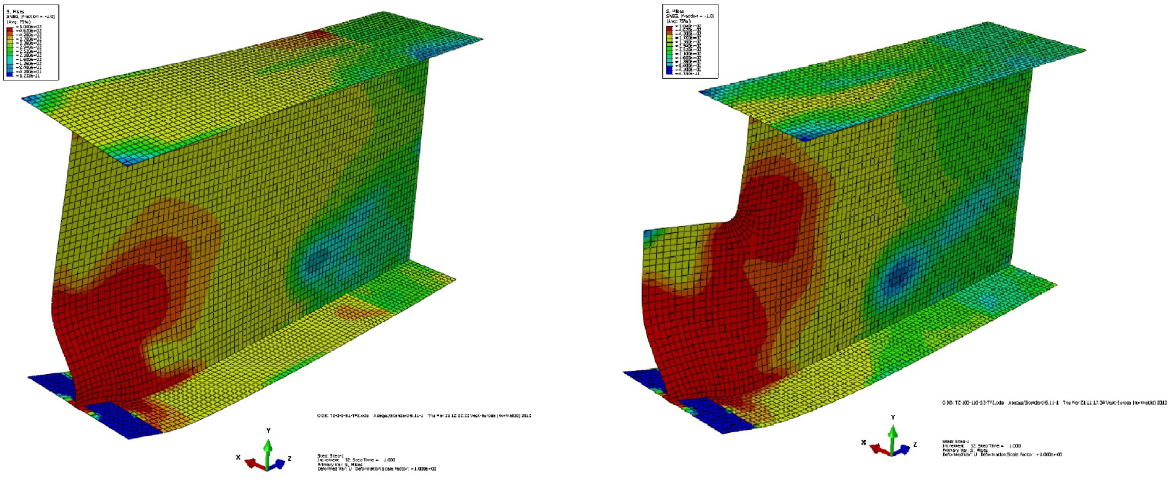

FIGURE 4.3: Stress distribution for a) Uncoped beam and b) Coped beam 100-110 with web thickness of 13.8 mm.

4.2 Effect of Restraining the Web at the Coped End

Bonkerud modeled the beam as simply supported with the web free to move or rotate in every direction over the beams length. However, it is customary to restrain the end of the beam in some way, either with a welded-on endplate or with a bolted connection. Therefor, the models strength and behaviour were investigated when doing so. At first, the web at the loaded end was restrained from moving sideways. This was done for all of the cope details. Secondly, coped end was also restrained from rotation about the vertical axis. The purpose of this study was to see how the boundary conditions were affecting the beams strength and behaviour for the different cope details. The restrainment was meant to reduce the webs buckling length in order to increase the buckling capacity. Restraining the web from rotating as well was belived to increase the buckling strength even more. The assumption was that for shorter copes, where the buckled shape reach the web's free end, the coped beam's strength would be increased. For longer copes however, the buckle originating from the stress concentration at the coped corner would not reach the web's free end and would not be affected much by the restrainment.
The model with web thickness of 6.9 mm was choosen and for each of the models, coped and uncoped the web at the loaded end was restrained from lateral translation ($U1 = 0$). The web

was also restrained from rotating about the vertical axis ($U1 = R2 = 0$). The results were compared with the results if the unrestrained beams.

4.2.1 Results and Discussion

Figure 4.4 and table 4.2 shows the results in terms of maximum reaction force relative to cope ratio obtained for all cope dimensions, both restrained and unrestrained. $R_{max,0}$ denotes the capacity of the unrestrained beam, while $R_{max,U1}$ and $R_{max,U1,R2}$ denotes the restrained beam's capacity, respectivily for the end prevented from moving sideways and rotating about its vertical axis.

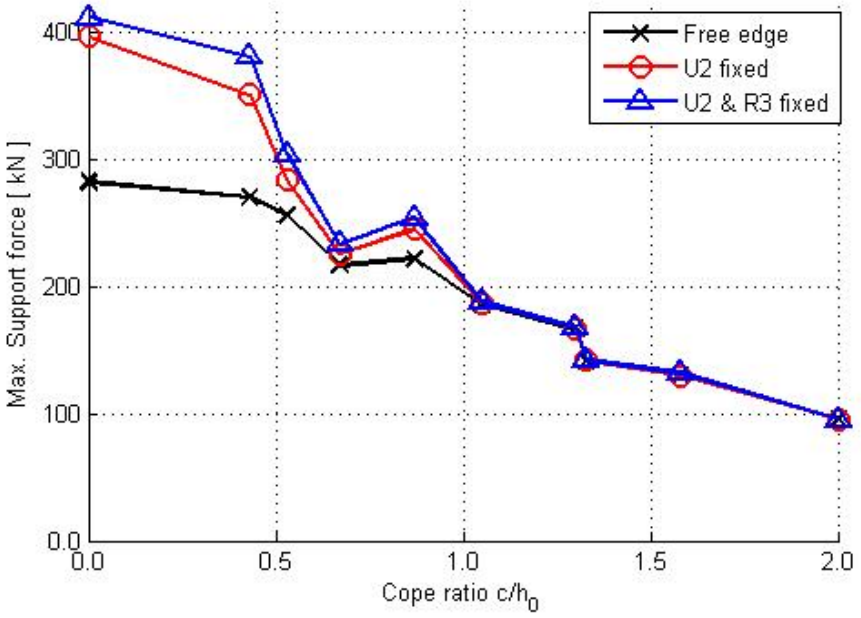

FIGURE 4.4: Max. reaction force vs cope ratio.

See from table 4.2 that the gain in strength is largest for small cope ratios. For cope ratio $c/h_0 = 0.43$ the capacity was increased by 30 % when restraining the web from lateral translation ($U1 = 0$) and by 41 % when additionally restrained from rotating about the vertical axis ($U1 = R2 = 0$). For higher cope ratios the gain in capacity falls quickly and when exceeding 1 the ratio between the restrained and unrestrained coped beam's capacity reduces to approximately 1.00, thus the gain in capacity for such cope dimensions seems negligible. This strongly implies the previous proposed statement that for beams with copes of a certain length restraining the coped end will not affect the capacity in any particular manner. Thus, as seen from figure 4.4 for cope lengths of 200 mm or higher ($c \leq 200$) the distance from the coped corner to the restrained end is large enough that the buckled shape is not affected by the restraining. This

Cope ratio	Max. reaction force Restrained DOF's			Deviation	
c/h_0	Unrestrained [N]	Restrained U1 [N]	Restrained U1 & R2 [N]	$\frac{R_{max,U1}}{R_{max,0}}$	$\frac{R_{max,U1,R2}}{R_{max,0}}$
0.00	281 883				
0.43	269 579	350 474	380 028	1.30	1.41
0.53	255 896	283 214	303 346	1.11	1.19
0.67	216 355	225 635	233 199	1.04	1.08
0.87	221 676	244 381	253 715	1.10	1.14
1.05	185 594	186 782	187 743	1.01	1.01
1.30	166 401	166 796	167 204	1.00	1.00
1.33	141 097	141 492	141 562	1.00	1.00
1.58	129 453	129 912	131 968	1.00	1.02
2.00	95 314	95 352	95 401	1.00	1.00

TABLE 4.2: Max. support force for restrained coped end.

is shown schematically in figures 4.5 and 4.6, where the lateral displacement $U1$ are compared for the restrained and unrestrained beams with cope lenghts of respectivily 100 mm and 200 mm. See that for the shorter cope length the buckling pattern changes when restraining the end, while it stays nearly unaltered for the longer cope length.

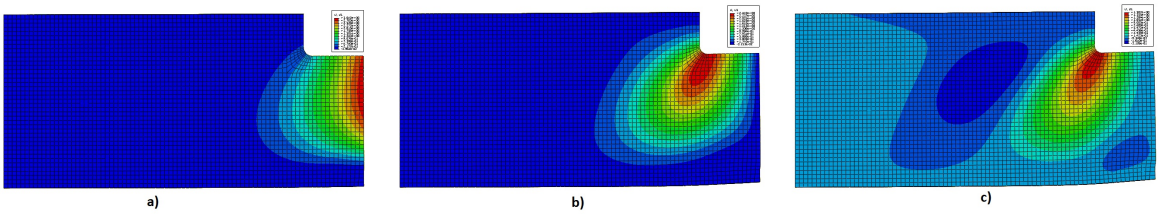

FIGURE 4.5: Lateral deflection pattern for a) Unrestrained, b) Restrained from lateral translation c) Restrained from lateral translation and rotation.

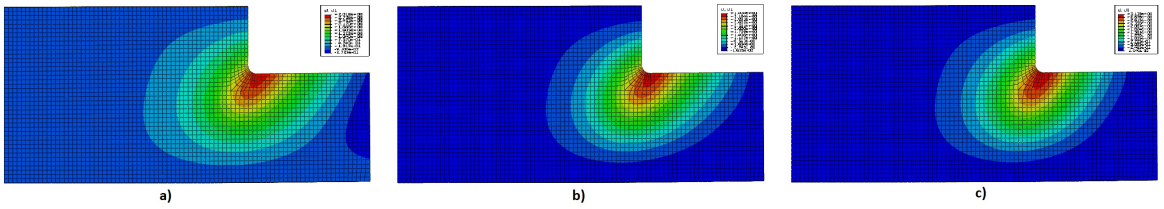

FIGURE 4.6: Lateral deflection pattern for a) Unrestrained, b) Restrained from lateral translation c) Restrained from lateral translation and rotation.

However, even though the effect of end restriction of the coped beams becomes more and more insignificant with increasing cope length, it will be more precise to consider the effect in terms of cope ratio, which takes into account the cope's depth as well. As seen from figure 4.4, the gain

in strength is seen to drop significantly with increasing cope depth. While the gain in capacity for beams with cope length 100 mm and cope depth 70 mm were as high as 41 %, it drops to a maximum of 19 % for a cope depth of 110 mm and reduces further to 8 % for a cope depth of 150 mm. The test specimen with cope ratio 0.87 experiences a gain in strength of 14 % for the most restrained case, even though the cope length is 200mm. Thus, the effect of restraining the reduced section at the coped end with an endplate seems negligible for cope ratios higher than or equal to 1 ($c/h_0 \geq 1$).

4.3 Summary

From the previous study of the elementmodel by Bonkerud certain parameters have been altered in order to change the coped beam's strength and behaviour. The topics investigated were:

1. Doubling of the flanges thickness at the fixed end in an attempt to avoid yielding and eventually failure at this end.
2. Restraining the web at the loaded end from lateral translation and rotation about the vertical axis

For the first topic the attempt was successfull. By doubling the thickness of both flanges over a length of 20 elements (elementsize = 7 mm), buckling of the beam's top flange was prevented. Also, the beam's increased cross-section prevented large stresses to form at the fixed end, instead forcing failure to occur at the loaded end only. The behaviour of the modified model for all cope geometries were made similar to that of the models with lesser flange thicknesses, as desired. A slightly increase of the capacity for the test specimens were also obtained, but in most cases the improved strength were negligible.

The second topic showed that the effect on the beam's strength when restraining it's web at the free end was less and less significant with increasing cope length (c). Also, the gain in capacity was reduced with a higher cope depth (d_c). The beam's cope ratios includes both the cope length and depth, thus the beams capacities were plotted against their respective cope ratios, see figure 4.4. The effect of restraining the free end seemed negligible for cope ratio exceeding 1 or equal to 1 ($c/h_0 \geq 1$), while for cope ratios lesser than 1 ($c/h_0 < 1$) the gain in strength increased with lowering cope ratio. For the smallest cope dimension tested ($c/h_0 = 0.43$), the max. capacity increased with 41 % when restrained from both lateral translation and rotation. However, it is practically impossible to fully restrain the beams end. In real life the restrained end will be able to move slightly, as the endplate or bolted conncetion will not act completely rigid and the end restrainment will be subjected to straining. Hence, a more realistic approach

would be to model the restraining of the free end as either an endplate welded to the coped beam, or restraining the other nodes of the free end with a series of springs given appropriate stiffnesses. However, the results obtained in this thesis provides some insight of how the coped beams behave when subjected to such restrainment, though the obtained solutions might not be that conservative.

Chapter 5

Numerical Analysis: Reinforced Coped Beams

5.1 General

Coping of the beam can lower it's capacity significantly, due to local web buckling and to the beam's reduced cross sectional properties at the coped section. A way to increase the coped beam's capacity is to reinforce the coped end with stiffeners. The stiffened coped beam's behaviour has been subject to several studies, but with varying results. In the study conducted by Cheng et.al (1984) [7] design recommendations were provided for three stiffener details, referring to figure 2.4. They stated that yielding would control the coped section's capacity for horizontal stiffeners extension lengths not shorter than the copes depth ($e_x d_c$). This however contradicts with the conclusions drawn from a later study conducted by Yam et al. (2007) [2]. Here the reinforced coped beams failed due to instability of the coped section instead of material yielding, resulting in a design reaction force significantly lower than the reaction forces corresponding to the yield moment capacity and shear yielding resistance of the web at the coped section.
A more comprehensive experimental study was conducted by Yam et al. (2011) [8] and followed by a numerical study conducted by Yam and Chung (2012) [9]. For both studies, the strength and behaviour of steel I-beams with varying cope dimensions were investigated. The coped beams were strengthened with end plates and stiffeners, as shown in figure 5.1.

In the experimental study 10 full scale specimens were tested. They showed that the reinforced coped beam specimens mainly failed by yielding of the full beam section near the loading position, followed by either a flange local buckling or rigid body movement of the longitudinal stiffeners due to web crippling [8]. Similar behaviour was observed in the numerical study. For all cases examined, non of the reinforced coped beams experienced flexural failure in the coped

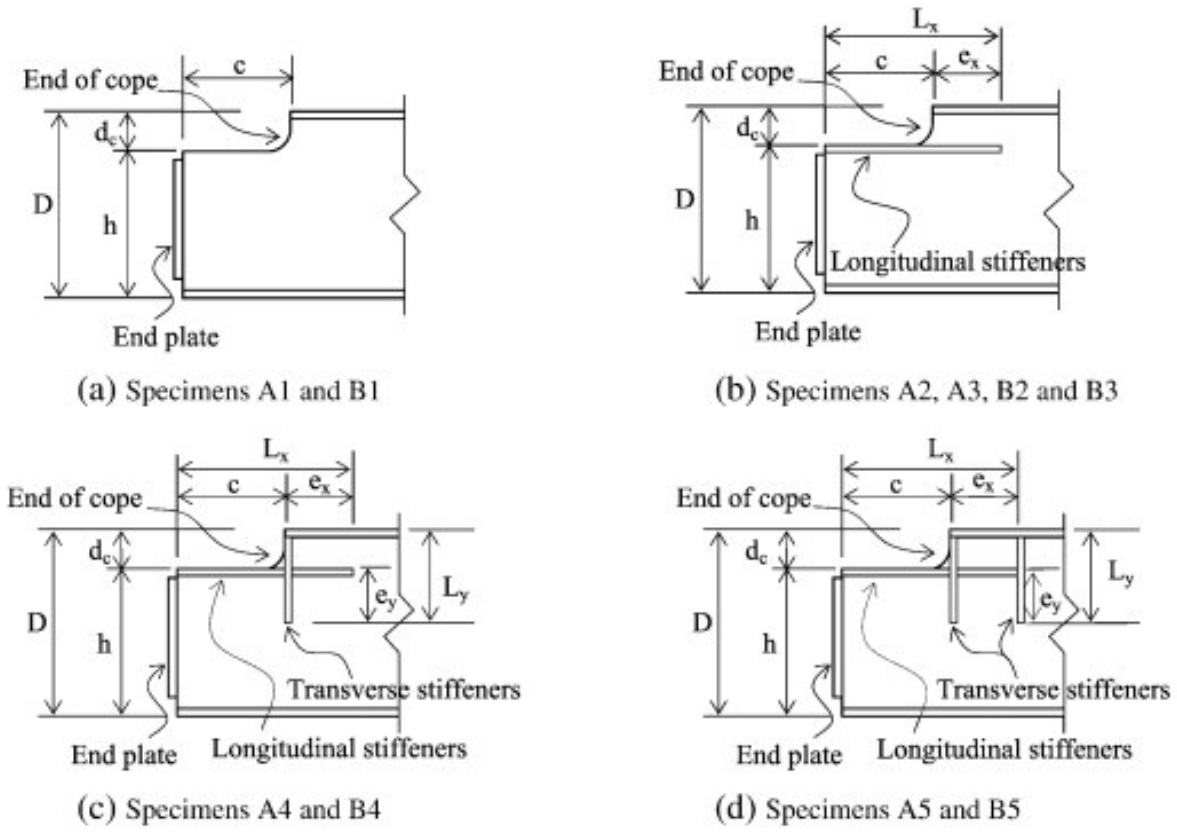

FIGURE 5.1: Reinforcement details.

region. Instead failure due to flexural yielding of the full beam section near the loaded position and shear yielding in the coped section were observed. The final failure mode included either rigid body movement of the longitudinal stiffeners due to web crippling or flange local buckling near the loaded position.

It was of interest to further investigate the strength and behaviour of coped beam's reinforced with stiffeners. Thus, a numerical study was conducted with use of the finite element analysis software ABAQUS/CAE [25]. The model developed and validated in chapter 3 was chosen, representing an I-steel beam, 1000 mm long, with one end restrained from translation in every direction and the other end simply supported on a rigid block. This block was also used to load the beam at a distance of 970 mm from the beams fixed end. The coped beams were reinforced with either longitudinal stiffeners only, or in combination transverse stiffeners. The beams cross-sectional dimensions were modelled similar to the $IPE300$-profile, which is categorized in cross sectional class 1 [22].

The reinforced coped beams were tested both in linear elastic buckling analyses and in nonlinear analyses. In the nonlinear analysis an initial imperfection was introduced to the beam in order to allow for buckling of the web near the coped region. The imperfection was obtained from the buckled shape corresponding to the beam's lowest eigenmode and assigned a scaling factor of

Cope Detail	c [mm]	d_c [mm]	Cope Ratio c/h_0
A	100	50	0.40
B	150	70	0.65
C	200	110	1.05

TABLE 5.1: Dimensions of coped regions.

c	d_c [mm]	$R_{M,pl}$ [kN]	$R_{V,pl\&el}$ [kN]	$R_{M,pl,red}$ [kN]	$R_{V,pl\&el,red}$ [kN]	$R_{M,el}$ [kN]	$R_{M,el,red}$ [kN]
100	50	229.8	436.6	1104.1	363.8	203.8	469.6
150	70	229.8	436.6	546.6	334.7	203.8	238.6
200	110	229.8	436.6	264.4	276.5	203.8	122.1

TABLE 5.2: Results elastic and plastic moment and shear capacity of the full and reduced beam section.

1.0, assumed to be appropriate considering the distortions the web experience during welding of the stiffeners. The beams were loaded to failure, where the force displacement curve is seen to drop. If not, the beams max. capacity was evaluated at a vertical displacement of 35 mm. Choose three cope geometries for testing, namely cope details A, B and C, with dimensions listed in table 5.1. Refering to figure 1.1, coping of the beam's end is usefull in connecting secondary beams to the main girder. Hence, the copes dimensions were chosen to provide enough clearance to a hypothetical adjacent main girder.

The reinforcements main objective is to prevent failure in local web buckling, at any loaction of the beam. Thus, the stiffeners have to be arranged such that the beam eventually fails in flexural yielding or shear yielding of the full beam section. Further increase of the beam's strength is not possible and would demand additionally reinforcement along the beam's length, which is not considered in this study. Hence, the results from the finite element analyses are compared to the representative coped beams moment and shear capacities listed in table 5.2. Also, rigid body movement and bending and torsional twisting of the stiffeners should be prevented.

5.2 Effects of Longitudinal Stiffeners

5.2.1 General

Use of longitudinal stiffeners are provided in order to improve the coped beam's strength. By forcing the coped beam to fail in flexural yielding of the full beam section the increased strength can be significant.

Several design recommendations have been proposed for use of stiffeners. Yam et al. (2007) recommended an extension length of both the horizontal and vertical stiffeners of min. d_c for cope length-to-beam hight ratios lesser than 1 ($c/h < 1$), while for $c/h > 1$ the extension

length should be min. $2d_c$ [2]. In the study by Yam et al. (2012) use of only longitudinal stiffeners were recommended for coped beams with web depth-to-thickness ratios (d/t_w) equal to or lesser than 52.7, cope depth-to-beam depth ratios (d_c/D) equal to or lesser than 0.3 and cope length-to-beam depth ratios (c/h) equal to or lesser than 0.75 [9], with stiffeners lengths as follows

$$L_x = c + e_x \qquad \text{where} \qquad e_x = 2d_c \tag{5.1}$$

However, as the stiffeners experienced sideways rigid body movement due to web crippling it is assumed that the provided stiffeners lengths were not long enough to provide properly anchorage of the stiffeners. Thus, the coped beams were tested for reinforcement in the longitudinal direction with increasing stiffener lenght (L_x).
The stiffeners material properties were the same as the beam, as seen in tableMaterialProperties. The stiffener lengths (L_x) equals the copes length (c) plus an extension length (e_x), hence $L_x = c + e_x$. The longitudinal reinforced solution is shown in figure 5.2.

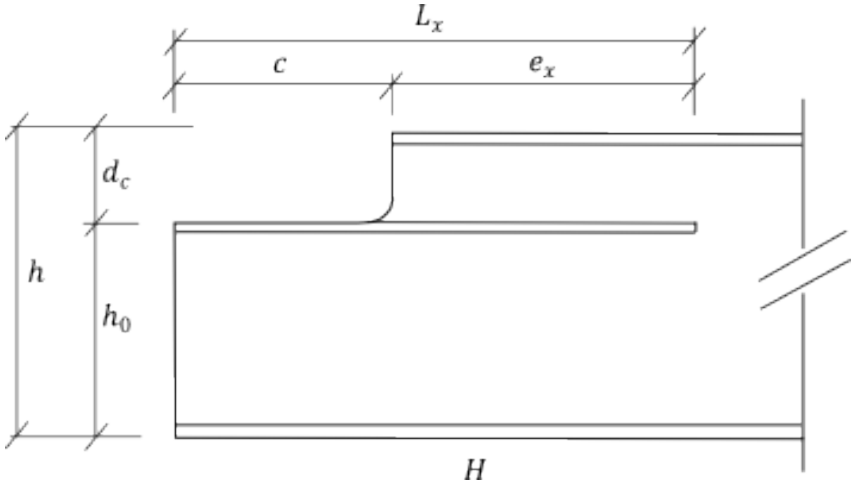

FIGURE 5.2: Reinforcement detail for coped beam with horizontal stiffener.

The stiffener dimensions tested are listed in table 5.3. The stiffeners bending- and torsional stiffness should be large enough to prevent the stiffeners to deform together with the beam [1]. Thus, had to provide adequate dimensions for stiffener width (b_x) and thickness (t_x). Intially those were set to respectivily 7.1 mm and 75 mm, but were further increased to see the effect on the coped beams strength. The dimensions tested in the parametric study are listed in table 5.4.

The FE model developed in chapter 3 was used for testing. The stiffeners were modeled with use of 4-noded shell elements with reduced integration ($S4R$-elements) and attached to the web with a TIE-constraint. The reinforced model is shown schematicaly in figure 5.3, where the stiffeners are placed at the top of the coped section. Normally there would be a couple of millimeters of clearance to allow for welding, but in order to simplify the modelling the stiffeners were placed

Stiffener Length L_x	Cope Dimension (c x d_c) 100 x 50 e_x [mm]	L_x/c	150 x 70 e_x [mm]	L_x/c	200 x 110 e_x [mm]	L_x/c
0	0	0	0	0	0	0
200	100	2	50	1.33	0	0.75
300	200	3	150	2	100	1.50
400	300	4	250	2.67	200	2
600	500	6	450	4	400	3
750	650	7.50	600	5	550	3.75
800	700	8	650	5.33	600	4
1000	900	10	850	6.67	800	5

TABLE 5.3: Dimensions and cope details of specimens.

Model name	Stiffener width $b_x[mm]$	Stiffener thickness t_x [mm]
MODEL-1	75	7.1
MODEL-2	75	10.7
MODEL-3	150	7.1
MODEL-4	150	10.7

TABLE 5.4: Longitudinal stiffener dimensions.

as specified. The model's behaviour was tested in both linear elastic buckling analyses and nonlinear analyses.

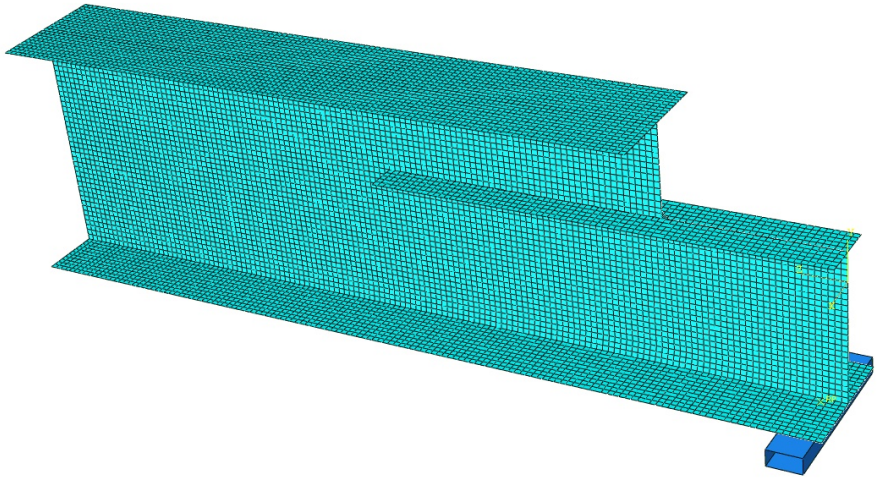

FIGURE 5.3: Elementmodel reinforced coped beam.

5.2.2 Results

Linear Buckling Analysis

L_x [mm]	MODEL-1	MODEL-2	MODEL-3	MODEL-4
		Cope detail A (100x50)		
0	629 233	629 233	629 233	629 233
200	788 186	803 701	795 323	808 242
300	828 054	844 204	840 683	850 458
400	845 385	857 050	853 960	863 653
600	846 756	868 481	859 616	878 751
800	848 402	876 619	865 984	895 791
1000	853 051	891 546	884 337	941 142
		Cope detail B (150x70)		
0	510 790	510 790	510 790	510 790
200	621 085	639 860	629 311	643 958
300	703 128	739 808	719 546	750 584
400	736 299	778 941	757 630	795 278
600	763 375	809 697	792 858	834 695
800	773 639	823 556	815 653	860 659
1000	783 368	840 146	862 889	919 815
		Cope detail C (200x110)		
0	348 744	348 744	348 744	348 744
200	421 610	424 581	421 719	424 481
300	520 175	590 162	545 942	621 120
400	548 348	618 941	572 278	655 348
600	606 092	677 414	637 529	721 503
800	630 028	706 532	681 363	763 896
1000	640 454	726 233	734 771	823 001

TABLE 5.5: Critical buckling load for longitudinal reinforced coped beams.

The reinforced coped beam's strength and behaviour was investigated in linear buckling analyses in order to provide the beams critical buckling load (R_{cr}), in ABAQUS given by the critical Eigenmode from solution of the eigenvalueproblem [4]. The corresponding buckled shape was further implemented in the nonlinear analyses as an initial imperfection assigned a scaling factor of 1.0.
The obtained critical buckling loads (R_{cr}) are presented in table 5.5 and plotted relative to longitudinal stiffener length (L_x) in figure 5.4.

See that the coped beam's resistance to elastic buckling increases with increased reinforcement length, with the largest gain in strength obtained when the unreinforced beam was provide a stiffener with lenght of 400 mm. However, for stiffener lengths exceeding 400 mm, the gain in strength was insignificant. For cope detail A the buckling capacity was increased with up to 37 % when reinforced with such stiffeners, but for reinforcement lengths up to 1000 mm the capacity was increased further with only 9 %. For cope detail B the capacity increased with respectivily 56 % and 16 %, while for cope detail C the capacity increased with 88 % and 26 %.

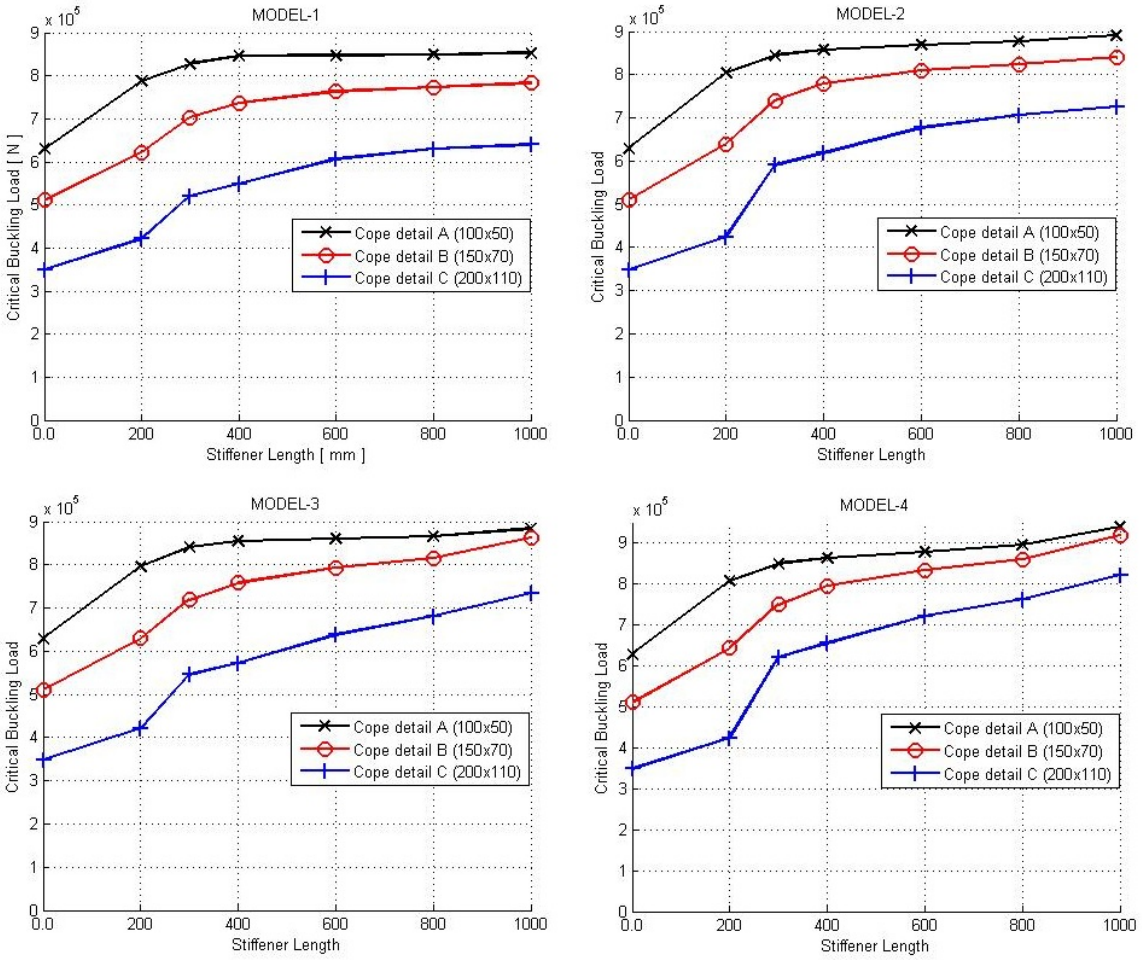

FIGURE 5.4: Critical buckling load for longitudinal reinforced coped beams.

Considering figure **??**, the buckled shape of cope detail B varied little with increasing stiffener length. For all specimens, the beam buckled outwards at the top end of the cope and remained undistorted at its fixed end.

Thus, the effect of extending the longitudinal stiffeners on the coped beam's capacity seems insignificant, even when increasing the stiffeners cross sectional properties. The behaviour were further investigated in nonlinear analyses.

Nonlinear Analysis

The coped beam's strength and behaviour was analyzed in nonlinear analyses when reinforced with longitudinal stiffeners. The results are presented in table 5.6 in terms of max. applied force (R_{max}) at the contact surface between the rigid block and the lower flange. As the effect of increasing stiffener length was of interest, the results were plotted as the ratio with max. reaction force for stiffener length of 1000 mm ($R_{max}/R_{max,1000}$), relative to stiffener length (L_x), as seen in figure 5.5. The beam experienced the following failure modes (FM)

Longitudinal stiffener H MODEL-1									
	Cope detail A (100x50)			Cope detail B (150x70)			Cope detail C (200x110)		
L_x	R_{max} [N]	$\frac{R_{max}}{R_{M,pl}}$	FM	R_{max} [N]	$\frac{R_{max}}{R_{M,pl}}$	FM	R_{max} [N]	$\frac{R_{max}}{R_{M,pl}}$	FM
0	241 665	1.05	WB1	237 162	1.03	WB1	177 371	0.77	WB2
200	249 374	1.08	WB1	248 317	1.08	WB1	181 877	0.79	WB2
300	248 891	1.08	WB1	247 848	1.08	WB1	233 074	1.01	WB2
400	247 317	1.08	WB1	247 556	1.08	WB1	245 816	1.07	WB2
600	245 330	1.07	WB1	247 433	1.08	WB1	246 846	1.07	WB1
800	243 858	1.06	WB1	247 470	1.08	WB1	246 868	1.07	WB1
1000	247 522	1.08	WB1	251 278	1.09	WB1	248 460	1.08	WB1

TABLE 5.6: FEM results of coped beam reinforced with horizontal stiffener.

- Local web buckling at the loaded position (WB1)
- Local web buckling at the coped corner (WB2)

For cope details A ($c/h_0 = 0.40$) and B ($c/h_0 = 0.65$) the beam's increased strength when reinforced with longitudinal stiffeneres was insignificant. Even when extending the stiffeners to full length ($L_x = 1000$ mm), the gain in strength compared to the unreinforced beam was only 24 % for cope detail A and 6 % for cope detail B. For cope detail C ($c/h_0 = 1.05$) however, the beam's capactiy was raised with up to 40 % compared to the unreinforced beam.
From the output files in ABAQUS of the coped beam's deformed shape and stress distribution it is possible to follow the coped beam's behaviour as the loading proceeds. Cope detail A and B showed similar behaviour for all stiffener lengths, where yielding was triggered quite early at the coped corner and in the web near the loaded position. The final failure mode was identified as local buckling of the lower part of the web, followed by a sideways displacement of the horizontal stiffeners. This behaviour was also observed for the unreinforced coped beams, thus reinforcement seems excessibly. However, the provision of stiffeners reduced the sideways movement of the coped end, increasingly with elongated stiffener length. Figures 5.6 and 5.7 show the lateral translation pattern for the two cope details at failure.
Localized buckling of the top flange at the fixed end was also observed, but that is rather seen as a result of the stress concentrations arising from the lateral movement following the local web buckling.

For cope detail C the behaviour was somewhat different. Referring to the figure 5.5 and table 5.6, the beam's capacity increased with 39 % from the unreinforced state up to a horizontal stiffener length of 400 mm ($L_x/c = 2$). Further gain in strength was negligible, with only 1 % for stiffener length 1000 mm ($L_x/c = 5$). Due to the longer coped lenght ($c = 200$ mm),

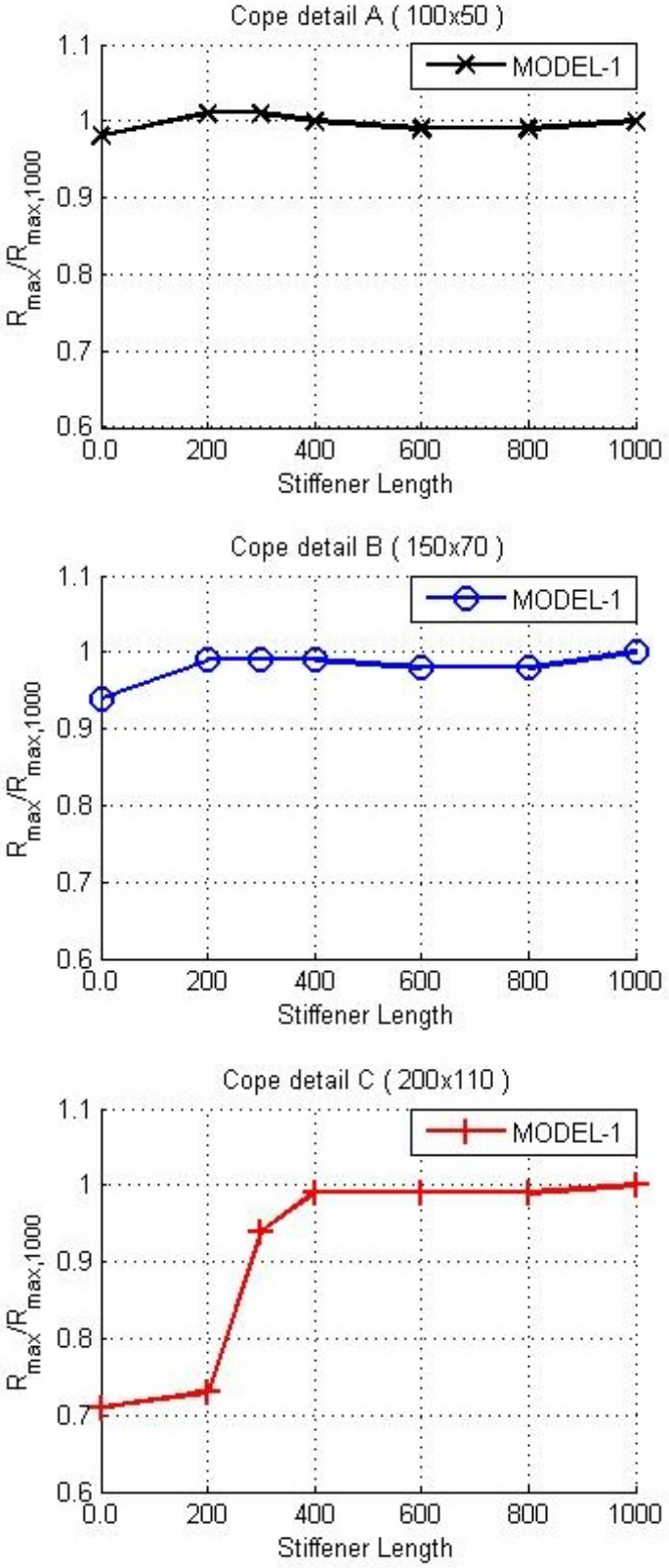

FIGURE 5.5: Max. reaction force longitudinal reinforced coped beams.

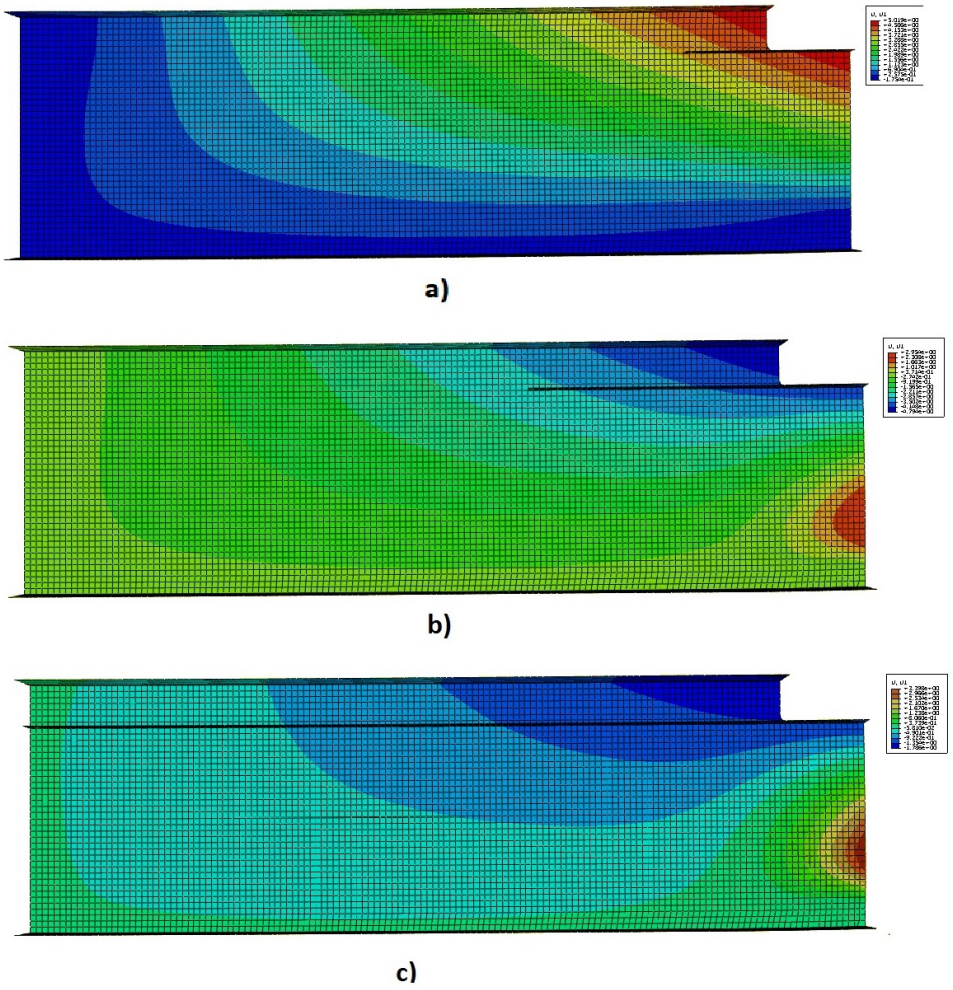

FIGURE 5.6: Lateral deflection pattern of longitudinally reinforced beam with stiffener length L_x
a) 200 mm, b) 400 mm and c) 1000 mm.

the shortest stiffeners did barely extend into the web, providing little support. For the shortest longitudinal stiffener ($L_x/c = 1$) the extension length equal zero. In that case the reduced web buckling length was somewhat lowered, increasing the beam's capacity some (3 %). But the buckling length of the full section at the coped corner remained unaltered and because of the large stress consentrations located at that point, the beam failed in buckling at the coped corner followed by severe sideways movement of the horizontal stiffener. By elongating the stiffener lengths the behaviour was successfully improved, forcing the beam to fail at the loaded position. Figure 5.8 shows the lateral deflection pattern at failure for increasing stiffener length (L_x).

The effect of increasing the stiffeners thickness and width on the reinforced coped beam's capacity was investigated in a parametric study. The results are presented in table 5.7 and in figures 5.9, 5.10 and 5.11, in terms of ratio of max. support force to max. support force of the longest stiffener length ($R_{max}/R_{max,1000}$).

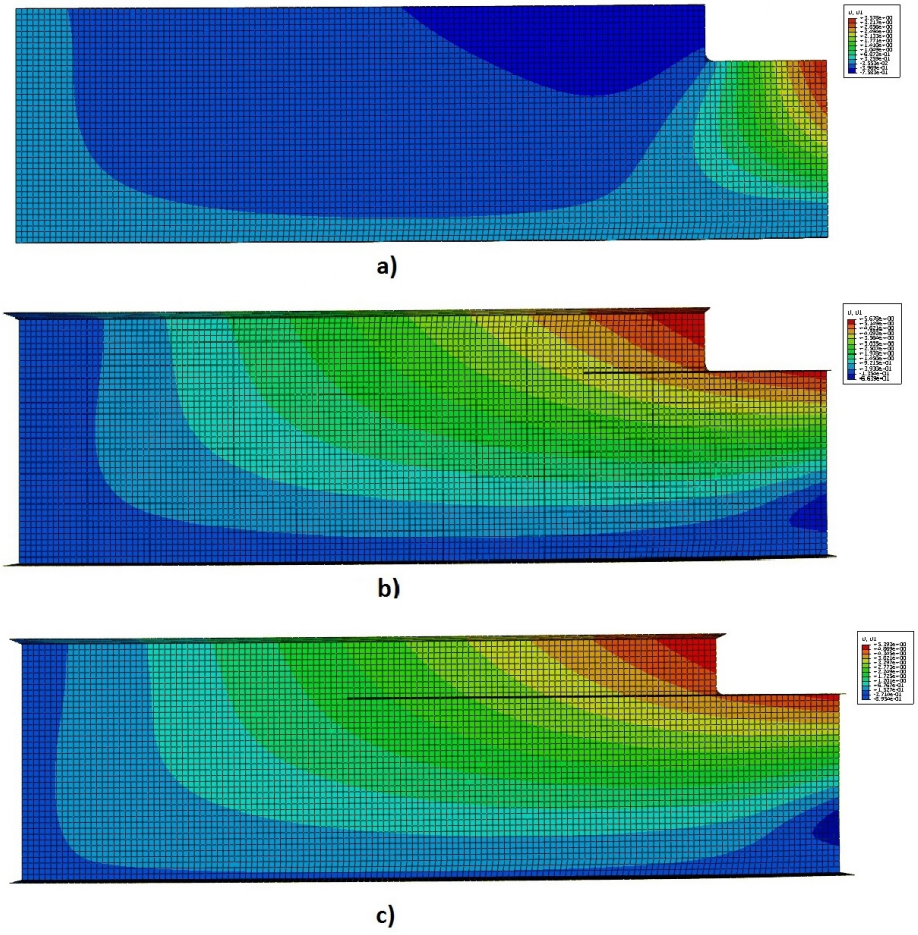

FIGURE 5.7: Lateral deflection pattern of longitudinally reinforced beam with stiffener length L_x
a) 0 mm, b) 300 mm and c) 600 mm.

See that the increased cross sectional dimensions of the longitudinal stiffeners had little or no effect on the coped beams strength. This was rather expected as the coped beams were seen to fail mostly in local buckling of the web below the horizontal reinforcement. Thus, increasing the stiffeners thickness and width would not prevent this from happen as the web's buckling length remained the same.
But, some of the results might seem a little odd. Observe from figures 5.9 and 5.11 that when increasing the stiffeners thickness, the coped beams capacities drops below the ones for the original model for stiffener lengths up to 600 mm. As the failure mode stays unaltered and with the stiffened beams increased cross section, the opposite would be expected to happen. The drop was quit small however, for all cases concerned the less than one procent. Thus, this behaviour migth just be a result of the nonlinear effects taken into account in the model, for instance a different buckling shape implemented as the models inital imperfections.

See from the obtained results that provision of horizontal stiffeners for cope detail A ($c/h_0 =$

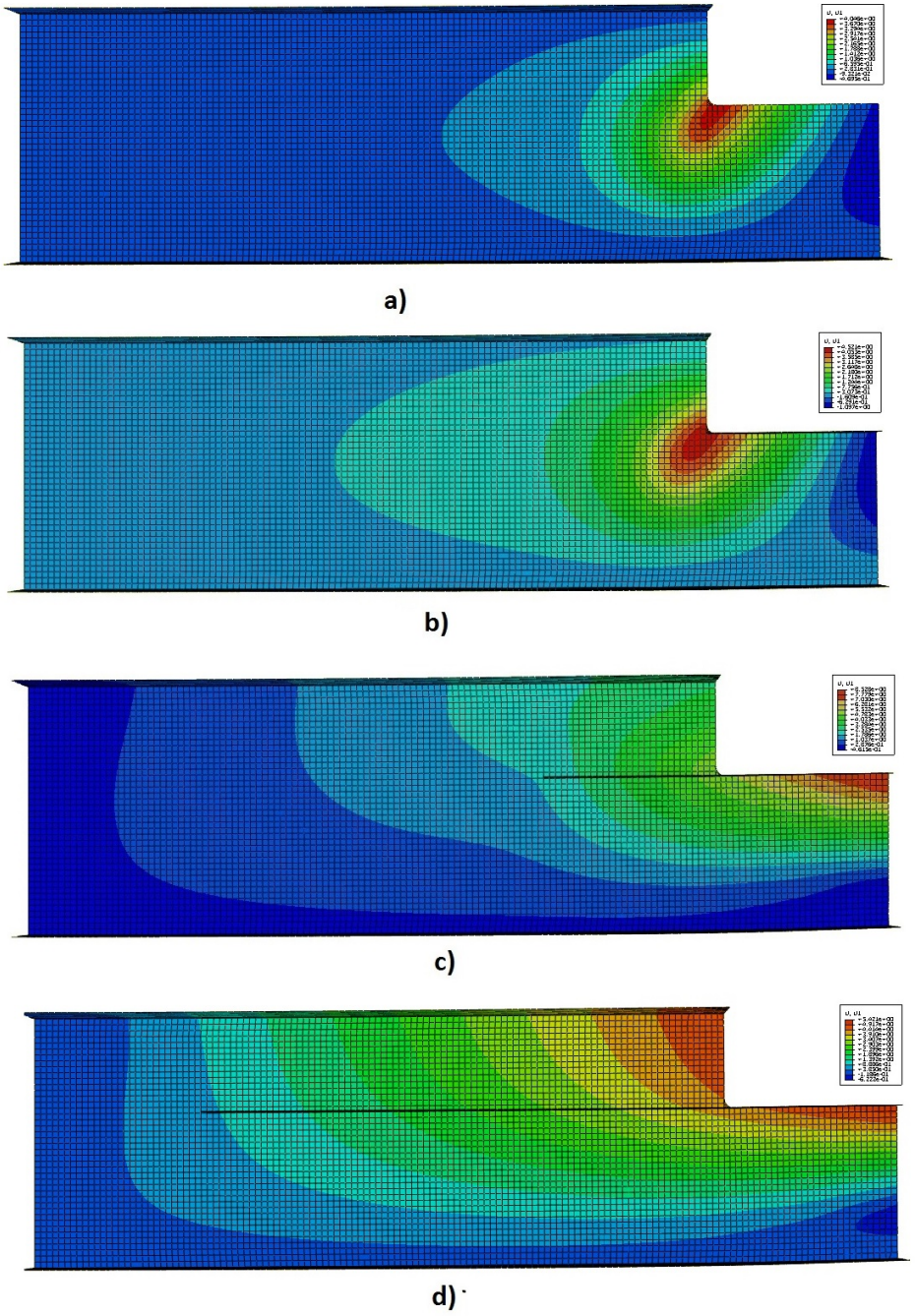

FIGURE 5.8: Lateral deflection pattern of longitudinally reinforced beam with stiffener length L_x
a) 0 mm, b) 200 mm, c) 400 mm and d) 800 mm.

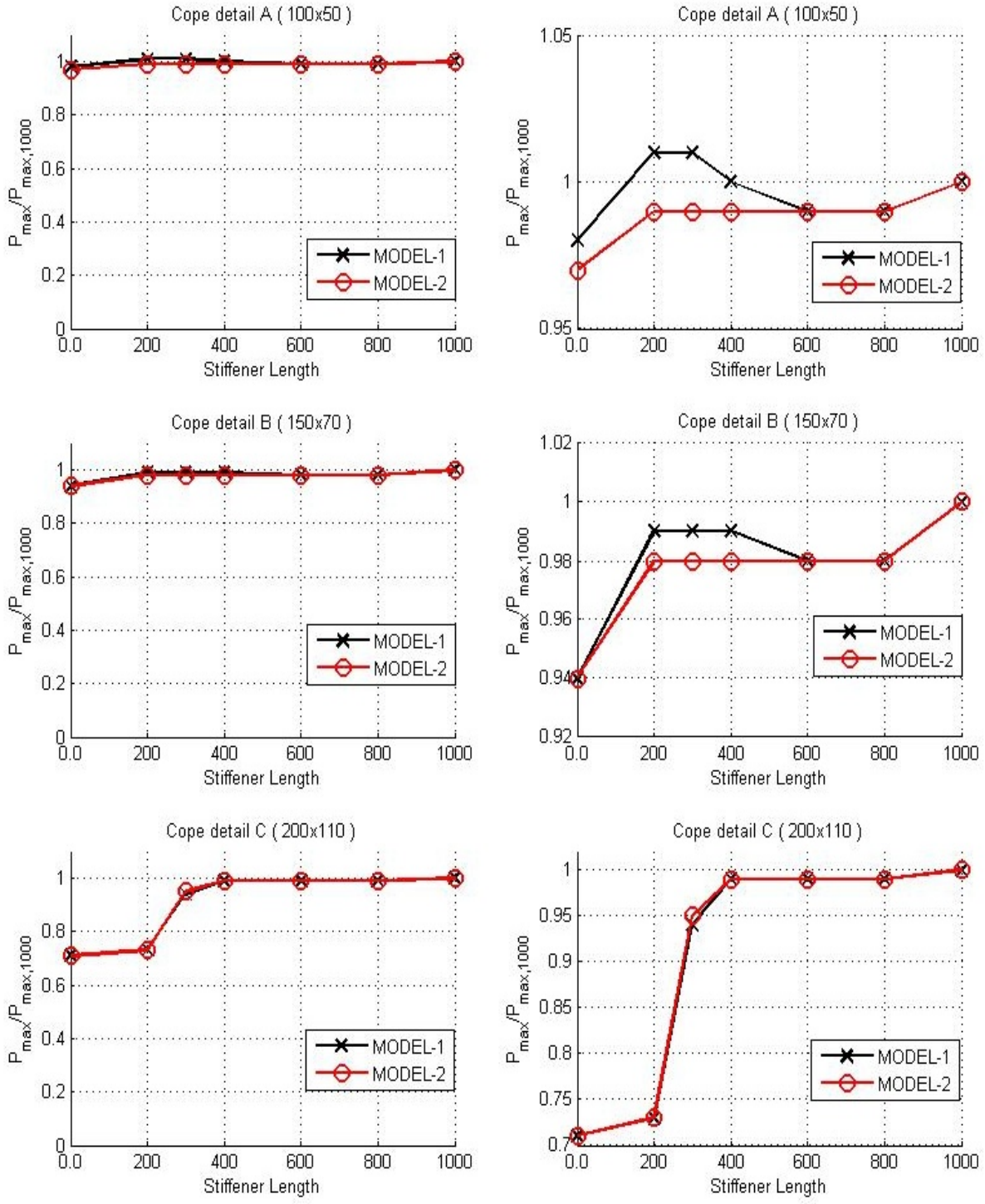

FIGURE 5.9: Max. reaction force for longitudinal reinforced coped beams MODEL-2 vs MODEL-1.

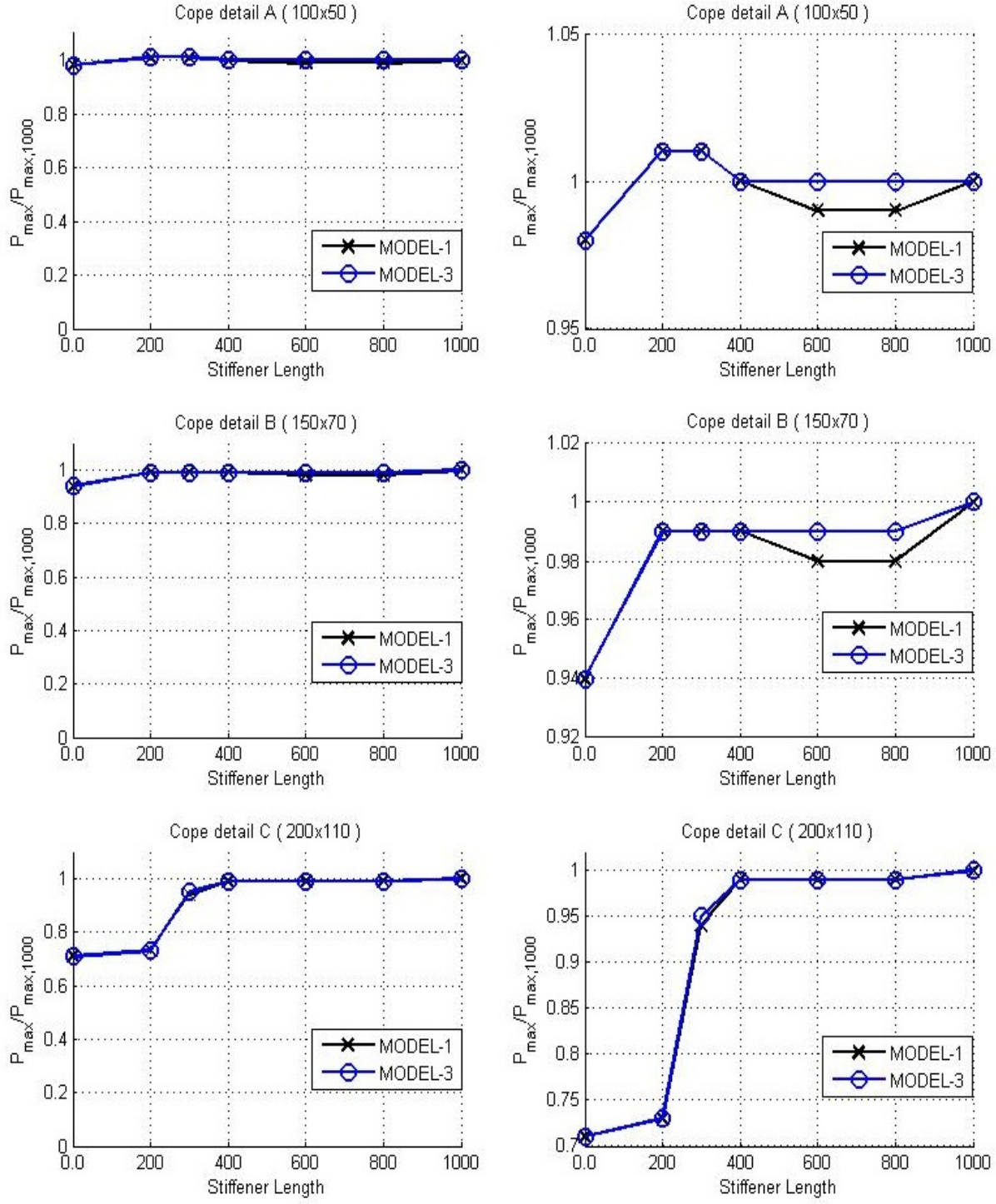

FIGURE 5.10: Max. reaction force for longitudinal reinforced coped beams MODEL-3 vs MODEL-1.

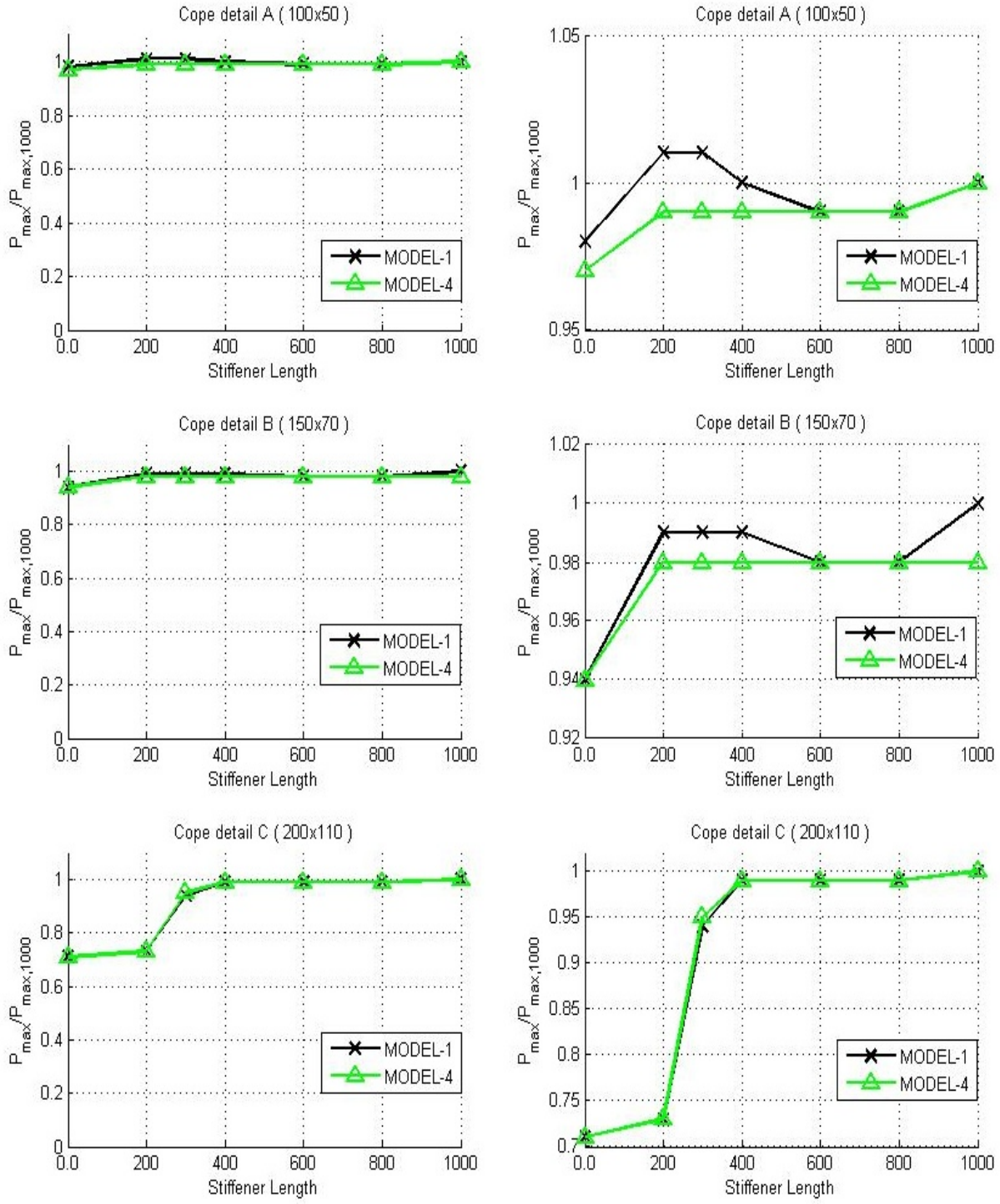

FIGURE 5.11: Max. reaction force for longitudinal reinforced coped beams MODEL-4 vs MODEL-1.

Cope detail	MODEL-2 $t_x = 10.7$ mm $b_x = 75$ mm Stiffener length L_x [mm]						
	0	200	300	400	600	800	1000
A (100x50)	241 665	248 608	247 925	247 015	248 189	248 546	250 285
B (150x70)	237 162	247 393	248 173	247 953	247 951	248 067	253 000
C (200x110)	177 371	182 503	238 048	247 924	247 729	247 780	250 054

Cope detail	MODEL-3 $t_x = 7.1$ mm $b_x = 150$ mm Stiffener length $L_x[mm]$						
	0	200	300	400	600	800	1000
A (100x50)	241 665	248 934	247 884	247 142	246 889	246 719	246 564
B (150x70)	237 162	247 995	247 958	247 662	247 508	247 502	251 066
C (200x110)	177 371	182 075	235 511	247 326	247 247	247 164	248 819

Cope detail	MODEL-4 $t_x = 10.7$ mm $b_x = 150$ mm Stiffener length $L_x[mm]$						
	0	200	300	400	600	800	1000
A (100x50)	241 665	248 470	247 788	247 688	247 815	247 977	249 790
B (150x70)	237 133	247 133	248 297	248 140	248 273	248 494	253 200
C (200x110)	177 371	182 640	239 131	248 363	248 270	248 430	250 763

TABLE 5.7: Max. reaction force for longitudinal reinforced coped beams.

0.40) and B ($c/h_0 = 0.65$) did not improve the beams capacity efficiently compared to the unreinforced state. For cope detail C ($c/h_0 = 1.05$) the beam's capacity was successfully improved, but extending the stiffener lengths over 400 mm ($L_x/c \leq 2$) would provide almost no further gain in strength.

This results compared well with the conclusions drawn by Yam et al. (2007), which stated that increasing of the horizontal stiffeners length would not increase the local web buckling capacity of the coped beam in an efficient manner [2]. However, this happened just for cope details A and B. The results for cope detail C compared well with the design recommendations presented by Yam and Chung (2012), that for coped beams with $d/t_w \geq 52.7$, $d_c/h \geq 0.3$ and $c/h \geq 0.75$ use of only longitudinal stiffeners with an extension length of $2d_c$ was sufficient [9]. In this case $d/t_w = 35.0$, $d_c/h = 0.37$ and $c/D = 0.67$, and with a recommended stiffener length of $L_x = c + 2d_c = 420$ mm. This compared well with the results presented in figure 5.5, where the beam reached its max. capacity for a stiffener length of 400 mm.

The different behaviour can be explained in terms of the coped sections dimensions relative to the beams cross sectional properties. The reinforced coped beams capacities against flexural yielding at the coped section was seen to drop with increasing cope ratio, as seen in table 5.6 As a result, the reinforced coped sections capacities against local web buckling were less than the corresponding yield moment capacities, so that strengthening of the coped section with

horizontal stiffeners would be less efficient. That seemed to be the case for cope details A and B, with cope ratio of respectivily 0.40 and 0.65, and cope depth to beam hight d_c/h of 0.17 and 0.23, where provision of horizontal stiffeners hardly raised the beams capacities at all. For cope detail C however, where $c/h_0 = 1.05$ and $d_c/h = 0.37$, the beams capacity increased with nearly 40 % when reinforced with a horizontal stiffener length of 400 mm, which corresponds well with the design recommendations proposed by Yam and Chung (2012). But, an increased strength of 40 % is not quite significant. Also, for non of the tested specimens the coped beams failed in flexural yielding or shear yielding at the fixed end.

5.3 Effects of Combined Horizontal and Vertical Stiffeners

5.3.1 General

In the previous section it was concluded that reinforcing of the coped sections with just horizontal stiffeners would not strengthen the coped beams in any efficient manner. Hence, vertical stiffeners were added to the horizontal stiffeners.
The horizontal stiffeners location and dimensions stayed unaltered, and all stiffener lengths L_x were tested. The vertical stiffeners were placed based on the observed location of the failure modes from the previous section. Since the beam most usually failed due to local web buckling at the loaded position, an obvious placement of the vertical stiffeners would be at the coped region rigth above the loading, here refered to as vertical stiffener $V1$. The coped corner was also particular vulnerable, thus vertical stiffeners were provided at that section, refered to as vertical stiffener $V2$. The vertical stiffeners dimensions and material properties were equal to the horizontal stiffeners. Thus, both vertical stiffeners $V1$ and $V2$ were assigned a thickness and width of respectivily 7.1 mm and 75 mm. Unlike the combined stiffened solution analyzed by Yam et al. (2007) where the vertical stiffeners length would cover only a part of the web [2], the vertical stiffeners lengths were in this case extended over the webs hight. Thus, at the reduced coped region, $L_{y1} = h_0 - t_f = h_{w,red}$, while at the uncoped section, $L_{y2} = h - 2t_f = h_w$.
The coped beams strength and behaviour were analyzed for three types of combinations of vertical and horizontal stiffeners for all lengths L_x, namely

- H + $V1$: Horizontal stiffener and vertical stiffener at the loaded position
- H + $V1$: Horizontal stiffener and vertical stiffener at the coped corner
- H + $V1$ + $V2$: Horizontal stiffener and vertical stiffeners at both locations

The combined reinforced solutions are shown in figure 5.12 with the details listed in table 5.8.

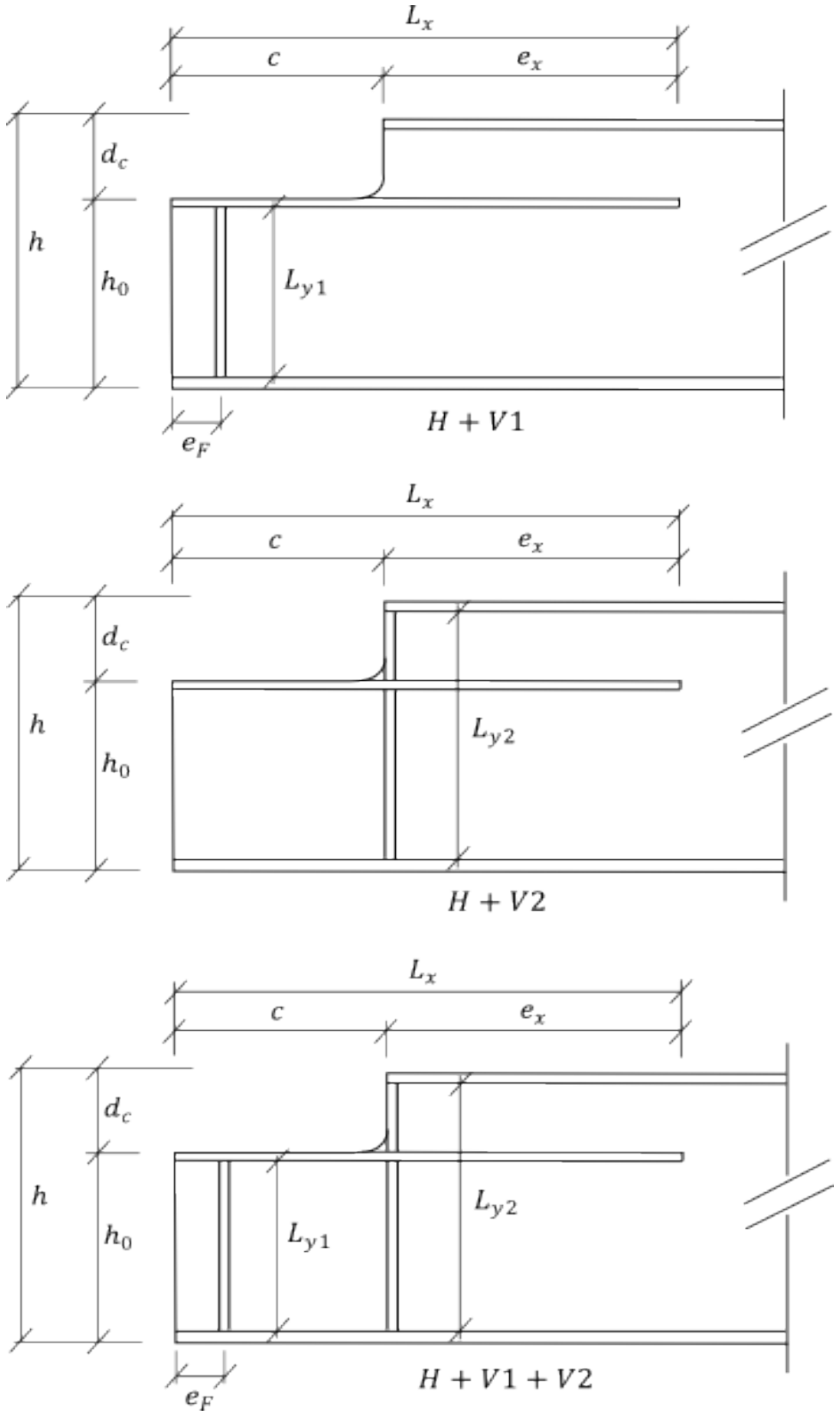

FIGURE 5.12: Reinforcement details for coped beams.

$b_x = 75$ mm $t_x = 7.1$ mm $b_{y1} = 75$ mm $t_{y1} = 7.1$ mm $b_{y2} = 75$ mm $t_{y2} = 7.1$ mm

	H + V1			H + V2	H + V1 + V2			
L_x [mm]	L_{y1} [mm]			L_{y2} [mm]	L_{y1} [mm]			L_{y2} [mm]
	A	B	C	A, B & C	A	B	C	A, B & C
0	232.2	212.2	172.2	278.6	232.2	212.2	172.2	278.6
200	232.2	212.2	172.2	278.6	232.2	212.2	172.2	278.6
300	232.2	212.2	172.2	278.6	232.2	212.2	172.2	278.6
400	232.2	212.2	172.2	278.6	232.2	212.2	172.2	278.6
600	232.2	212.2	172.2	278.6	232.2	212.2	172.2	278.6
800	232.2	212.2	172.2	278.6	232.2	212.2	172.2	278.6
1000	232.2	212.2	172.2	278.6	232.2	212.2	172.2	278.6

TABLE 5.8: Dimensions of vertical and horizontal stiffeners.

Both the horizontal and vertical stiffeners were modelled with use of $S4R$ elements and attached to the beams flange and web with a TIE-constraint which also was used to weld the stiffeners together. Figure 5.13 show the complete meshed element model for the different stiffener combinations.

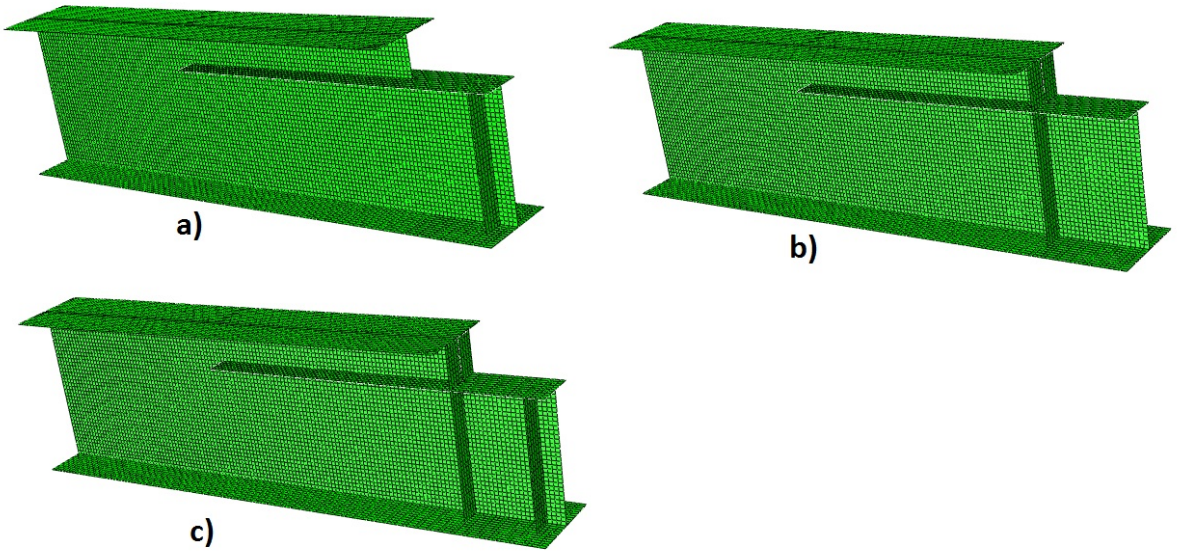

FIGURE 5.13: Element model reinforced beam for stiffener combination a) H + V1, b) H + V2 and c) H + V1 + V2.

5.3.2 Results

Nonlinear Analysis

The coped beams strength and behaviour are analyzed in a nonlinear manner for three different combinations of vertical and horizontal stiffeners, as shown in figure 5.12.

The results are presented in tables 5.9, 5.10 and 5.11 where the stiffened coped beams capacities are given in terms of the max. reaction force (R_{max}) at the contact surface between the rigid block and lower flange. The different failure modes (FM) which the beam where seen to experience are as follows

- Flexural failure of the full beam section at the fixed end, followed by buckling of compressional flange (FF)
- Flexural failure of the full beam section at the fixed end, followed by sideways movement of stiffeners (FR)
- Local web buckling at the loaded position (LWB1)
- Local web buckling at coped corner (LWB2)

For most of the cases examined in this study, the beam failed in flexural yielding at the fixed end (FF). Thus, the results are also presented as the ratio of max. reaction force and plastic moment capacity of the full beam section, ($R_{max}/R_{M,pl}$), and plotted relative to the longitudinal stiffener length (L_x), as seen in figures 5.14, 5.15 and 5.16.

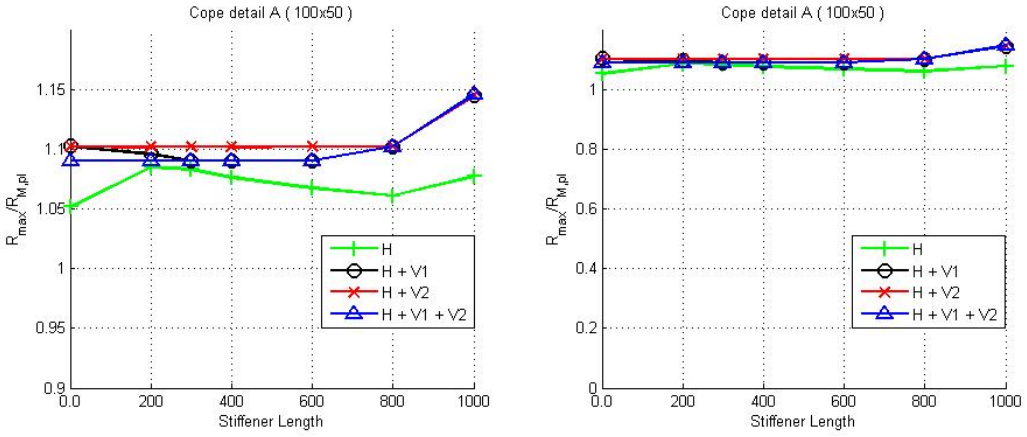

FIGURE 5.14: FEM results of reinforced coped beam A.

For cope detail A ($c/h_0 = 0.40$) that the beam failed in flexural yielding at the fixed end followed by buckling of the compressional flange (FF), for all placements of the vertical stiffeners and horizontal stiffener length (L_x). Thus, provison of vertical stiffeners succeeded in preventing local web buckling at the coped section from happening, regardless of their location. See also that it was no occurance of severe sideways movement of the coped end.
In terms of the beams capacity, the applied load exceeded the moment capacity at the full beam section ($R_{M,pl}$) with $9 - 10$ %. For the longest horizontal stiffener length ($L_x = 1000$ mm) the moment capacity was exceeded with $14 - 15$ %, but in that case the FE models max. capacity was not reached unless a very large vertical displacement of the coped end was provided, hence

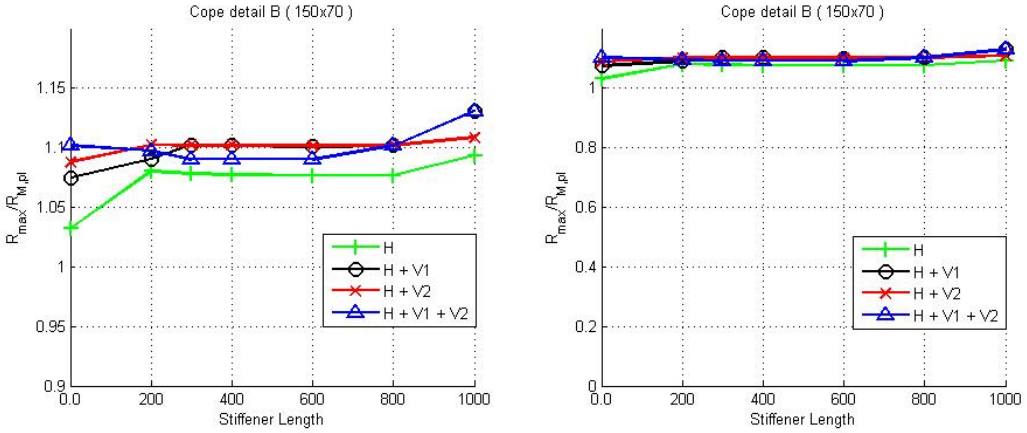

FIGURE 5.15: FEM results of reinforced coped beam B.

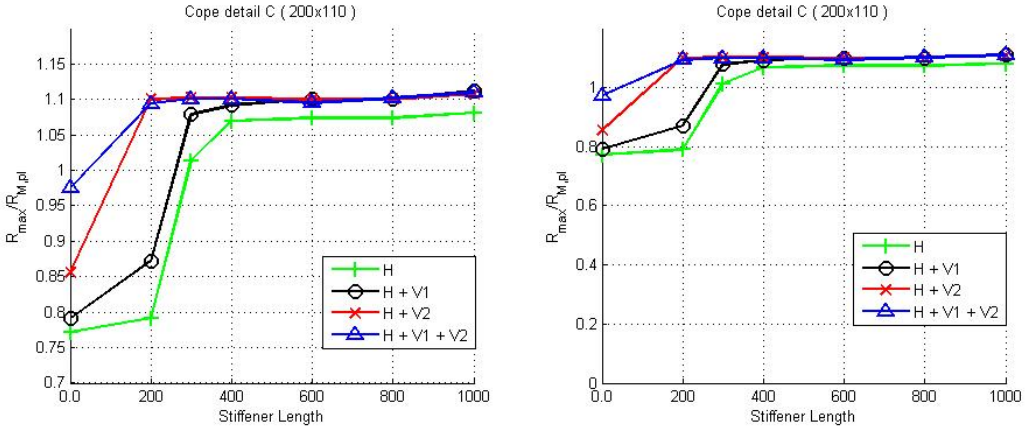

FIGURE 5.16: FEM results of reinforced coped beam C.

Combined stiffener H + V1									
	Cope detail A (100x50)			Cope detail B (150x70)			Cope detail C (200x110)		
L_x	R_{max} [N]	$\frac{R_{max}}{R_{M,pl}}$	FM	R_{max} [N]	$\frac{R_{max}}{R_{M,pl}}$	FM	R_{max} [N]	$\frac{R_{max}}{R_{M,pl}}$	FM
0	253 353	1.10	FF	247 021	1.07	WB2	181 846	0.79	WB2
200	251 881	1.10	FF	250 677	1.09	FR	200 470	0.87	WB2
300	250 591	1.09	FF	253 342	1.10	FF	247 976	1.08	WB2
400	250 603	1.09	FF	253 261	1.10	FF	250 903	1.09	FR
600	250 611	1.09	FF	253 029	1.10	FF	253 012	1.10	FF
800	253 282	1.10	FF	253 295	1.10	FF	252 940	1.10	FF
1000	263 019$^{(*)}$	1.14	FF	259 883$^{(*)}$	1.13	FF	255 579	1.11	FF

TABLE 5.9: FEM results of coped beam reinforced with horizontal stiffener and vertical stiffener at loaded position.

Combined stiffener H + V2									
	Cope detail A (100x50)			Cope detail B (150x70)			Cope detail C (200x110)		
L_x	R_{max} [N]	$\frac{R_{max}}{R_{M,pl}}$	FM	R_{max} [N]	$\frac{R_{max}}{R_{M,pl}}$	FM	R_{max} [N]	$\frac{R_{max}}{R_{M,pl}}$	FM
0	253 262	1.10	FF	250 044	1.09	WB1	196 753	0.86	WB2
200	253 199	1.10	FF	253 314	1.10	FF	252 885	1.10	WB1
300	253 204	1.10	FF	253 294	1.10	FF	253 338	1.10	FF
400	253 205	1.10	FF	253 271	1.10	FF	253 338	1.10	WB1
600	253 231	1.10	FF	253 258	1.10	FF	252 865	1.10	WB1
800	253 265	1.10	FF	253 267	1.10	FF	252 900	1.10	WB1
1000	263 098$^{(*)}$	1.14	FF	254 816	1.11	WB1	254 647	1.11	FF

TABLE 5.10: FEM results of coped beam reinforced with horizontal stiffener and vertical stiffener at coped corner.

Combined stiffener H + V1 + V2									
	Cope detail A (100x50)			Cope detail B (150x70)			Cope detail C (200x110)		
L_x	R_{max} [N]	$\frac{R_{max}}{R_{M,pl}}$	FM	R_{max} [N]	$\frac{R_{max}}{R_{M,pl}}$	FM	R_{max} [N]	$\frac{R_{max}}{R_{M,pl}}$	FM
0	250 551	1.09	FF	253 303	1.10	FF	224 073	0.97	WB2
200	250 579	1.09	FF	252 196	1.10	FF	251 599	1.09	FF
300	250 610	1.09	FF	250 568	1.09	FF	253 080	1.10	FF
400	250 628	1.09	FF	250 575	1.09	FF	252 994	1.10	FF
600	250 610	1.09	FF	250 559	1.09	FF	251 701	1.10	FF
800	253 318	1.10	FF	253 248	1.10	FF	253 259	1.10	FF
1000	263 296$^{(*)}$	1.15	FF	259 863$^{(*)}$	1.13	FF	255 035	1.11	FF

TABLE 5.11: FEM results of coped beam reinforced with horizontal stiffener and vertical stiffener at both locations.

the capacity was evaluated at a vertical displacement of 35 mm.

The capacities of the different stiffener combinations and horizontal stiffener lengths varied little, in figure 5.14 represented by an almost straight line. Compared to the case with reinforcement in only longitudinal direction, the difference in strength is almost insignificant where the max. applied load exceeded the moment capacity by $6 - 8$ % in reinforced state and 5 % in an unreinforced state. But as earlier stated, use of horizontal stiffeners only do not prevent the web from buckling at the coped end. Hence, because of the coped region's relativily small size the beam was already close to the moment capacity of the full section in an unreinforced state, so that only a small increase in strength was possible when reinforced.

For cope detail B ($c/h_0 = 0.65$) the behaviour was similar to that of cope detail A. The beam usually failed in flexural yielding at the fixed end followed by buckling of the top flange (FF). However, other failure modes were observed as well. When reinforced with vertical stiffener

at the loaded posistion only ($L_x = 0$ mm) the web would fail at the coped corner (WB2). Due to the inclined buckling line, shear was assumed to be critical [15]. This behaviour was however prevented when the vertical reinforcement was moved to the coped corner. But, due to lack of support of the coped end the beam still failed in local web buckling, now at the loaded position (WB1). Hence, vertical stiffeners at only one location did not prevent local web buckling from happening. That would demand stiffeners in the longitudinal direction as well, which was accomplished for all stiffener lengths as seen in figures 5.14 and 5.15. However, with one exeption. Extending the stiffener over the beams full length ($L_x = 1000$ mm) increased the beams capacity at its fixed end, forcing the web at the loaded position to buckle instead (WB1). When reinforced with vertical stiffeners at both locations (H + V1 + V2), local web buckling was prevented, both for vertical stiffeners only and for all stiffener lengths ($L_x = 0$ mm).
The capacities of the different stiffener combinations and stiffener lengths varied little, as seen in figure 5.15. For failure at the fixed end, the applied load exceeded the beam's moment capacity with $9 - 10$ %, regardless of stiffener combinations and horizontal stiffener length. For local web buckling the exceedance was 7 % when located at the coped corner and $9 - 11$ % at the loaded position, respectivily for $L_x = 0$ mm and $L_x = 1000$ mm. Similar to cope detail A, compared to the unreinforced beam and reinforced beam in longitudinal direction only, the effect of providing vertical stiffeners seems almost insignificant and exceeding the moment capacity with respectivily 3 % and $8 - 9$ %.

The behaviour of cope detail C ($c/h_0 = 1.05$) depended more on the vertical stiffeners location. When reinforced at the loaded position only (H + V1), the beam failed in local web buckling at the coped corner. This happened for the horizontal stiffeners of length 200 mm and 300 mm as well, which deflected laterally in rigid body motion. By increasing the stiffener length to 400 mm local web buckling was prevented, forcing the beam to fail in flexural yielding at it's fixed end. But, the horizontal stiffener would still deflect sideways in rigid body motion (FR). Hence, further elongation of the horizontal stiffeners ($L_x = 600 - 1000$ mm) were needed to provide enough sideways support.
When only vertical reinforcement was provided at the coped corner (H + V2) the webs shear capacity was exceeded, forming a plastic hinge along the vertical stiffener causing the web to buckle outwards. When horizontal stiffeners were added, the web buckling was located to the loaded position, except for the stiffener lengths of 300 mm and 1000 mm for which the beam failed in flexural yielding at its fixed end (FF).
When vertical reinforcement was provided at both locations (H + V1 + V2), local web buckling was prevented from happening for all stiffener lengths (L_x) and the beam failed in exceedance of the plastic moment capacity at its fixed end followed by buckling of the compressional flange (FF). Also, no significant sideways rigid body motion of the longitudinal stiffeners was observed.
When no reinforcement was provided in the longitudinal direction ($L_x = 0$ mm), buckling of the web was initiated along the vertical stiffener at the coped corner. However, the web was

prevented from any significant sideways movement by the stiffener at the loaded position.
The coped beams capacity did vary some for the different stiffener combinations and stiffener lengths, as seen in figure 5.16. For failure at the fixed end the applied load was similar to that of cope detail A and B, where the beam's moment capacity was exceeded with $9 - 11$ % regardless of stiffener combinations and stiffener lengths, similar to cope details A and B. The behaviour was also similar for local web buckling at the loaded position, where the beam's moment capacity was exceeded with 10 %. However, for buckling of the web at the coped corner the beam's capacity was reduced with a fair amount. The largest reduction was observed when vertical reinforcement were provided at the loaded position only (H + V1), where the applied load was either $21 - 13$ % under or 8 % over the beam's moment capacity, respectivily for stiffener lengths of 0 mm, 200 mm and 300 mm. For the other combined stiffener solutions, the behaviour was somewhat improved. For vertical stiffener at the coped corner (H + V2) the applied load was 14 % under the beam's moment capacity, while for vertical stiffeners at both locations the difference was only 3 %.
Compared to the unreinforced beam and reinforced beam in longitudinal direction only, the effect of providing vertical stiffeners depended on their location. But, as seen in figure 5.16 the difference were almost insignificant for stiffener lengths of 400 mm or higher ($L_x \geq 400$ mm).

But, can these results be treated as accurate? First of all, the occurence of exceeded moment capacity might seem a little strange. However, the results obtained from the FEA are expected to disagree some with the mathematical model, here represented by the plastic moment capacity formula ($M_{pl} = f_y W_{pl}$). As the mathematical model is only a simplification, certain details of the actual problem might be omitted. Also, error can arise from pourly discretization of the model. As the mathematical model consist of an infinite number of dof's but finite in the FE model, the FEA solutions are clearly influenced by the chosen element size, number of element nodes, integration rules and other formulation details [5]. Thus, assume that the observed exceedance of the beams moment capacity of magnitude up to 11 % are acceptable.
The results obtained from the FEA compared well with Yam and Chungs (2012) study on reinforced coped beams [9], where the reinforced coped beams failed due to web crippling or in flange local buckling at the location of max. moment. Also, the behaviour was similar in that the max. applied load to the beam's plastic moment capacity at the full section, in their study represented by the M_{max}/M_{pl}) ratio, would decrease with increasing d_c/h ratio.
In their recommendations for design of reinforced coped beams, use of combined longitudinal and double transverse stiffeners should be provided for coped beams with $52.7 < d/t_w \leq 57.1$, $d_c/h \leq 0.3$ and $c/h \leq 0.9$. The stiffener lengths were set to respectivily $L_x = c + e_x$ and $L_y = c + e_y$, where $e_x = e_y = d_c$. While for coped beams with $h_w/t_w \leq 52.7$, $d_c/h \leq 0.3$ and $c/h \leq 0.75$, they recommended use of only longitudinal stiffeners, where $L_x = c + 2d_c$. However, transferring those design recommendations is not easy. In the present study, the beam's slenderness $h_w/t_w = 35.0$ and cope to beam ratios $d_c/h = 0.17 - 0.37$ and $c/h = 0.33 - 0.67$. In

c	d_c [mm]	$R_{M,pl}$ [kN]	$R_{V,pl\&el}$ [kN]	$R_{M,pl,red}$ [kN]	$R_{V,pl\&el,red}$ [kN]	$R_{M,el}$ [kN]	$R_{M,el,red}$ [kN]
100	50	204.2	246.0	631.2	205.0	169.1	312.2
150	70	204.2	246.0	312.6	188.6	169.1	157.2
200	110	204.2	246.0	152.2	155.8	169.1	78.9

TABLE 5.12: Results elastic and plastic moment and shear capacity of the full and reduced beam section.

following those recommendation, reinforcement should be provided in the longitudinal direction only. This would increase the strength for all cope details, but would not prevent the beam to fail at the coped end. Hence, the design recommendations proposed by Cheng and Yura might not be applicable.

5.4 Effects of Reduced Web Thickness for Combined Reinforced Coped Beam

As seen from the results, the difference in the beam's strength for the different failure modes was quite small. Due to the modeled IPE300 beams low slenderness, the resistance to web crippling and local web buckling is relativily high compared to the plastic moment capacity. Hence, the applicabilty for the different reinforcement details are tested for more slender webs. Of present the slenderenss is defined by $h_w/t_w = 35.0$, which categorizes it in cross sectional class 1. By reducing the web thickness to 4.0 mm the slenderness is reduced to $h_w/t_w = 62.2$, now categorized in cross sectional class 2 [22].
The coped beams moment and shear capacities were updated for the reduced web thickness and listed in table 5.12

5.4.1 Procedure

The coped beam was tested for a reduced web thickness of 4.0 mm for all stiffener combinations and cope dimensions tested in the previous section, as listed in table 5.8. No changes on the element model was conducted and the vertical and horizontal stiffener dimensions remained unaltered ($t_x = 7.1 = t_{y1} = t_{y2} = 7.1$ mm). Also, the extra material at the intersection of the web and flanges were modeled as earlier with a doubling of the web thickness at its extremities, now 8 mm thick.
The element model was tested only in nonlinear analyses, as the critical buckled shapes obtained from previous section are used to implement the initial imperfections in the model.

5.4.2 Results

Nonlinear Analysis

The results are presented in tables 5.13, 5.14 and 5.15, with the stiffened coped beams capacities given in terms of the max. reaction force (R_{max}). In figures 5.17, 5.18 and 5.19 the response is plotted as the ratio of max. applied load to the beam's full moment capacity ($R_{max}/R_{M,pl}$) relative to horizontal stiffener length (L_x).

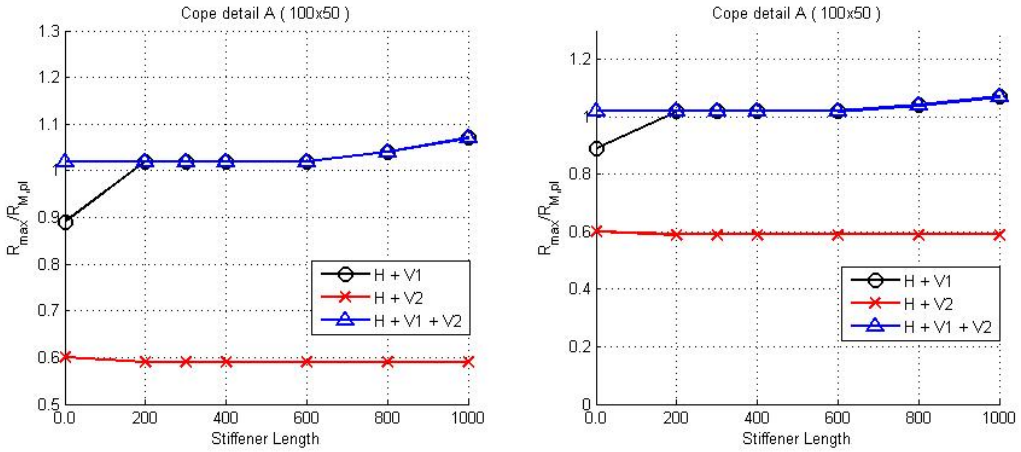

FIGURE 5.17: FEM results of reinforced coped beam A.

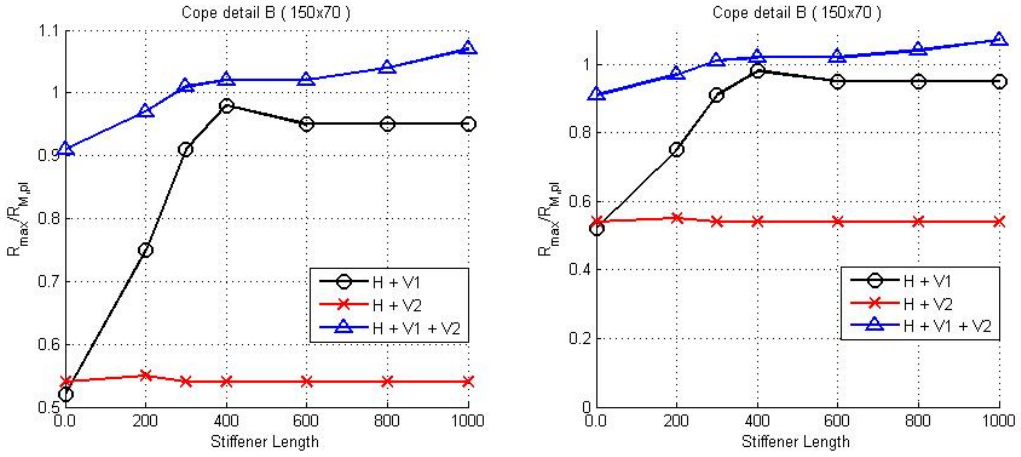

FIGURE 5.18: FEM results of reinforced coped beam B.

From the results it is clear that the reduced web thickness decreases the beams capacity. See that provision of combined horizontal and vertical stiffener at the coped corner (H + V2) did not improve the beams strength and behaviour in any significant manner. For all specimens tested, the beam failed in local web buckling at the loaded position (WB1), with the applied load ranging in the area of 60 % of the beams moment capacity, as seen from table 5.14.

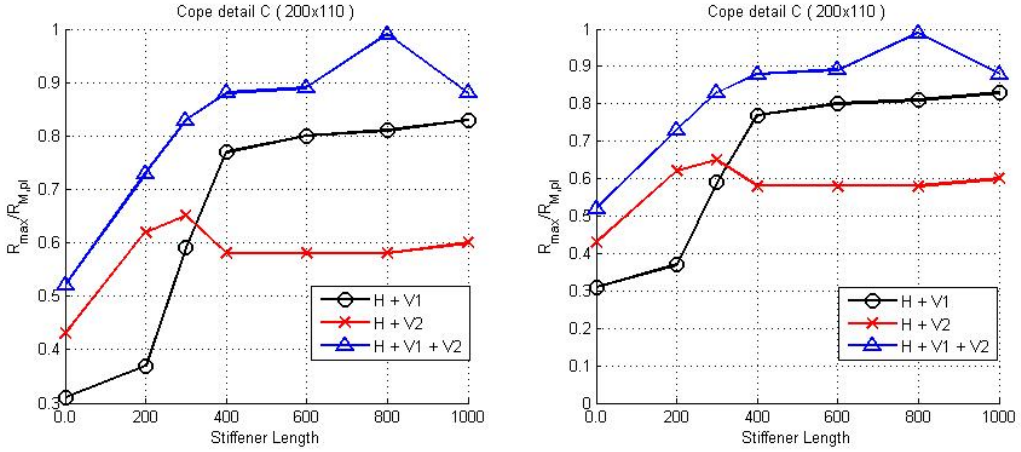

FIGURE 5.19: FEM results of reinforced coped beam C.

Combined stiffener H + V1									
	Cope detail A (100x50)			Cope detail B (150x70)			Cope detail C (200x110)		
L_x	R_{max} [N]	$\frac{R_{max}}{R_{M,pl}}$	FM	R_{max} [N]	$\frac{R_{max}}{R_{M,pl}}$	FM	R_{max} [N]	$\frac{R_{max}}{R_{M,pl}}$	FM
0	181 025	0.89	RM	105 853	0.52	WB1	63 819	0.31	WB2
200	208 500	1.02	RM	152 464	0.75	WB1	75 897	0.37	WB2
300	209 058	1.02	FF	185 454	0.91	WB1	120 300	0.59	RM
400	209 057	1.02	FF	199 118	0.98	WB1	157 710	0.77	WB2
600	250 587	1.23	FF	194 516	0.95	WB1	163 480	0.80	WB2
800	253 309	1.24	FF	194 376	0.95	WB1	165 996	0.81	WB2
1000	258 488$^{(*)}$	1.27	FF	193 464	0.95	WB1	168 764	0.83	WB2

TABLE 5.13: FEM results of coped beam reinforced with horizontal stiffener and vertical stiffener at loaded position.

Combined stiffener H + V2									
	Cope detail A (100x50)			Cope detail B (150x70)			Cope detail C (200x110)		
L_x	R_{max} [N]	$\frac{R_{max}}{R_{M,pl}}$	FM	R_{max} [N]	$\frac{R_{max}}{R_{M,pl}}$	FM	R_{max} [N]	$\frac{R_{max}}{R_{M,pl}}$	FM
0	121 699	0.60	WB1	110 792	0.54	WB1	87 942	0.43	WB1
200	119 720	0.59	WB1	112 493	0.55	WB1	125 785	0.62	WB1
300	120 372	0.59	WB1	110 821	0.54	WB1	132 102	0.65	WB1
400	120 421	0.59	WB1	110 703	0.54	WB1	119 249	0.58	WB1
600	120 577	0.59	WB1	110 799	0.54	WB1	119 357	0.58	WB1
800	120 811	0.59	WB1	109 678	0.54	WB1	119 210	0.58	WB1
1000	121 188	0.59	WB1	110 446	0.54	WB1	121 886	0.60	WB1

TABLE 5.14: FEM results of coped beam reinforced with horizontal stiffener and vertical stiffener at coped corner.

Combined stiffener H + V1 + V2									
	Cope detail A (100x50)			Cope detail B (150x70)			Cope detail C (200x110)		
L_x	R_{max} [N]	$\frac{R_{max}}{R_{M,pl}}$	FM	R_{max} [N]	$\frac{R_{max}}{R_{M,pl}}$	FM	R_{max} [N]	$\frac{R_{max}}{R_{M,pl}}$	FM
0	209 167	1.02	FF	185 484	0.91	WB2	105 831	0.52	WB2
200	209 234	1.02	FF	197 905	0.97	WB2	148 113	0.73	WB2
300	209 238	1.02	FF	207 149	1.01	WB2	170 000	0.83	WB2
400	209 237	1.02	FF	207 768	1.02	WB2	180 263	0.88	WB2
600	209 144	1.02	FF	207 783	1.02	FF	181 148	0.89	WB
800	212 696	1.04	FF	211 715	1.04	FF	201 875	0.99	WB
1000	219 203	1.07	FF	219 300	1.07	FF	179 901	0.88	WB

TABLE 5.15: FEM results of coped beam reinforced with horizontal stiffener and vertical stiffener at both locations.

However, provision of vertical stiffeners at the loaded position successfully improved the coped beams behaviour. For cope detail A ($c/d_c = 0.40$), the beam's full moment capacity was exceeded for a min. horizontal stiffener length of 200 mm ($e_x/c = 1$). For cope detail B ($c/d_c = 0.65$) the capacity was brought close to the beams moment capacity (up to 98%) when $L_x \geq 300$ mm ($e_x/c = 1$), but never exceeding it. In stead, the beam failed due to exceedance of the shear capacity of the coped section.

For cope detail C ($c/d_c = 1.05$) provision of vertical stiffener at loaded position increased the beams capacity, however efficiently only for a min. horizontal length of 400 mm ($e_x/c = 1$). Up to such a stiffener length, failure of the beam was due to web crippling at the coped corner, followed by sideways rigid body movement of the horizontal stiffener. Elsewhere, failure was due to local web buckling of the coped section followed by bending of the horizontal stiffener.

As expected, provision of vertical stiffeners at both locations improved the coped beam's strength and behaviour the most. For cope detail A and B, failure was due to exceedance of the beam's full moment capacity at the fixed end. For cope detail B, the max. capacity was obtained for a horizontal stiffener length of min. 300 mm ($e_x/c = 1$), while for cope detail A the max. capacity was nearly constant regardless of L_x.

For cope detail C, the beam's max. capacity was reached for a min. horizontal stiffener length of 400 mm ($e_x/c = 1$). Up to that point, the beam would fail due to local web buckling at the full beam section (WB2). Elsewhere, buckling of the web was located to the reduced section between the vertical stiffeners (WB).

5.5 Proposed Reinforcement of Coped Beams

The effect of reinforcing the coped beam with stiffeners in either longitudinal, vertical or in both directions is clearly affected by the copes dimensions. In terms of increasing the coped beam's strength, cope detail A and B were hardly affected at all, regardless of type of stiffener combinations and horizontal stiffener length.
For cope detail A ($c/h_0 = 0.40$), the applied load exceeded the beam's moment capacity at its full section for every reinforced case examined, even the unreinforced one. However, provision of stiffeners in the vertical direction did improve the beam's behaviour in an important aspect that local web buckling at the coped end was prevented.
For cope detail B ($c/h_0 = 0.65$), the beam's capacity for the different stiffener combinations did not vary in any particular way. However, local web buckling was prevented when vertical stiffeners were provided in addition to horizontal stiffeners with a min. length of $200 - 300$mm when vertically reinforced at one location only.
For cope detail C ($c/d_c = 1.05$), the coped beam's response to the different stiffener combinations did vary some, but as seen from figure 5.16 the strength reached a constant value for a min. horizontal stiffener length of $200 - 400$ mm. In order to prevent local web buckling, stiffener combination H + V1 + V2 seems to be the best option, given a min. horizontal stiffener length of 200 mm ($e_x/c = 0.0$). However, a longer stiffener will be more resistent to rigid body movement. Hence, a min. length of $300 - 400$ mm is preferable.

For the coped beam with reduced web thickness, the strength and behaviour was more susceptible to reinforcement. From the results it is clear that stiffener combination H + V2 did not increase the coped beam's strength in any significant way, neither did it prevent the web from buckling.
Stiffener combinations H + V1 and H + V1 + V2 were more efficient in that manner. For cope detail A, the difference seemed negligible given that a min. hor. stiffener length of 200 mm was provided for stiffener combination H + V1. But, due to rigid-body movement of the hor. stiffener a length of 300 mm is prefered.
For cope detail B the beams strength was increased for both cases, however stiffener combination H + V1 + V2 was prefered in that local web buckling was prevented from happening. Both cases required a min. hor. stiffener length of 300 mm ($e_x/c = 1$) to act efficiently.
For cope detail C the beam's strength was increased for both cases, however stiffener combination H + V1 + V2 is preferable in that it provides a higher capacity. Both cases required a min. hor. stiffener length of 400 mm ($e_x/c = 1$) to act efficiently.

Based on the results of the parametric study, the following design recommendations for coped I-steel beams are proposed:

For coped beams with $(h/t)_w \leq 58$ and $c/h_0 < 1.00$ use of longitudinal stiffener in combination with vertical stiffener at the loaded position (H + V1) with stiffener lengths

$$L_x = c + e_x \quad \text{where} \quad e_x \geq c$$
$$L_{y1} = h_{w,red}$$

For coped beams with $(h/t)_w \leq 58$ and $c/h_0 \geq 1.00$ use of longitudinal stiffener in combination with vertical stiffener at the both locations (H + V1 + V2) with stiffener lengths

$$L_x = c + e_x \quad \text{where} \quad e_x \geq c$$
$$L_{y1} = h_{w,red}$$
$$L_{y2} = h_w$$

For coped beams with $58 < (h/t)_w \leq 67$ and $c/h_0 < 0.5$ use of longitudinal stiffener in combination with vertical stiffener at the loaded position (H + V1) with stiffener lengths

$$L_x = c + e_x \quad \text{where} \quad e_x \geq 2c$$
$$L_{y1} = h_{w,red}$$

For coped beams with $58 < (h/t)_w \leq 67$ and $c/h_0 \geq 0.50$ use of longitudinal stiffener in combination with vertical stiffener at the both locations (H + V1 + V2) with stiffener lengths

$$L_x = c + e_x \quad \text{where} \quad e_x \geq c$$
$$L_{y1} = h_{w,red}$$
$$L_{y2} = h_w$$

Chapter 6

Conclusion

The strength and behaviour of coped beams were investigated with use of the finite element method program ABAQUS/CAE. The finite element model used for testing was validated by comparison with numerical solutions from a similar study. In general, the two finite element models results compared well in terms of load deflection behaviour and stress distributions. The ratio of ultimate loads predicted by the FEM analyses to the comparative model ranges from 0.87 to 1.04.

Based on the validated FE model, a parametric study was conducted to investigate the effect of strenghtening the coped beam with different reinforcing measures. Those consists of either restrainment of the coped end from lateral translation, or reinforcing of the coped region with longitudinal stiffeners alone or in combination with vertical stiffeners. The study also included the cope dimensions relative to beam dimensions, here represented by the ratio of cope length-to-reduced web hight (c/h_0) and the web depth-to-thickness ratio (h_w/t_w).

Restraining of the coped end would not prevent local web buckling from happening, but an increase of coped beam's capacity was obtained due to improved stabilty of the coped end. However, this only complies to ratios of cope length-to-reduced web hight (c/h_0) lesser than 1. Otherwise the bucklig pattern remained nearly unaltered.

For reinforcement of the coped region in longitudinal direction only, all of the tested specimens experienced local web buckling at the coped end, regardless of the longitudinal stiffener length (L_x). For that purpose, provision of vertical stiffeners in addition is more suitable. Based on the results from the FEM analyses, a set of reinforcement details for strengthening of the coped section is recommended. Depending on the cope length-to-reduced-web hight (c/h_0) and web depth-to-thickness ratio (h_w/t_w) of the coped beams, the design recommendations includes use of longitudinal stiffeners combined with either vertical stiffeners at the loaded position only (H + V1) or double vertical stiffeners (H + V1 + V2).

Future work

On the topic of coped beams and reinforcement measures there are several parameters that can be subject to further research. The following proposals concerns end restrainment of the coped end and the provision of stiffeners:

1. Investigate the effect of restraining the coped end in a way that allow for a certain flexibility. A possible measure will be to restrain the end with a series of spring elements in longitudinal and/or lateral direction.

2. More testing on the proposed reinforcement details have to be conducted to expand and check their applicability. In this thesis only a limited selection of cope dimensions and beam dimensions were tested. Hence, it is of interest to test for a wider range of cope dimensions and beam cross sections. Also, the reinforcement applicability should be checked for different material properties, i.e. for aluminium.

Appendix A

Hand Calculations

A.1 Moment and shear capacity of coped beam

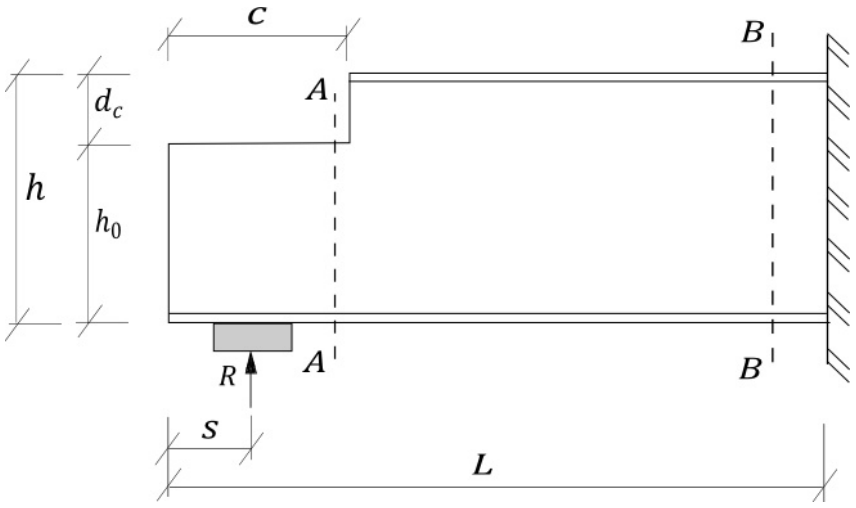

FIGURE A.1: Dimensions of coped beam

G	81 000	N/mm^2	h	300	mm
E	210 000	N/mm^2	b	150	mm
ν	0.3		t_w	7.1	mm
A	5380	mm^2	t_f	10.7	mm
I_{y-y}	83 600 000	mm^4	r	15	mm
W_{y-y}	557 000	mm^3	f_y	355	N/mm^2
S_y	314 000	mm^3			

TABLE A.1: Materail and cross sectional properties of the full beam section

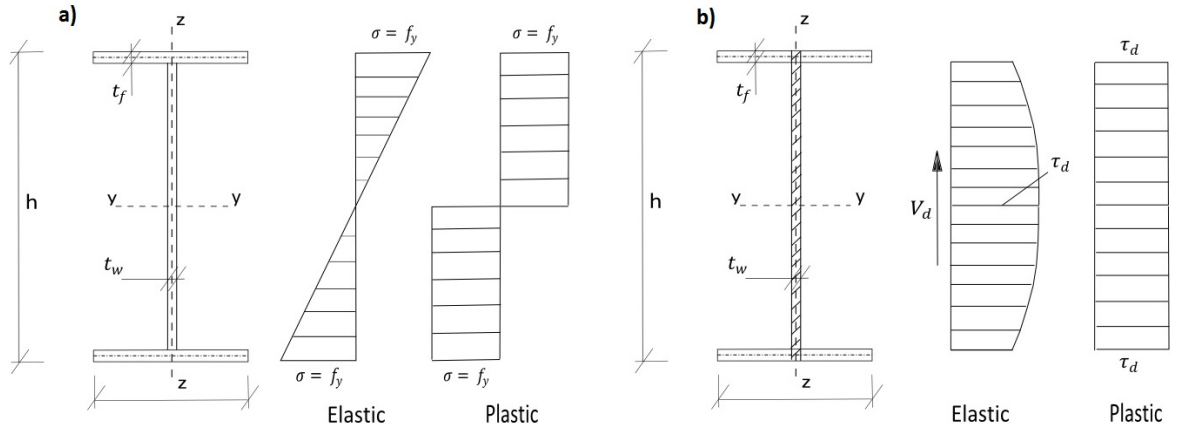

FIGURE A.2: a) Bending stress distribution over full beam section, b) Shear stress distribution over full beam section.

A.1.1 Section A-A - Full beam section

Elastic moment capacity

$$\begin{aligned} M_{el} &= f_y W_{el} = 355 \cdot 557000 \\ &= 197.735 \cdot 10^6 Nmm = 197.735 kNm \\ R_{M,pl} &= M_{M,el}/e = \frac{197.735 \cdot 10^6}{1000 - 30} \\ &= 203851N \approx 203.8kN \end{aligned}$$

Plastic moment capacity

$$\begin{aligned} M_{pl} &= f_y W_{pl} = f_y 2S_y = 355 \cdot 2 \cdot 314000 \\ &= 222.94 \cdot 10^6 Nmm = 222.94 kNm \\ R_{M,pl} &= M_{M,pl}/e = \frac{222.94 \cdot 10^6}{1000 - 30} \\ &= 229835N \approx 229.8kN \end{aligned}$$

Elastic & Plastic shear capacity

$$\begin{aligned} V_{el,Rd} = \tau_d A_v &= \frac{f_y}{\sqrt{3}\gamma_{M0}} A_v = \frac{f_y}{\sqrt{3}\gamma_{M0}} \cdot ht_w \\ &= \frac{355}{\sqrt{3} \cdot 1.0} \cdot 300 \cdot 7.1 \\ &= 436563N \approx 436.6kN \end{aligned}$$

A.1.2 Section B-B - Reduced beam section

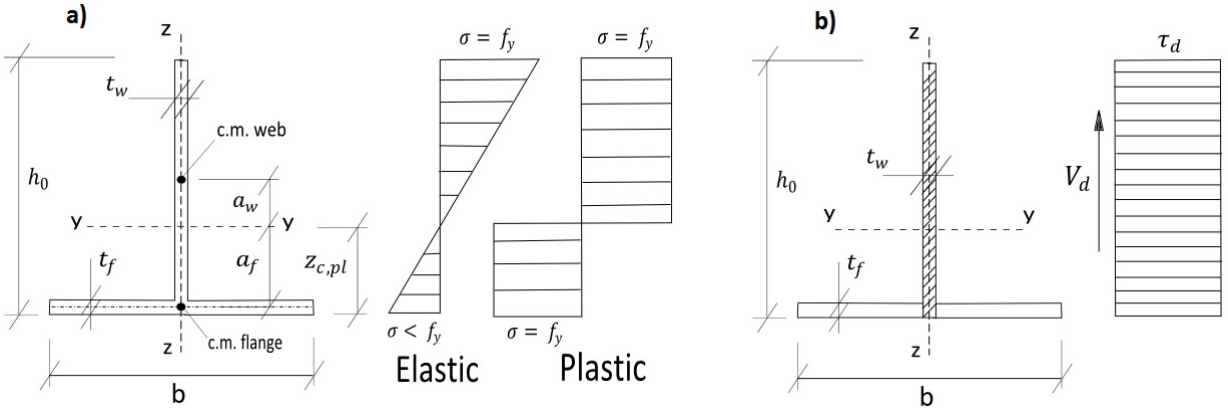

FIGURE A.3: a) Bending stress distribution over the reduced beam section, b) Shear stress distribution over the reduced beam section.

New location of elastic N.A.

$$\begin{aligned} z_{c,el} &= \frac{(a_w h_w t_w) + a_f t_f b}{A_w + A_f} \\ &= \frac{(\frac{h_0+t_f}{2})(h_0 - t_f)t_w + \frac{t_f^2 b}{2}}{t_w(h_0 - t_f) + bt_f} \\ &= \frac{(\frac{h_0+10.7}{2})(h_0 - 10.7) \cdot 7.1 + \frac{10.7^2 \cdot 150}{2}}{7.1 \cdot (h_0 - 10.7) + 150 \cdot 10.7} \end{aligned}$$

Distance from center of masses

$$\begin{aligned} z_f &= z_{c,el} - \frac{t_f}{2} = z_{c,el} - \frac{10.7}{2} \\ z_w &= \frac{h_0 + t_f}{2} - z_{c,el} = \frac{h_0 + 10.7}{2} - z_{c,el} \end{aligned}$$

c	d_c [mm]	h_0 [mm]	$z_{c,el}$ [mm]	z_w [mm]	z_f [mm]	$I_{y,red}$ $[10^6 \cdot mm^4]$
100	50	250	69.6	60.7	64.3	16.7
150	70	230	62.0	58.4	56.6	13.6
200	110	190	47.4	53.0	42.0	8.3

TABLE A.2: Reduced section properties.

$$\begin{aligned} I_{y,red} &= [(\frac{1}{12}bt_f^3) + (bt_f z_f^2)] + [\frac{1}{12}t_w(h_0 - t_f)^3 + t_w(h_0 - t_f)z_w^2] \\ &= [(\frac{1}{12} \cdot 150 \cdot 10.7^3) + (150 \cdot 10.7 \cdot z_f^2)] + [\frac{1}{12} \cdot 7.1 \cdot (h_0 - 10.7)^3 + 7.1 \cdot (h_0 - 10.7) \cdot z_w^2] \end{aligned}$$

New location of plastic N.A.

for $z_{c,pl} < h_w$:

$$\begin{aligned} z_{c,pl} &= \frac{(A_f + A_w)/2}{t_w} = \frac{(bt_f + h_w t_w)/2}{t_w} \\ &= \frac{(150 \cdot 10.7 + h_w \cdot 7.1)/2}{7.1} \end{aligned}$$

for $z_{c,pl} > h_w$:

$$\begin{aligned} z_{c,pl} &= \frac{(A_f + A_w)/2}{t_w} = \frac{(bt_f + h_w t_w)/2}{b} \\ &= \frac{(150 \cdot 10.7 + h_w \cdot 7.1)/2}{150} \end{aligned}$$

Distance from center of mass

$$\begin{aligned} a_w &= \frac{(h_0 - t_f)t_w[\frac{(h_0 - t_f)}{2} + (t_f - z_{c,pl}] + (t_f - z_{c,pl})b\frac{(t_f - z_{c,pl})}{2}}{(h_0 - t_f) + b\frac{(t_f - z_{c,pl}}{2}} \\ &= \frac{(h_0 - 10.7) \cdot 7.1 \cdot [\frac{(h_0 - 10.7)}{2} + (10.7 - z_{c,pl}] + (10.7 - z_{c,pl}) \cdot 150 \cdot \frac{(10.7 - z_{c,pl})}{2}}{(h_0 - 10.7) + 150 \cdot \frac{(10.7 - z_{c,pl}}{2}} \\ a_f &= \frac{z_{c,pl}}{2} \end{aligned}$$

Cope length c	Cope depth d_c [mm]	Reduced web hight h_w [mm]	Location N.A. $z_{c,pl}$ [mm]		a_w [mm]	a_f [mm]
100	50	239.3	17.3	(web)	116.3	11.7
150	70	219.3	10.5	(flange)	108.2	5.3
200	110	179.3	9.6	(flange)	80.4	4.8

TABLE A.3: Reduced section properties.

c	d_c [mm]	W_{pl} $[10^3 \cdot mm^3]$	A_v $[mm^2]$	$W_{pl,red}$ $[10^3 \cdot mm^3]$	$A_{v,red}$ $[mm^2]$
100	50	628.0	2130	217.7	1775
150	70	628.0	2130	184.7	1633
200	110	628.0	2130	126.6	1349

TABLE A.4: Reduced section properties.

Elastic Moment capacity

$$\begin{aligned} M_{el,red} &= f_y W_{el,red} = f_y \frac{I_{y,red}}{h_0 - z_{c,el}} \\ &= 355 \cdot \frac{I_{y,red}}{h_0 - z_{c,el}} \\ R_{M,el,red} &= \frac{M_{el,red}}{c - 30} \end{aligned}$$

Plastic Moment capacity

$$\begin{aligned} M_{pl,red} &= f_y W_{pl,red} = f_y \frac{A_{red}}{2}(a_w + a_f) \\ &= 355 \cdot \frac{A_{red}}{2}(a_w + a_f) \\ R_{M,pl,red} &= \frac{M_{pl,red}}{c - 30} \end{aligned}$$

Plastic & Elastic Shear capacity

$$\begin{aligned} V_{pl,Rd,red} &= \tau_d A_{v,red} = \frac{f_y}{\sqrt{3}\gamma_{M0}} A_{v,red} \\ &= \frac{f_y}{\sqrt{3}\gamma_{M0}} h_0 t_w = \frac{355}{\sqrt{3} \cdot 1.0} \cdot h_0 \cdot t_w \end{aligned}$$

c	d_c [mm]	$R_{M,pl}$ [kN]	$V_{pl\&el,Rd}$ [kN]	$R_{M,pl,red}$ [kN]	$V_{pl\&el,Rd,red}$ [kN]	$R_{M,el}$ [kN]	$R_{M,el,red}$ [kN]
100	50	229.8	436.6	1104.1	363.8	203.8	469.6
150	70	229.8	436.6	546.6	334.7	203.8	238.6
200	110	229.8	436.6	264.4	276.5	203.8	122.1

TABLE A.5: Results elastic and plastic moment and shear capacity of the full and reduced beam section $t_w = 7.1$ mm.

c	d_c [mm]	$R_{M,pl}$ [kN]	$V_{pl\&el,Rd}$ [kN]	$R_{M,pl,red}$ [kN]	$V_{pl\&el,Rd,red}$ [kN]	$R_{M,el}$ [kN]	$R_{M,el,red}$ [kN]
100	50	204.2	246.0	631.2	205.0	169.1	312.2
150	70	204.2	246.0	312.6	188.6	169.1	157.2
200	110	204.2	246.0	152.2	155.8	169.1	78.9

TABLE A.6: Results elastic and plastic moment and shear capacity of the full and reduced beam section $t_w = 4.0$ mm.

A.2 Moment of shear capacities of beam section with reduced web thickness

The calculations are similar as in previous section, now with $t_w = 4.0$ mm. However, need to update the cross sectional properties.

$$
\begin{aligned}
I_{y,1} &= \sum_i^n \int_A y^2 dA + a^2 A = 2\Big[\big(\frac{1}{12} \cdot 150 \cdot 10.7^3\big) + \big(10.7 \cdot 144.65^2\big)\Big] \\
&+ \big(\frac{1}{12} \cdot 4.0 \cdot 278.6^3\big) + 2\Big[\big(\frac{1}{12} \cdot 4.0 \cdot 15^3\big) + \big(4.0 \cdot 15\dot{1}31.8^2\big)\Big] \\
&= 69308126 \approx 69.3 \cdot 10^6 mm^4 \\
W_{el,1} &= \frac{I_{y,1}}{y} = \frac{69.3 \cdot 10^6}{150} = 462054 \approx 462000 mm^3 \\
S_{y,1} &= \sum_i^n \int_A {}_i y_i dA_i = (150 \cdot 10.7 \cdot 144.65) \\
&+ (4.0 \cdot 139.3 \cdot 69.65) + (4.0 \cdot 15 \cdot 131.8) \\
&= 278880.23 \approx 279000 mm^3 \\
W_{pl,1} &= 2S_{y,1} = 2 \cdot 279000 = 558000 mm^3
\end{aligned}
$$

G	81 000	N/mm^2	h	300	mm
E	210 000	N/mm^2	b	150	mm
ν	0.3		t_w	7.1	mm
A	5380	mm^2	t_f	10.7	mm
I_{y-y}	83 600 000	mm^4	r	15	mm
W_{y-y}	557 000	mm^3	s_s	40	mm
S_y	314 000	mm^3	c_s	10	mm
f_y	355	N/mm^2	h_w	278.6	mm

TABLE A.7: Materail and cross sectional properties of the reduced beam section

A.3 Resistance to transverse forces

Following calcultions are conducted on basis of the design recommendations found in NS-EN 1993 1-5

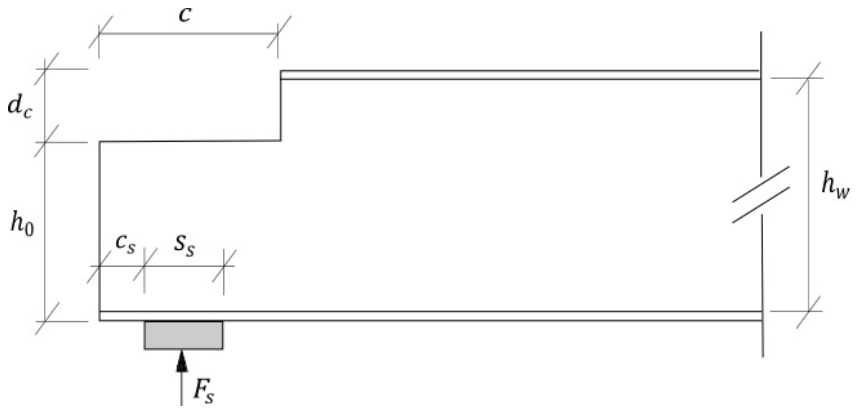

FIGURE A.4: Dimensions of coped beam.

$$k_F = 2 + \frac{6(s_s + c)}{h_w} \leq 6$$
$$= 2 + \frac{6 \cdot (40 + 10)}{278.6} = 3.077 < 6$$

$$F_{cr} = 0.9 k_F E \frac{t_w^3}{h_w} = 0.9 \cdot 3.077 \cdot 210000 \cdot \frac{7.1^3}{278.6}$$
$$= 747062N \approx 747kN$$

$$
\begin{aligned}
l_e &= \frac{k_F E t_w^2}{2 f_{yw} h_w} \leq s_s + c_s \\
&= \frac{3.077 \cdot 210000 \cdot 7.1^2}{2 \cdot 355 \cdot 278.6} = 164.66 > 50 \\
&= 50mm \\
m_1 &= \frac{f_{yf} b}{f_{yw} t_w} = \frac{355 \cdot 150}{355 \cdot 7.1} \\
&= 21.13 \\
m_2 &= 0.02 \left(\frac{h_w}{t_f}\right)^2 = 0.02 \cdot \left(\frac{278.6}{10.7}\right)^2 \\
&= 13.56
\end{aligned}
$$

$$
l_y = min \begin{cases}
{}_e + t_f \sqrt{\frac{m_1}{2} + \left(\frac{l_e}{t_f}\right)^2 + m_2} \\
= 50 + 10.7 \cdot \sqrt{\frac{21.13}{2} + \left(\frac{50}{10.7}\right)^2 + 13.56} \\
= 122.54mm \\
l_e + t_f \sqrt{m_1 + m_2} \\
= 50 + 10.7 \cdot \sqrt{21.13 + 13.56} \\
= 113.01mm
\end{cases}
$$

$$
l_y = 113.01mm
$$

$$
\begin{aligned}
\lambda_F &= \sqrt{\frac{f_{yw} t_w l_y}{F_{cr}}} = \sqrt{\frac{355 \cdot 7.1 \cdot 113.01}{747.06}} = 0.578 \\
\chi_F &= \frac{0.5}{\lambda_F} = \frac{0.5}{0.578} = 0.810
\end{aligned}
$$

$$
\begin{aligned}
F_{Rd} &= \frac{f_{yw} \chi_F l_y t_w}{\gamma_{M1}} = \frac{355 \cdot 0.810 \cdot 113.01 \cdot 7.1}{1.0} \\
&= 230727N \approx 230.7kN
\end{aligned}
$$

Appendix B

FEM Results

In the following pages are the FEM results for a selection of the reinforced coped beams presented. The results are presented in terms of the beams lateral displacement pattern at maximum applied load, the Von Mises stress distribution of the loaded coped beams and plots of the force-displacement relation. The selection includes the following tested specimens:

1. Cope details A ($c = 100$ mm, $d_c = 50$ mm), B ($c = 150$ mm, $d_c = 70$ mm) and C ($c = 200$ mm, $d_c = 110$ mm)
2. Coped beam reinforced with
   - Longitudinal reinforcement only (H) for stiffener lengths 200, 400 and 800 mm
   - Longitudinal reinforcement combined with vertical stiffeners at either loaded position (H + V1), at the coped corner (H + V2) or at both locations (H + V1 + V2) for longitudinal stiffener lengths 200, 400 and 800 mm
3. The web thickness is 7.1 mm

100-50-H-200-7.1

$F_{max} = 249.37$ **kN**
$U2_{max} = 9.55$ **mm**

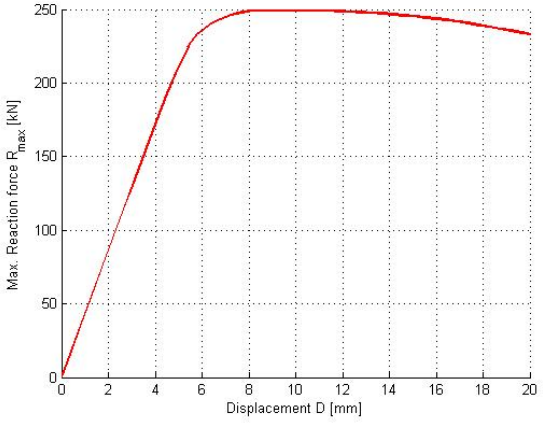

Lateral displacement at max. applied load

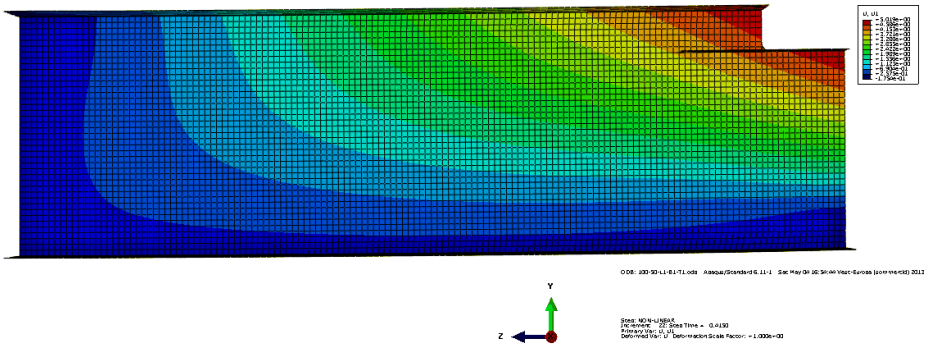

Mises stress distribution at $U2 = 30$ mm

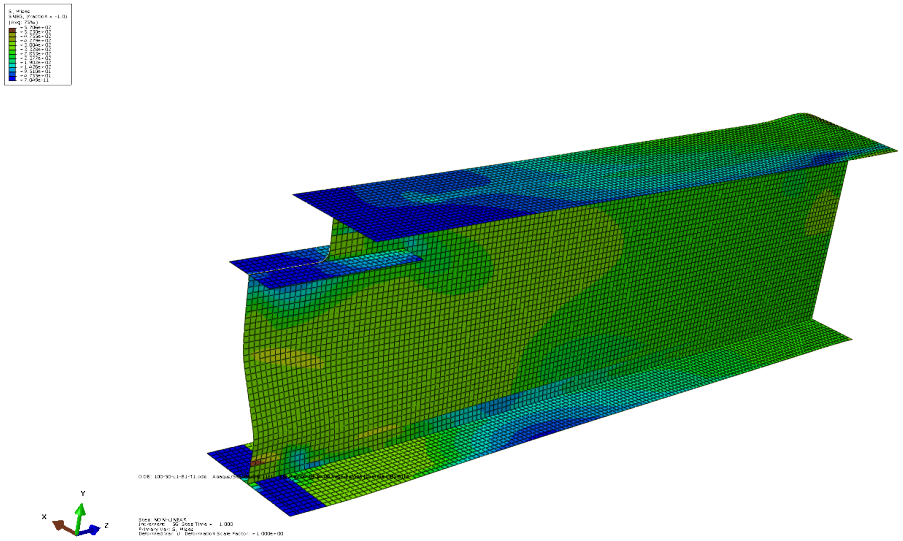

100-50-H-400-7.1

$F_{max} = 227.32$ **kN**
$U2_{max} = 8.63$ **mm**

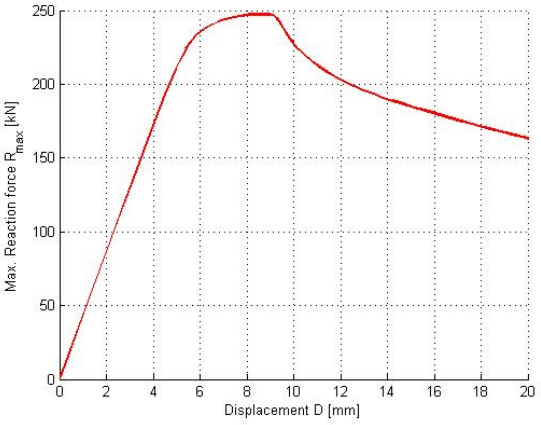

Lateral displacement at max. applied load

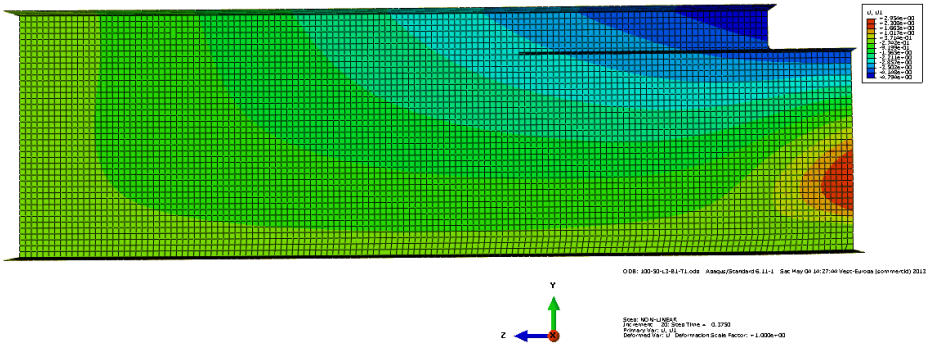

Mises stress distribution at $U2 = 30$ mm

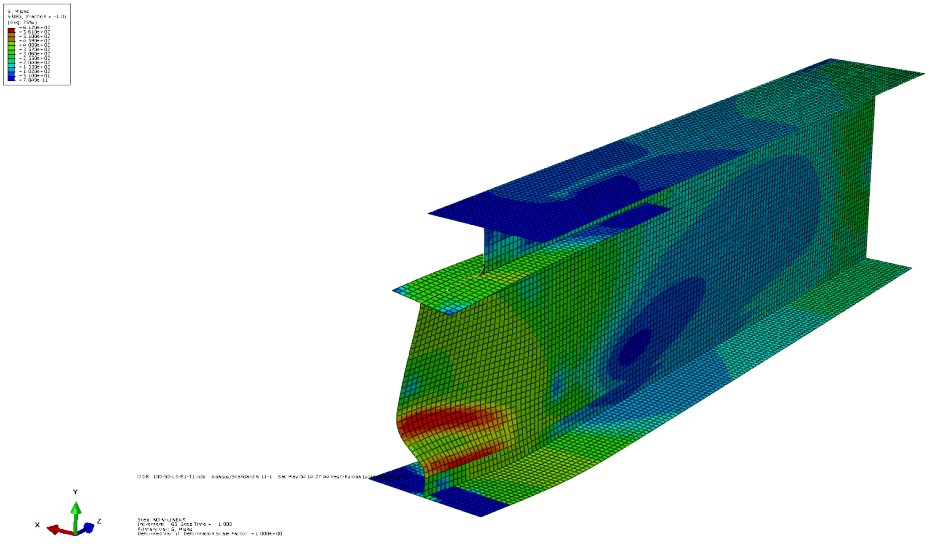

100-50-H-800-7.1

$F_{max} = 243.86$ **kN**
$U2_{max} = 7.65$ **mm**

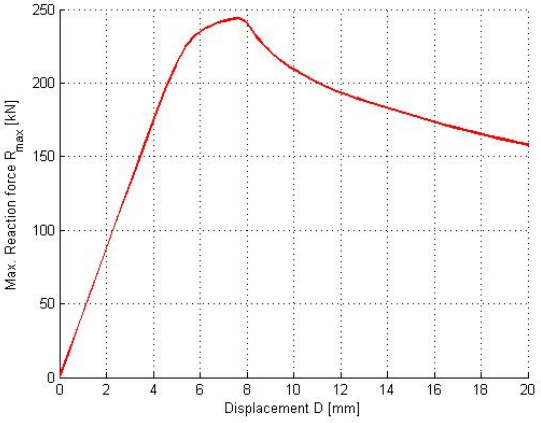

Lateral displacement at max. applied load

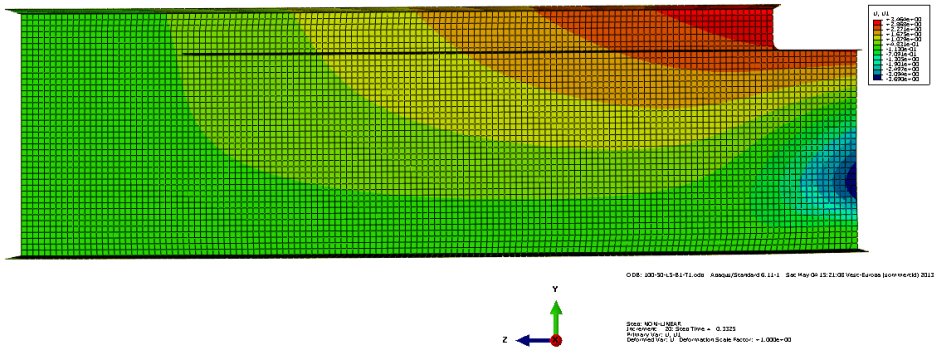

Mises stress distribution at $U2 = 30$ mm

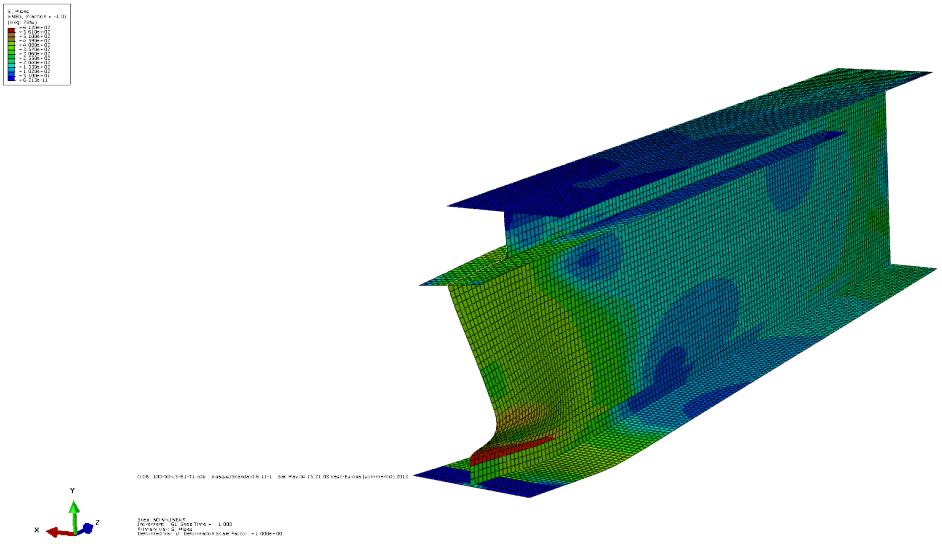

150-70-H-200-7.1

$F_{max} = 248.32$ **kN**
$U2_{max} = 8.63$ **mm**

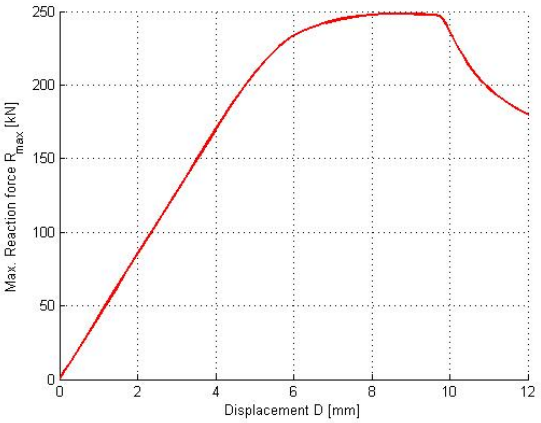

Lateral displacement at max. applied load

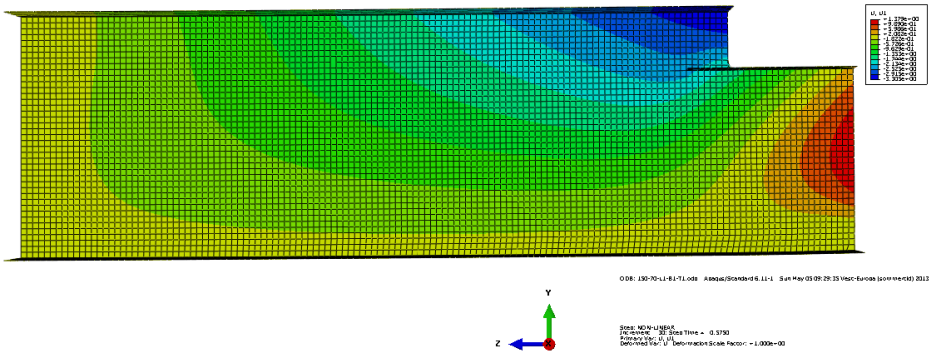

Mises stress distribution at $U2 = 30$ mm

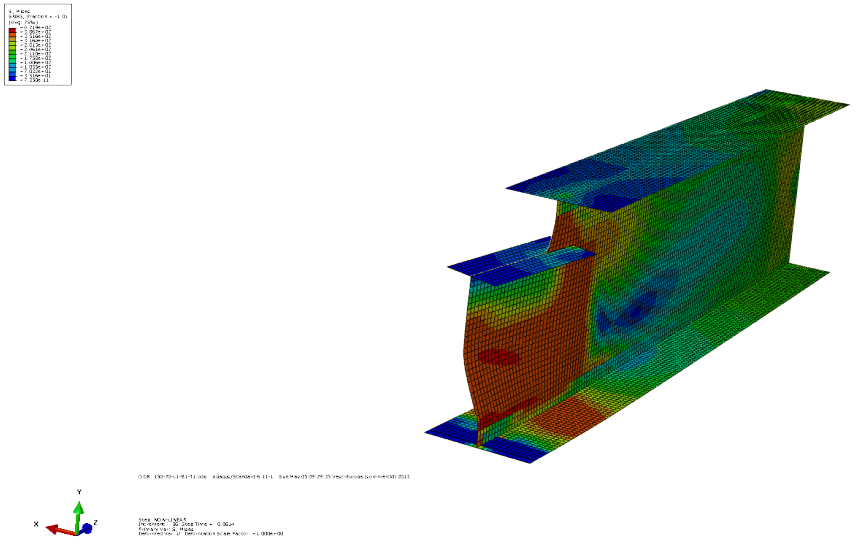

150-70-H-400-7.1

$F_{max} = 247.56$ **kN**
$U2_{max} = 9.23$ **mm**

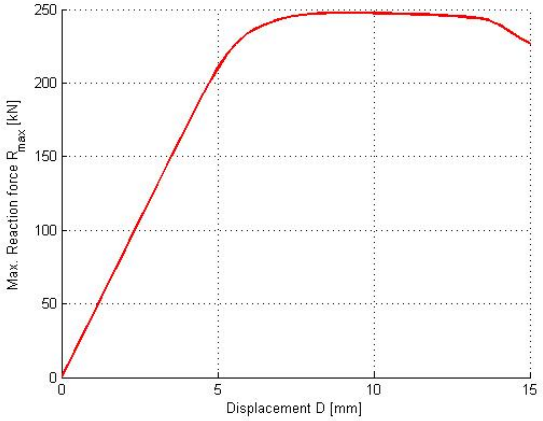

Lateral displacement at max. applied load

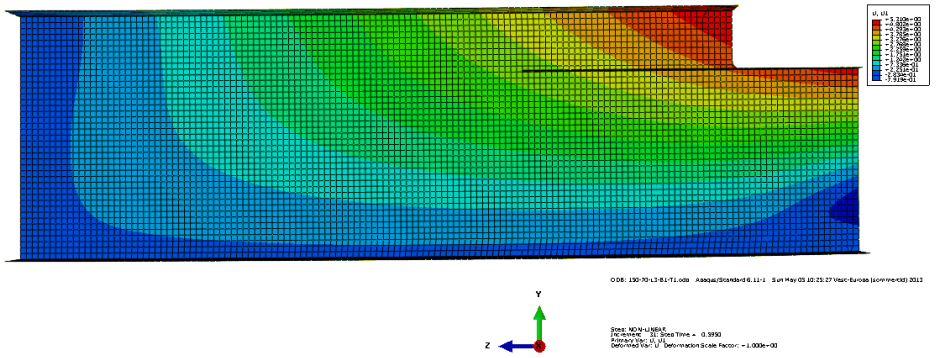

Mises stress distribution at $U2 = 30$ mm

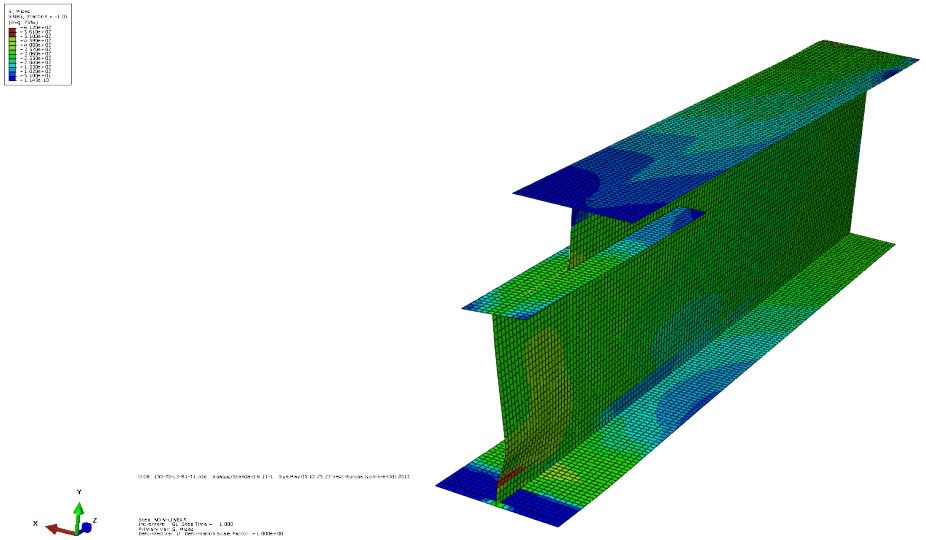

150-70-H-800-7.1

$F_{max} = 247.47\mathbf{kN}$
$U2_{max} = 9.23\mathbf{mm}$

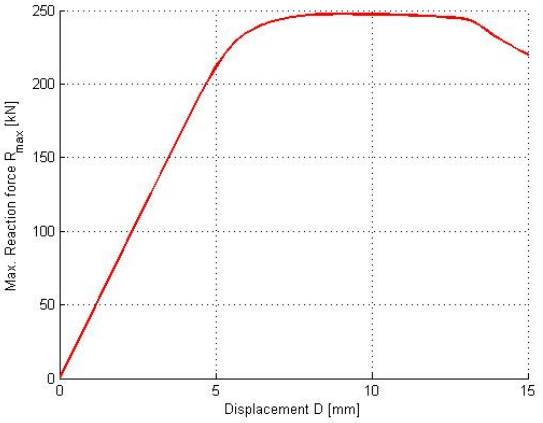

Lateral displacement at max. applied load

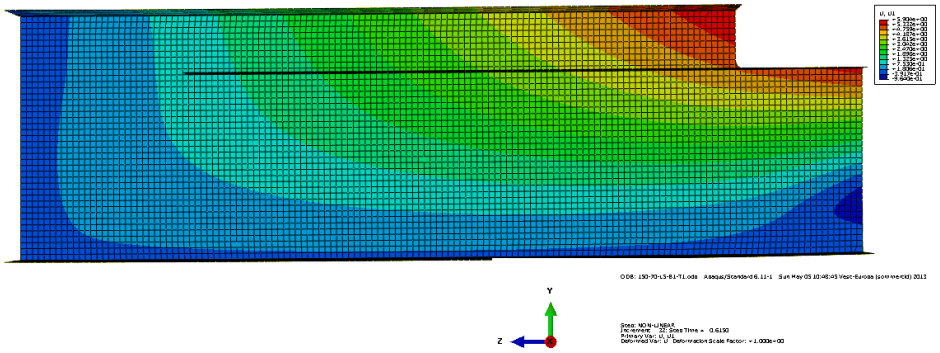

Mises stress distribution at $U2 = 30$ mm

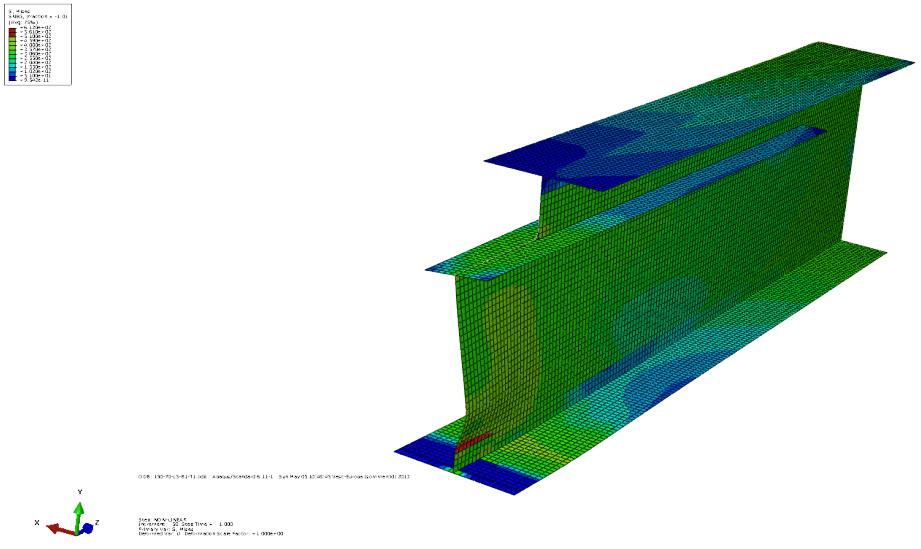

200-110-H-200-7.1

$F_{max} = 181.88$ **kN**
$U2_{max} = 5.55$ **mm**

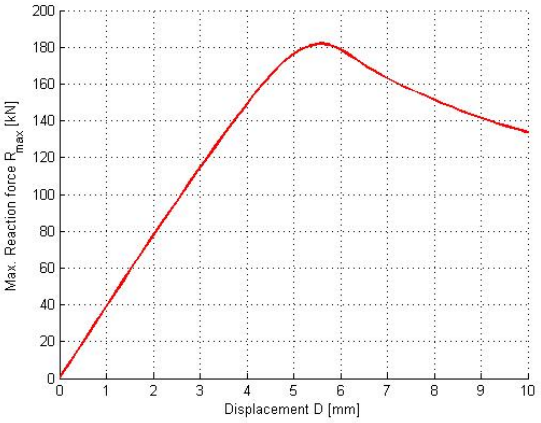

Lateral displacement at max. applied load

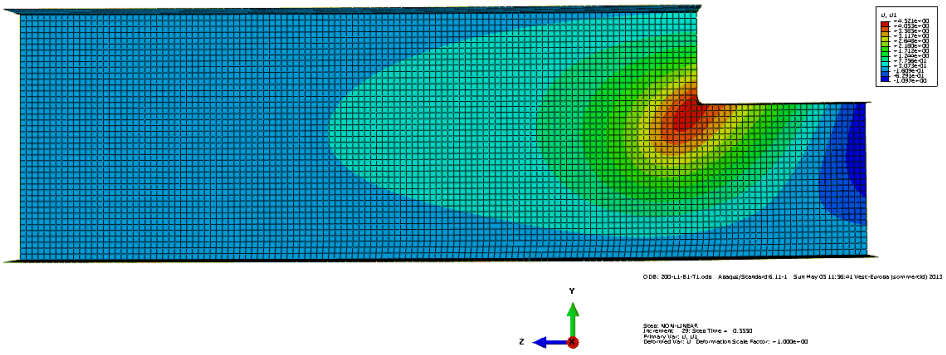

Mises stress distribution at $U2 = 10$ mm

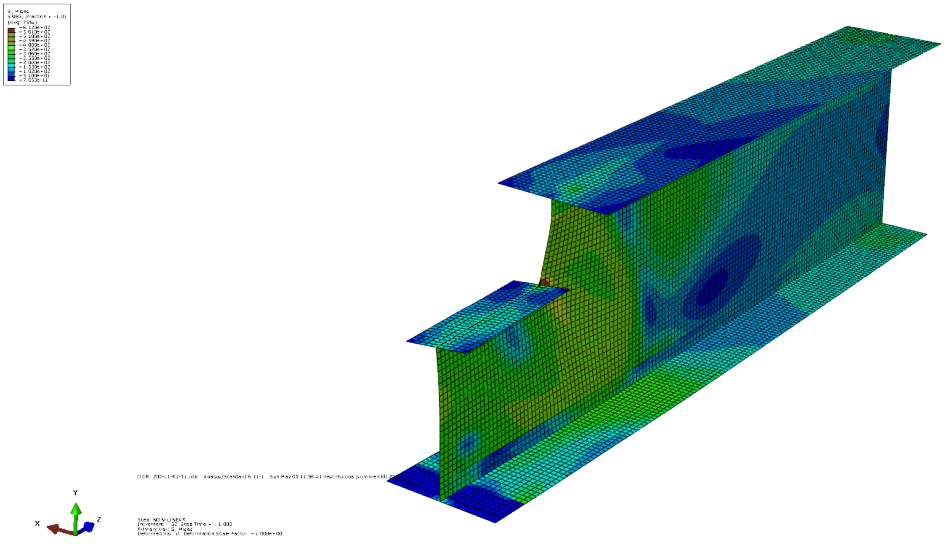

200-110-H-400-7.1

$F_{max} = 245.82$ **kN**
$U2_{max} = 10.01$ **mm**

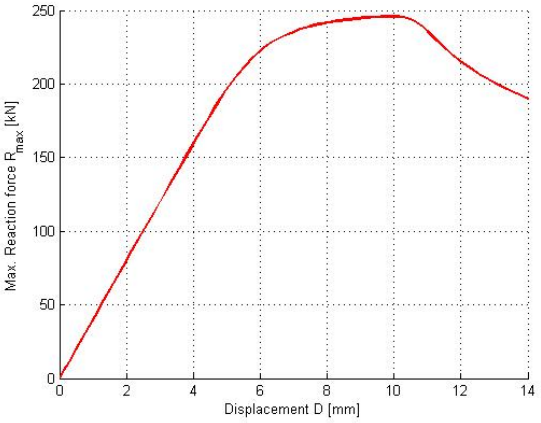

Lateral displacement at max. applied load

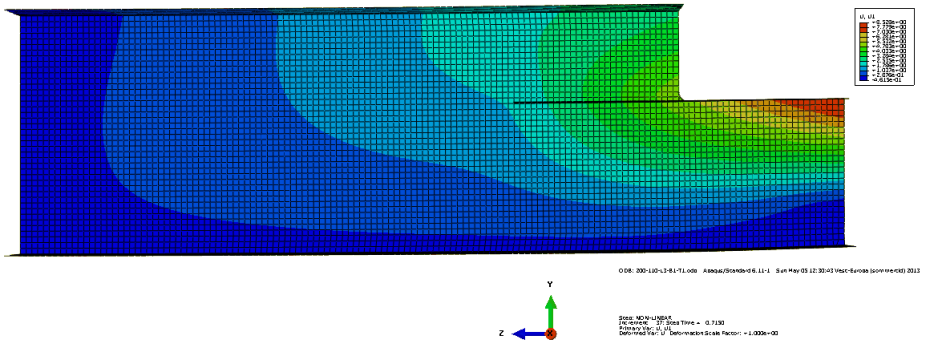

Mises stress distribution at $U2 = 14$ **mm**

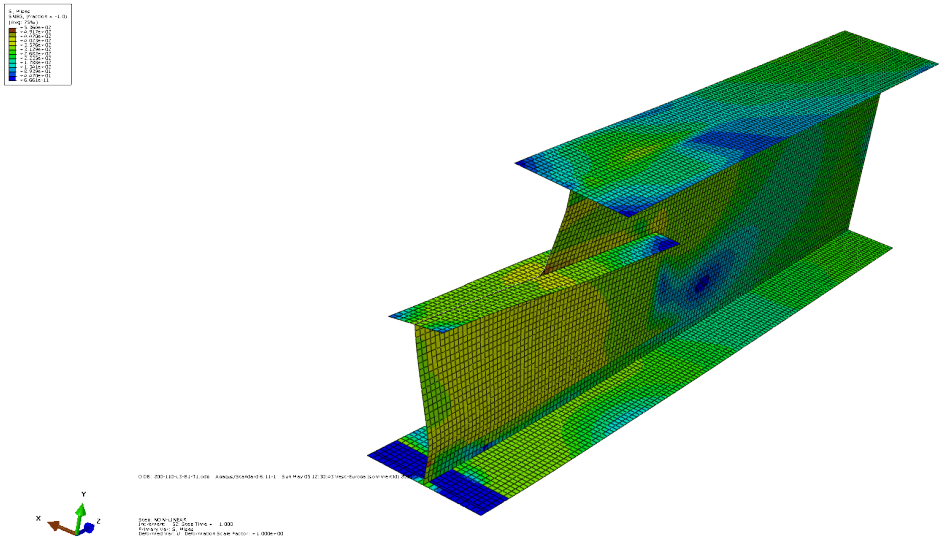

200-110-H-800-7.1

$F_{max} = 246.87$ **kN**
$U2_{max} = 10.35$ **mm**

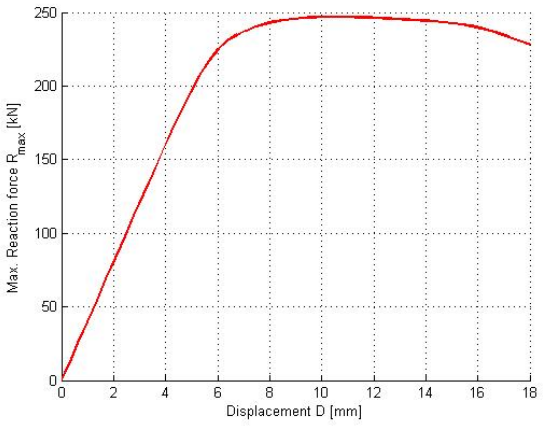

Lateral displacement at max. applied load

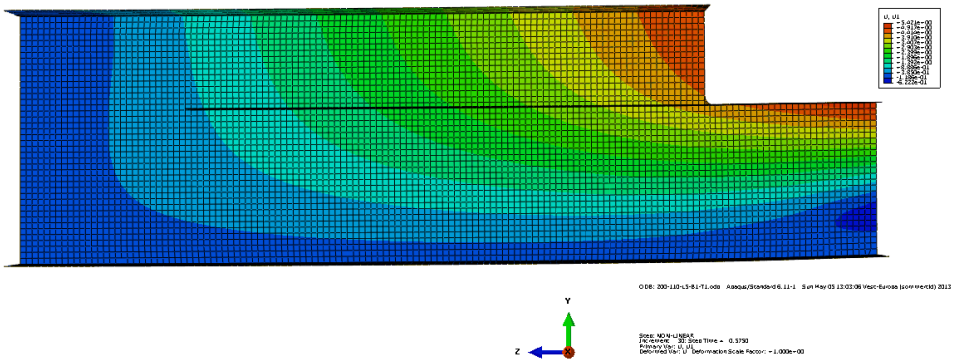

Mises stress distribution at $U2 = 18$ **mm**

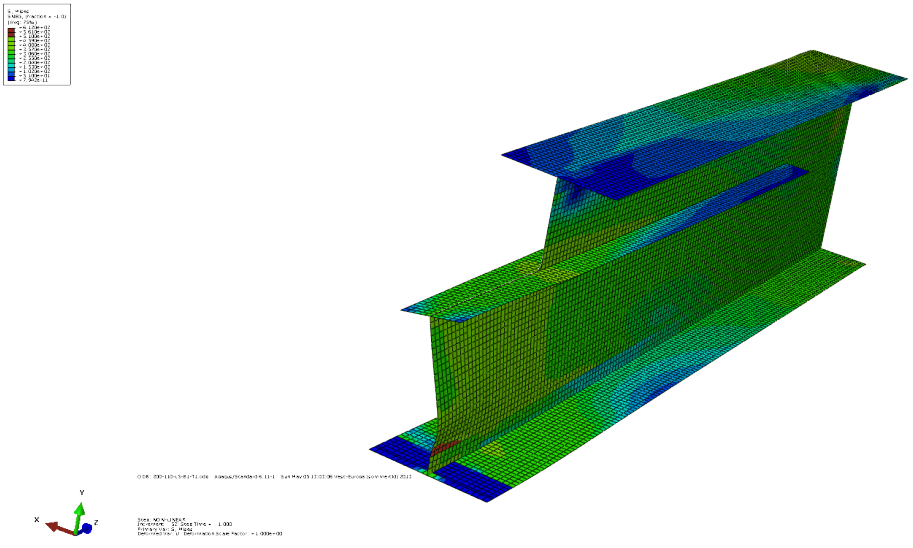

100-50-H+V1-200-7.1

$F_{max} = 251.88$ **kN**
$U2_{max} = 14.74$ **mm**

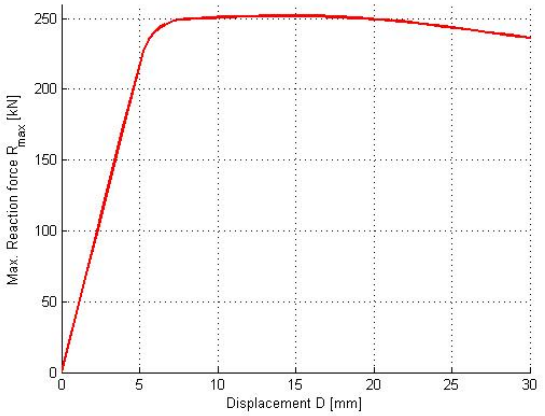

Lateral displacement at max. applied load

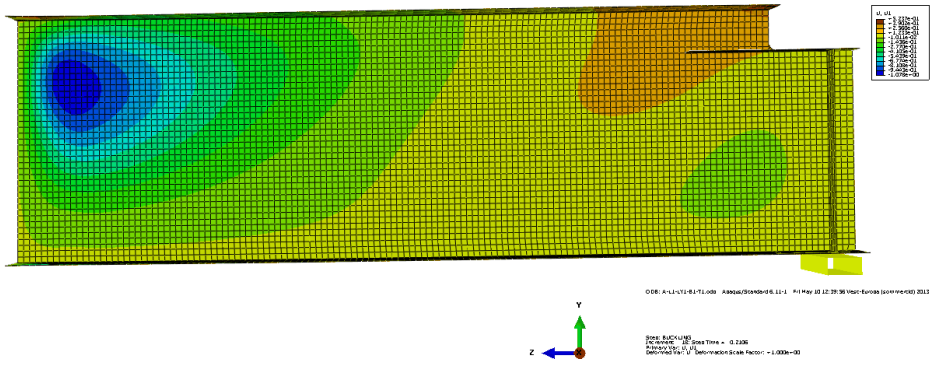

Mises stress distribution at $U2 = 30$ mm

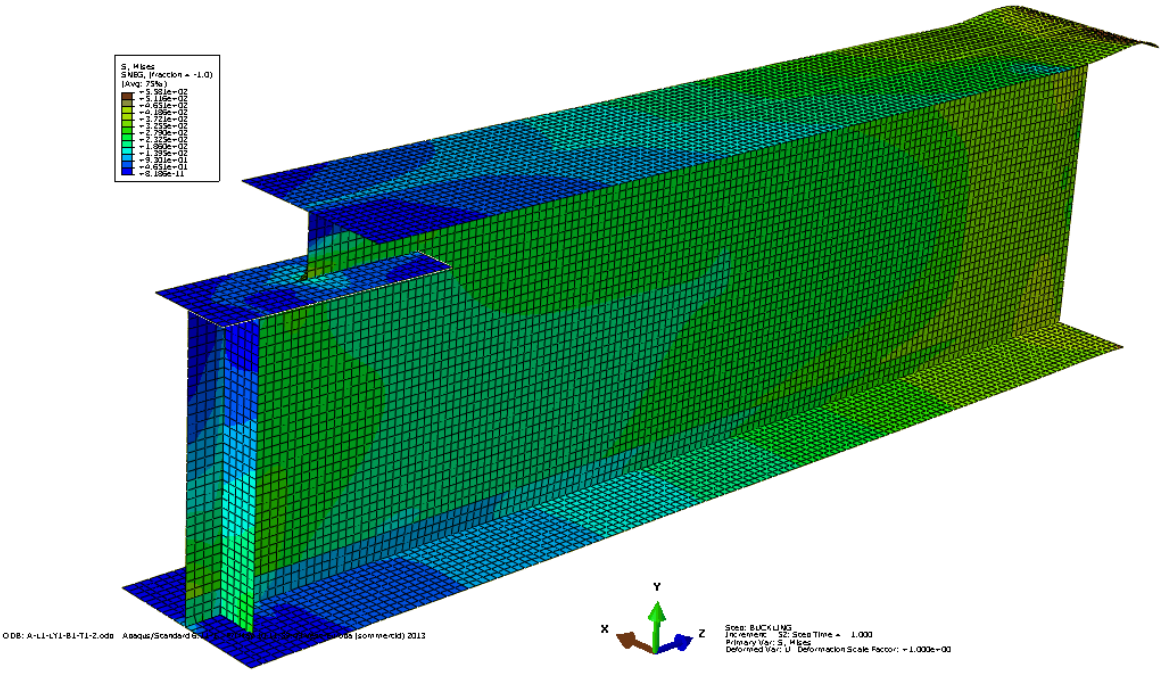

100-50-H+V1-400-7.1

$F_{max} = 250.60$ **kN**
$U2_{max} = 12.45$ **mm**

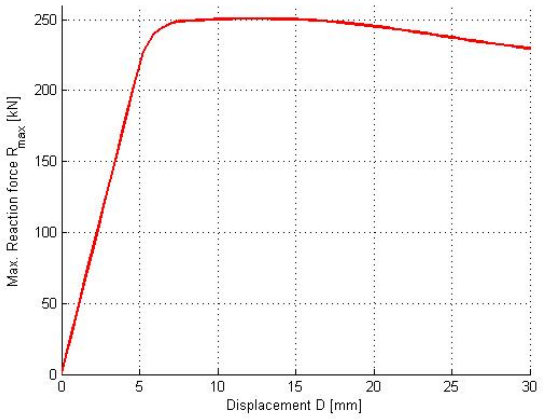

Lateral displacement at max. applied load

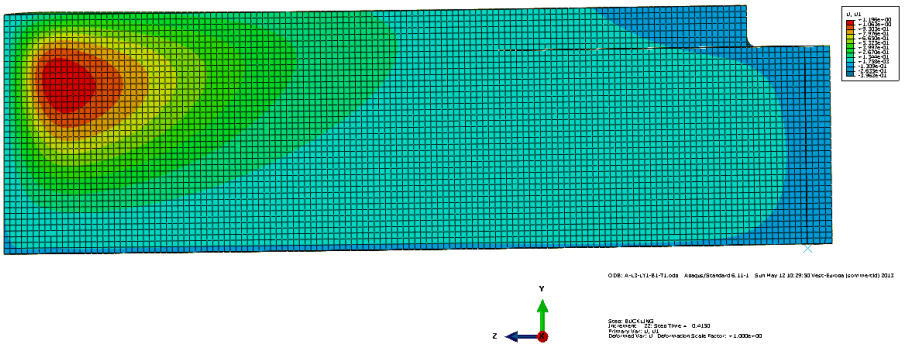

Mises stress distribution at $U2 = 30$ mm

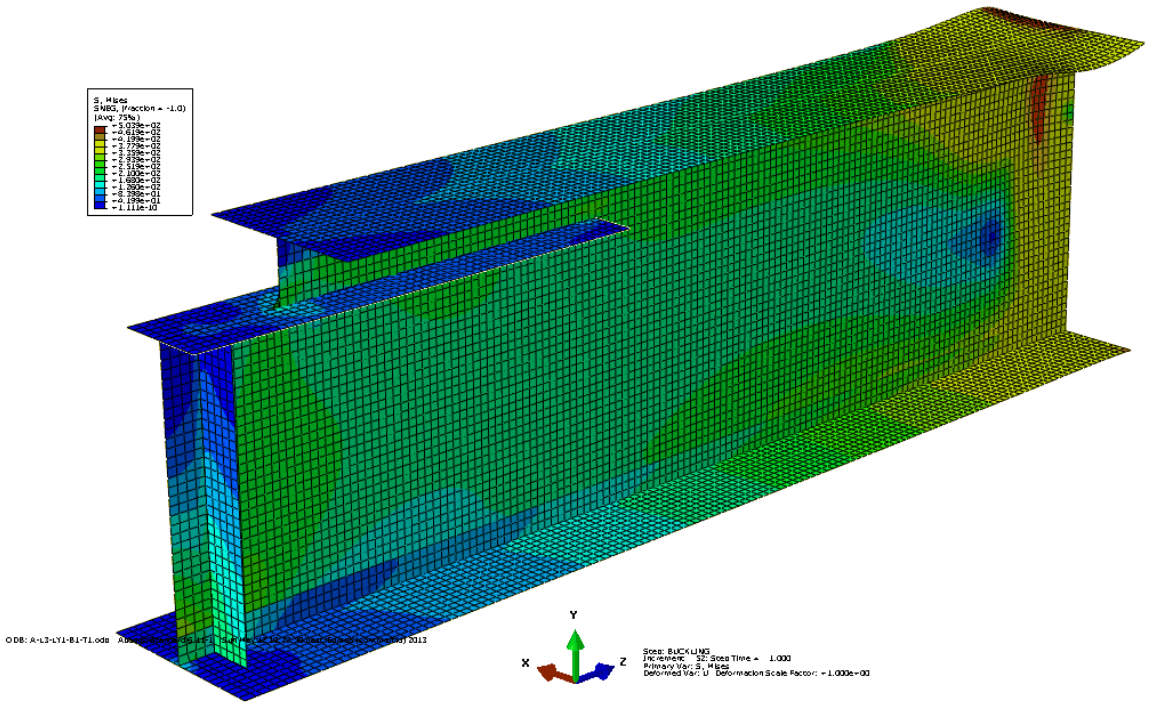

100-50-H+V1-800-7.1

$F_{max} = 253.28$ **kN**
$U2_{max} = 18.03$ **mm**

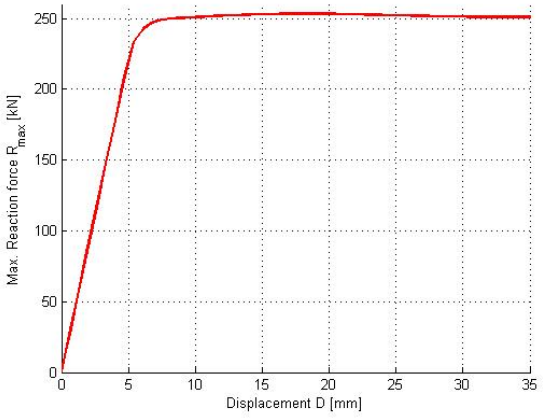

Lateral displacement at max. applied load

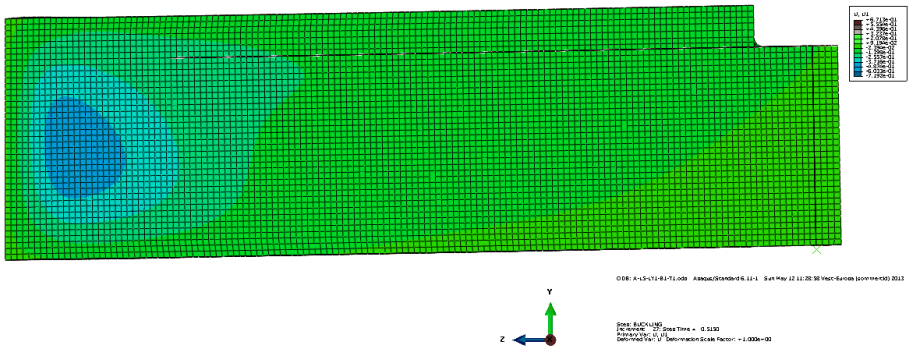

Mises stress distribution at $U2 = 35$ mm

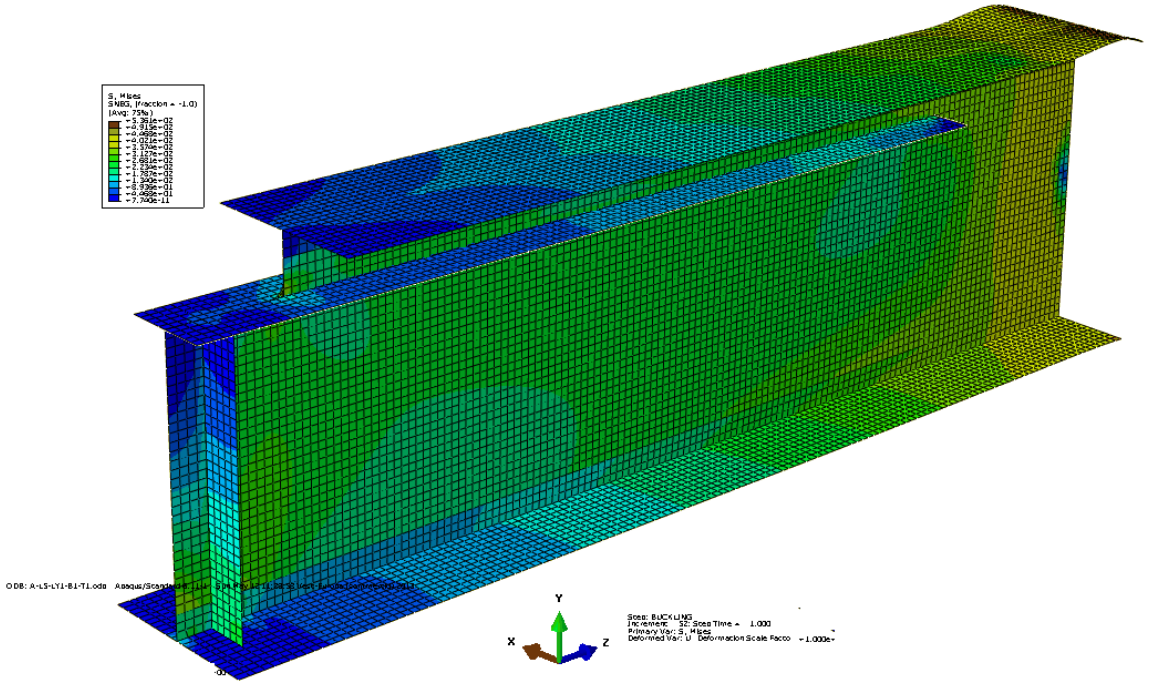

150-70-H+V1-200-7.1

$F_{max} = 250.68$ **kN**
$U2_{max} = 11.25$ **mm**

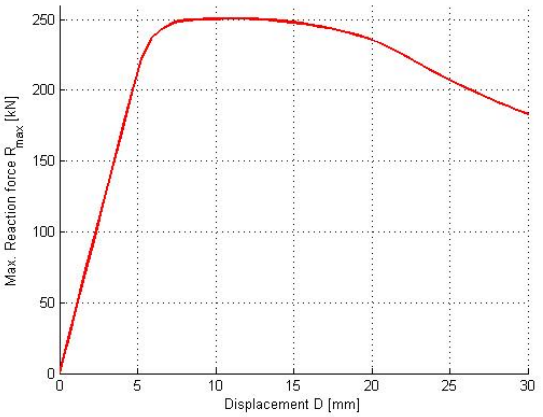

Lateral displacement at max. applied load

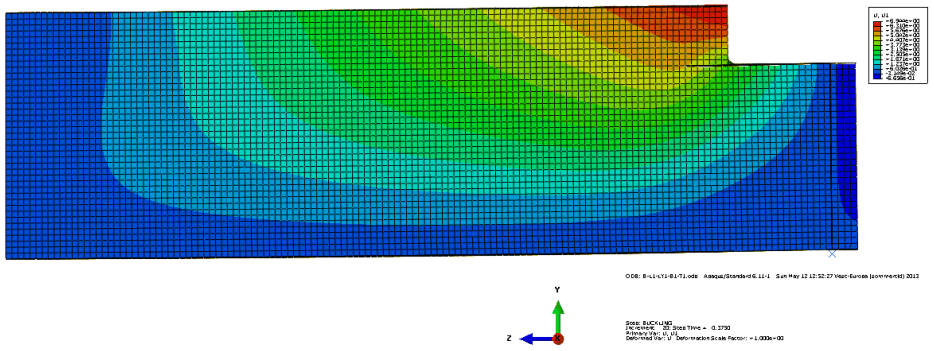

Mises stress distribution at $U2 = 30$ mm

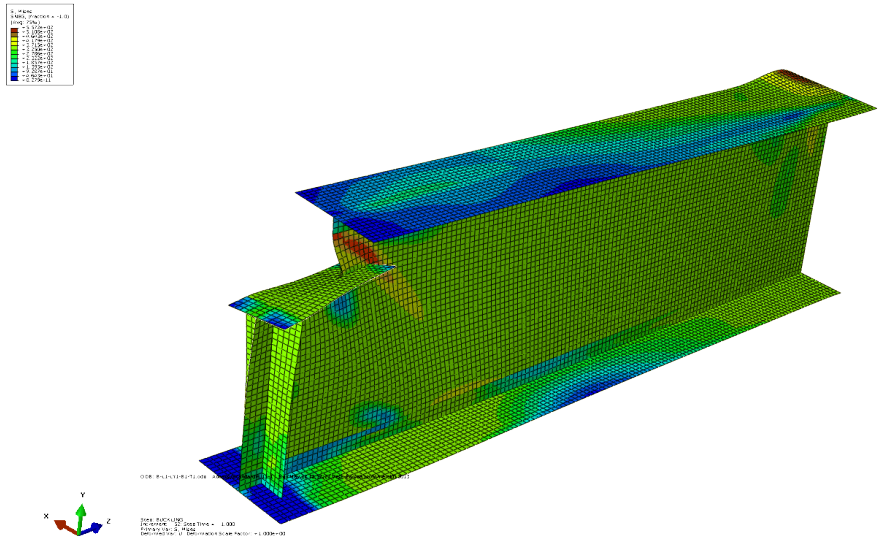

150-70-H+V1-400-7.1

$F_{max} = 253.26$ **kN**
$U2_{max} = 18.73$ **mm**

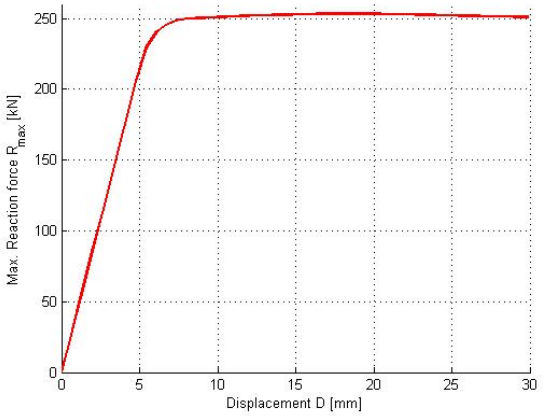

Lateral displacement at max. applied load

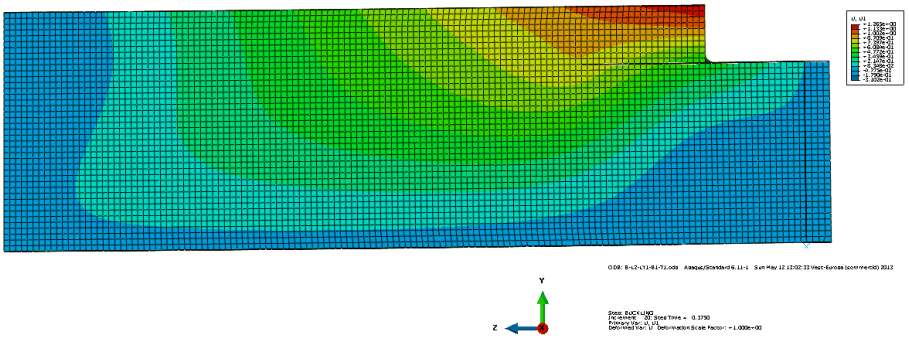

Mises stress distribution at $U2 = 30$ mm

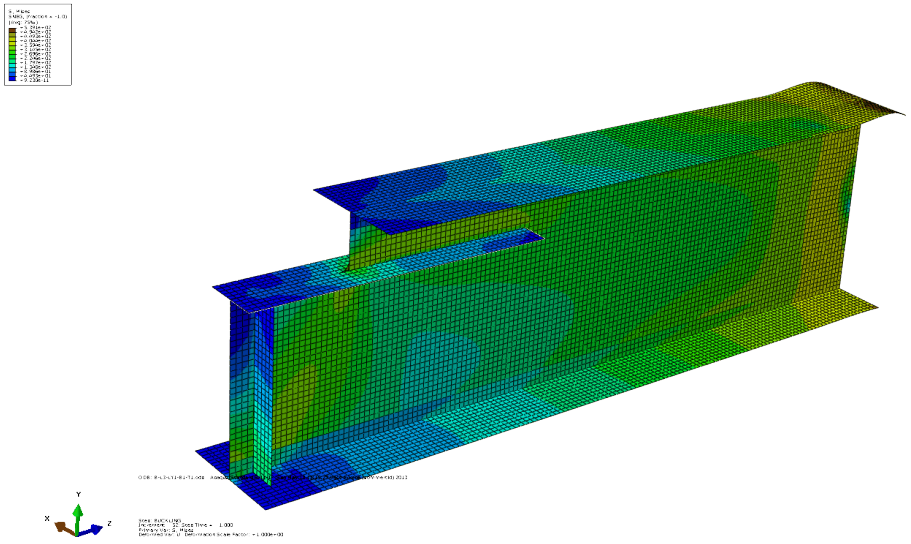

150-70-H+V1-800-7.1

$F_{max} = 253.30$ **kN**
$U2_{max} = 18.73$ **mm**

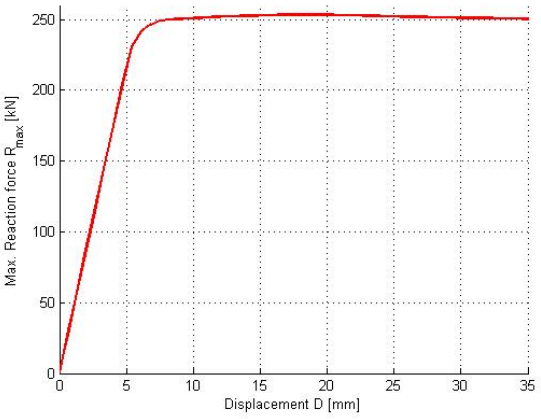

Lateral displacement at max. applied load

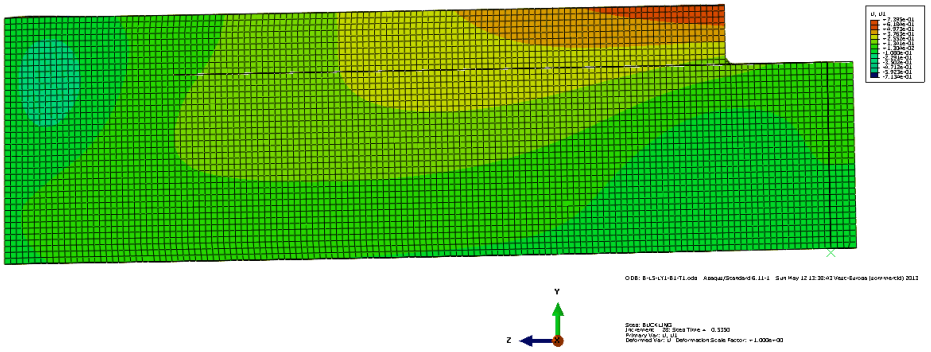

Mises stress distribution at $U2 = 35$ **mm**

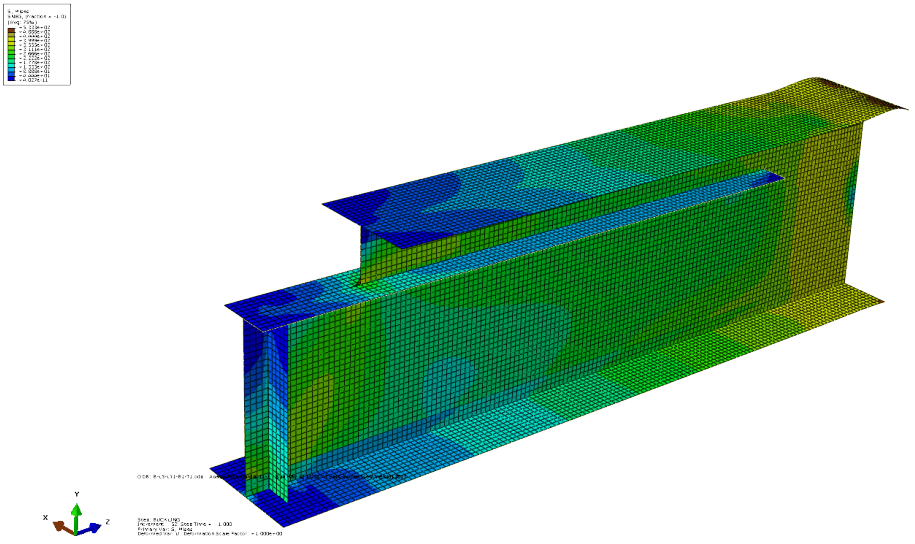

200-110-H+V1-200-7.1

$F_{max} = 200.47$ **kN**
$U2_{max} = 5.90$ **mm**

Lateral displacement at max. applied load

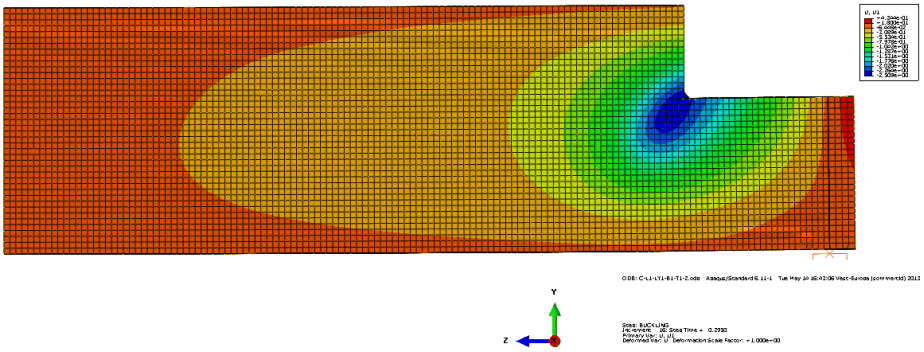

Mises stress distribution at $U2 = 10$ **mm**

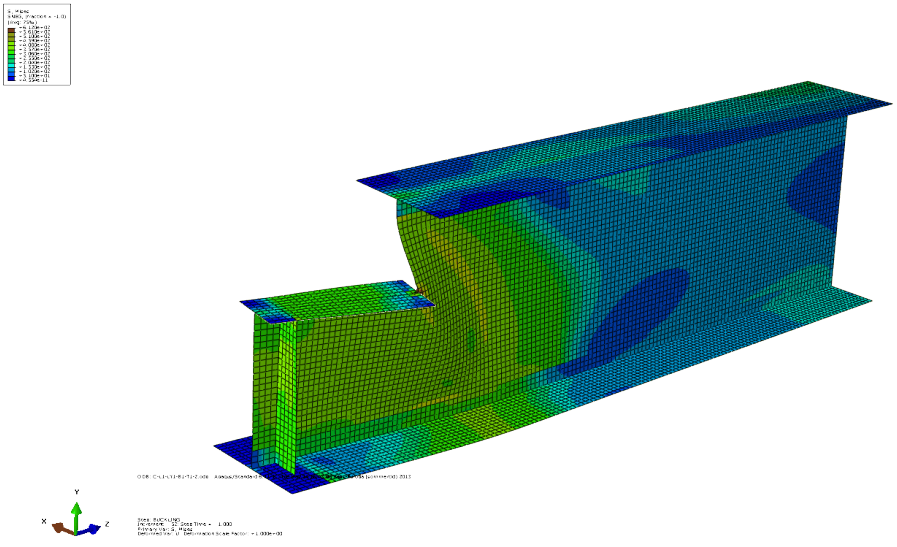

200-110-H+V1-400-7.1

$F_{max} = 250.90$ **kN**
$U2_{max} = 12.38$ **mm**

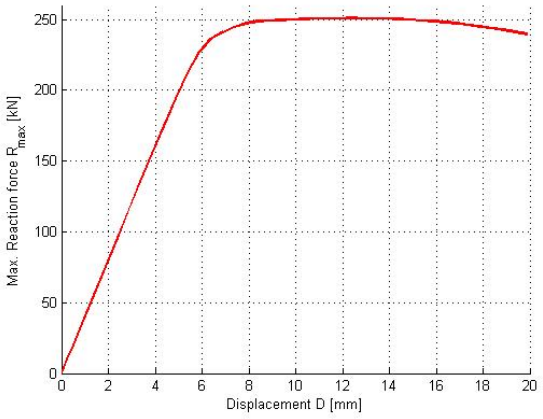

Lateral displacement at max. applied load

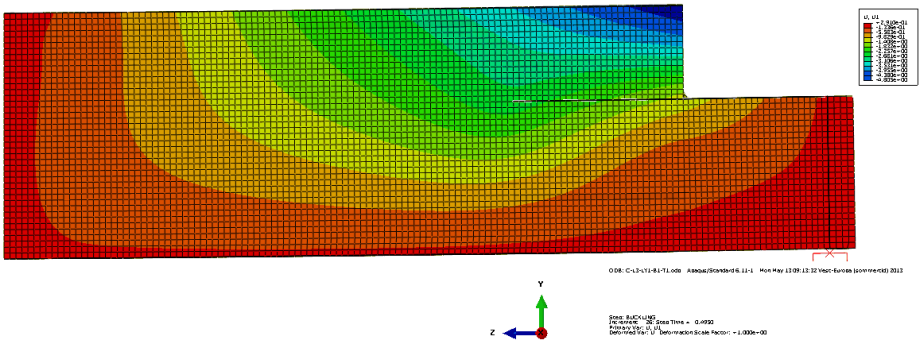

Mises stress distribution at $U2 = 20$ **mm**

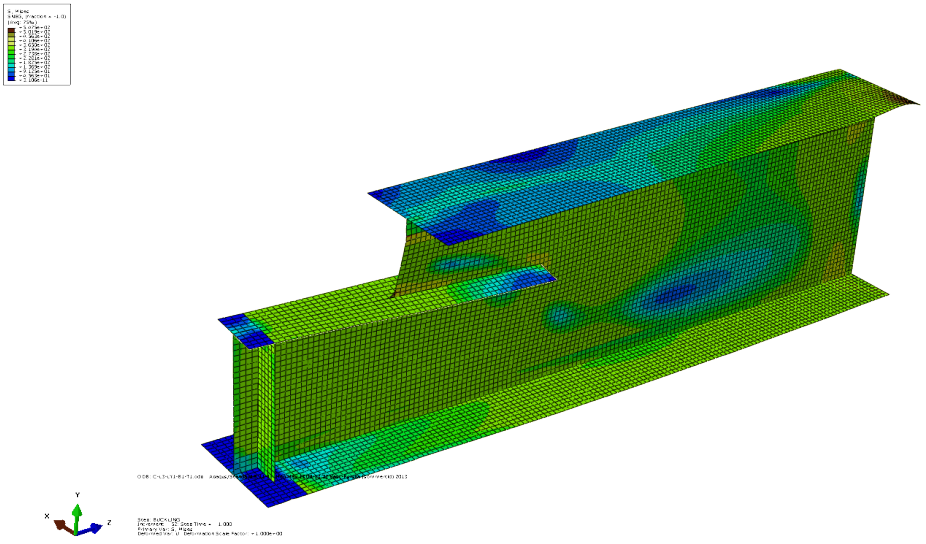

200-110-H+V1-800-7.1

$F_{max} = 252.94$ **kN**
$U2_{max} = 19.43$ **mm**

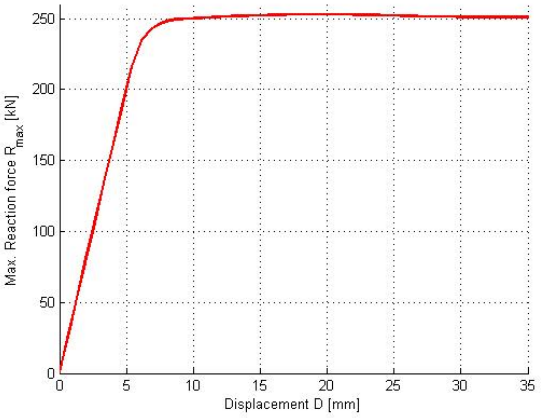

Lateral displacement at max. applied load

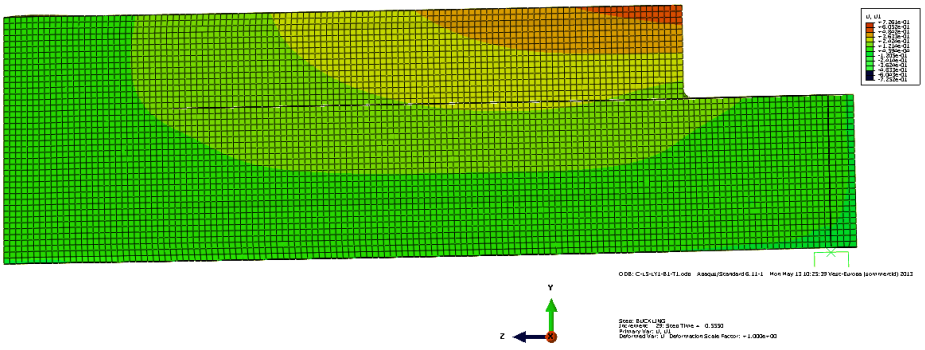

Mises stress distribution at $U2 = 35$ mm

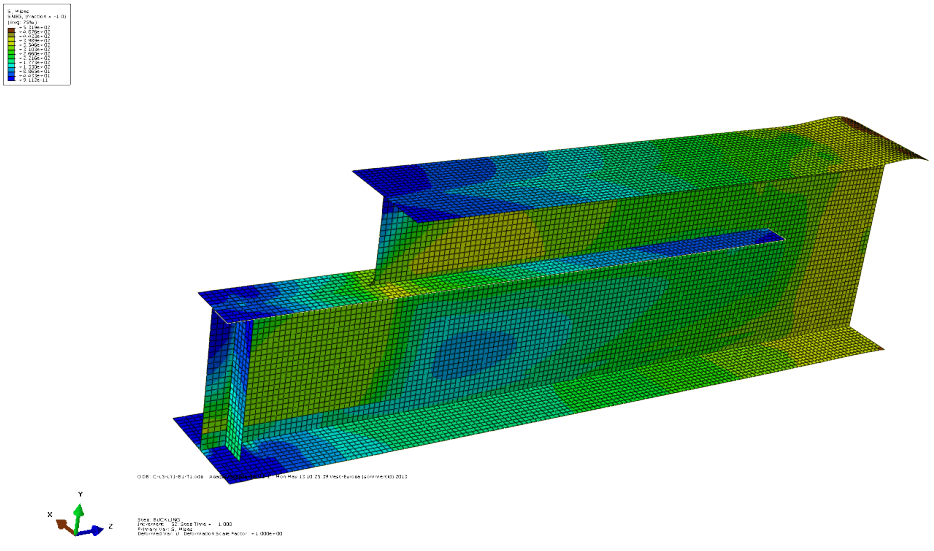

100-50-H+V2-200-7.1

$F_{max} = 253.20$ **kN**
$U2_{max} = 18.73$ **mm**

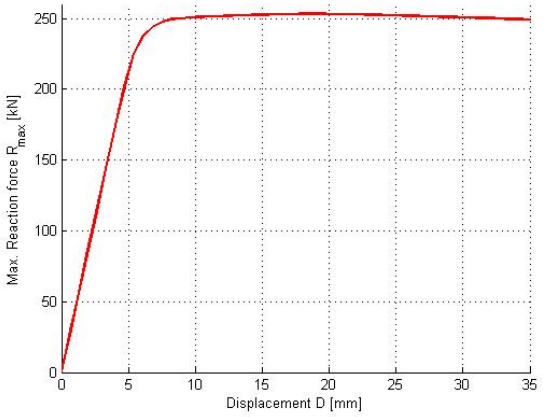

Lateral displacement at max. applied load

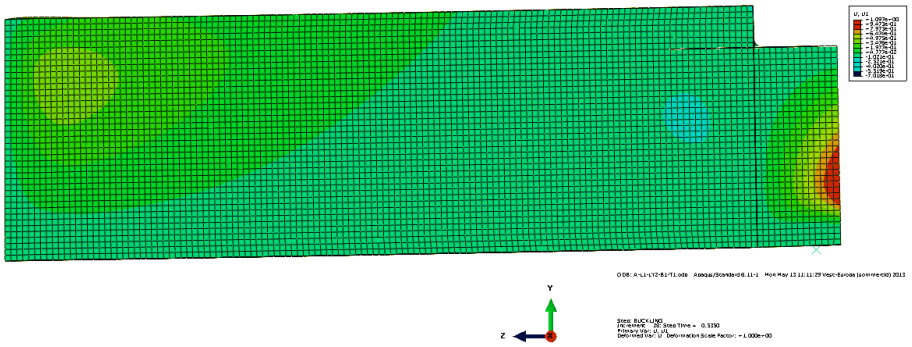

Mises stress distribution at $U2 = 35$ **mm**

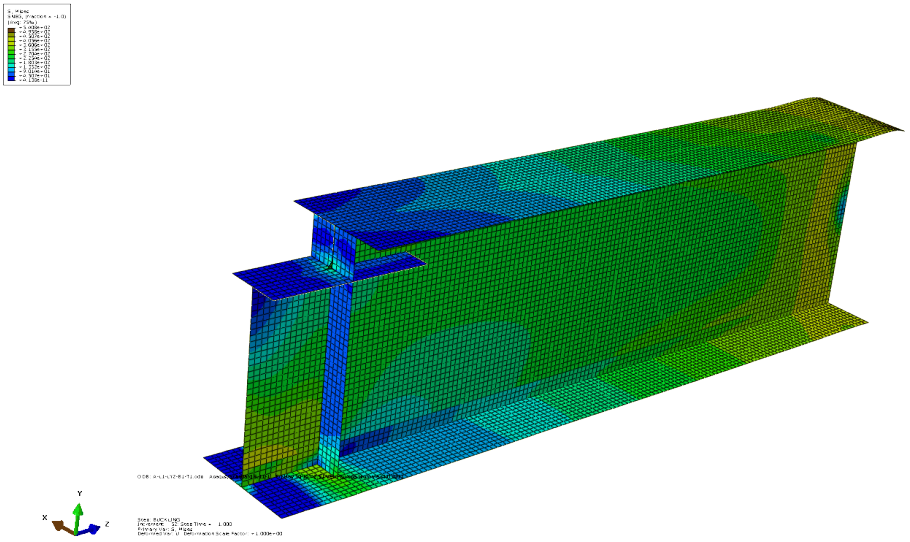

100-50-H+V2-400-7.1

$F_{max} = 253.21$ **kN**
$U2_{max} = 18.73$ **mm**

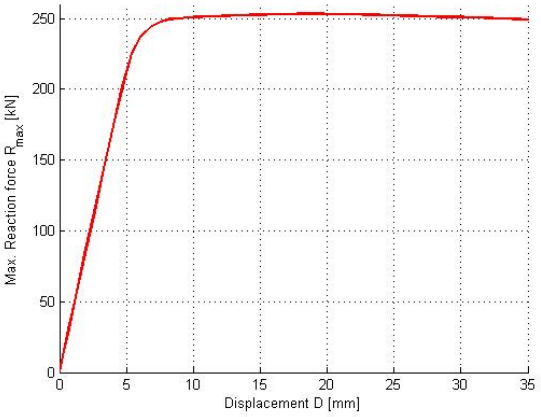

Lateral displacement at max. applied load

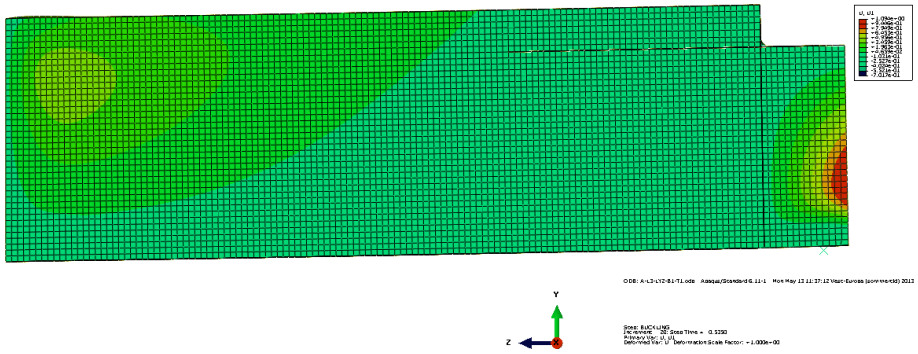

Mises stress distribution at $U2 = 35$ mm

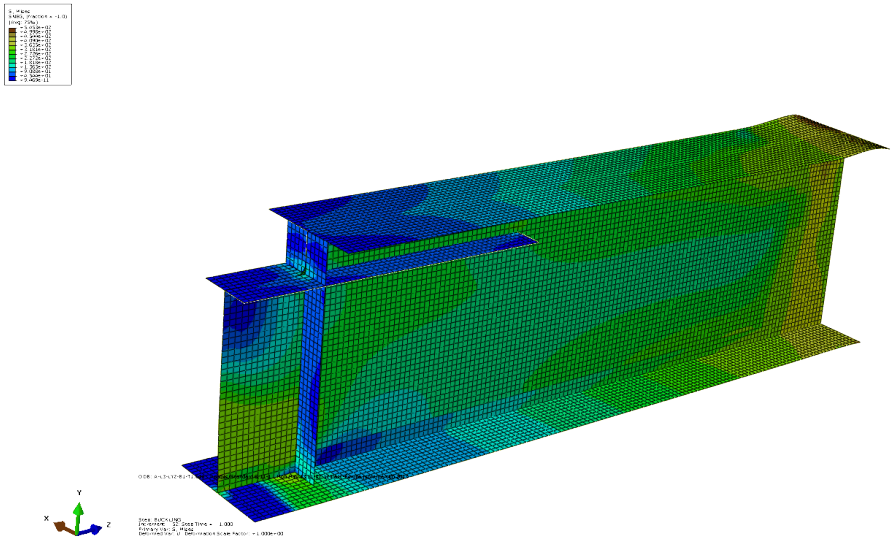

100-50-H+V2-800-7.1

$F_{max} = 253.27$ **kN**
$U2_{max} = 18.73$ **mm**

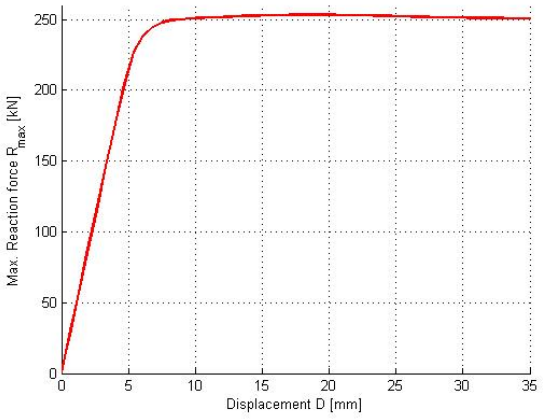

Lateral displacement at max. applied load

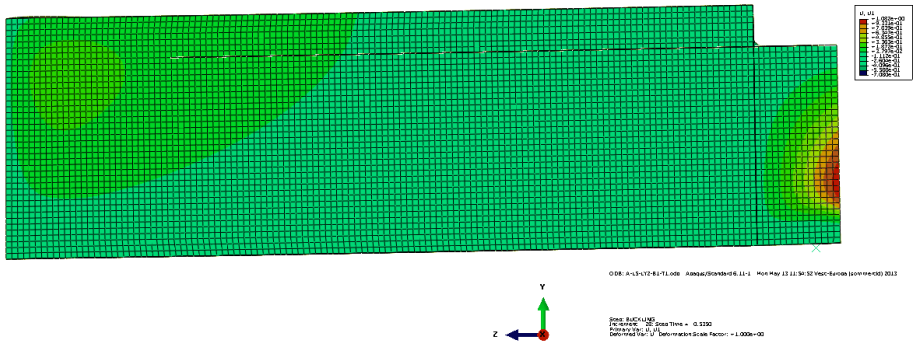

Mises stress distribution at $U2 = 35$ mm

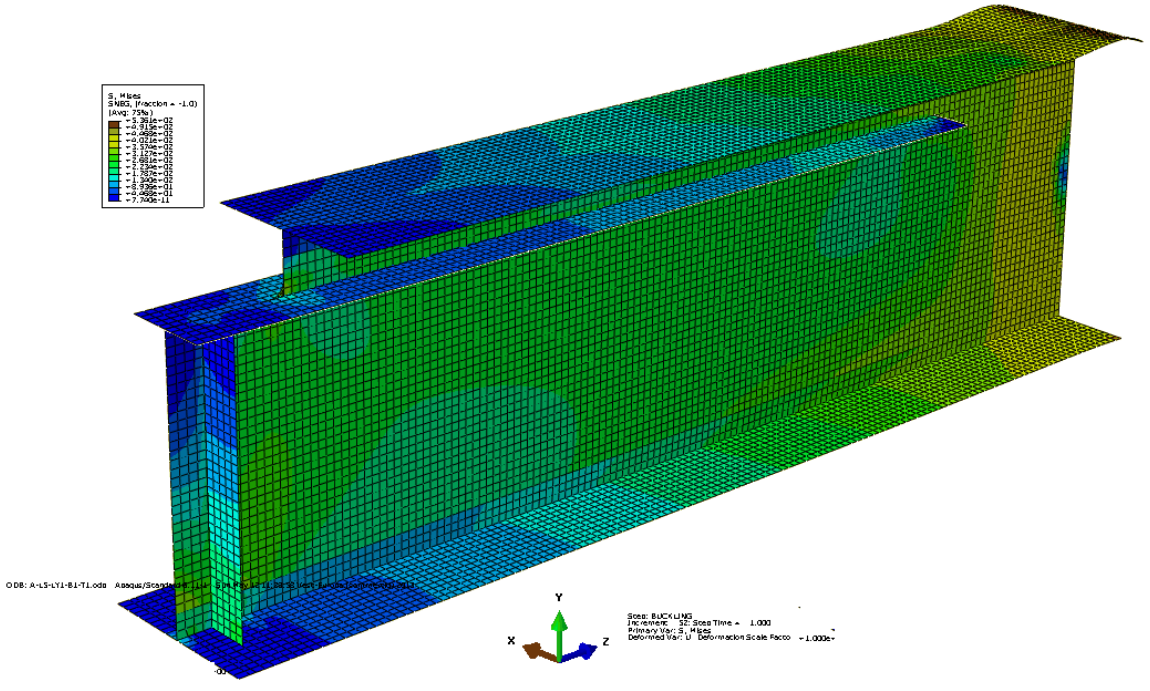

150-70-H+V2-200-7.1

$F_{max} = 253.31$ **kN**
$U2_{max} = 19.65$ **mm**

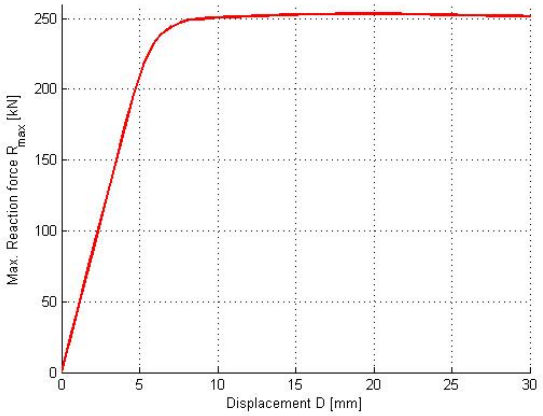

Lateral displacement at max. applied load

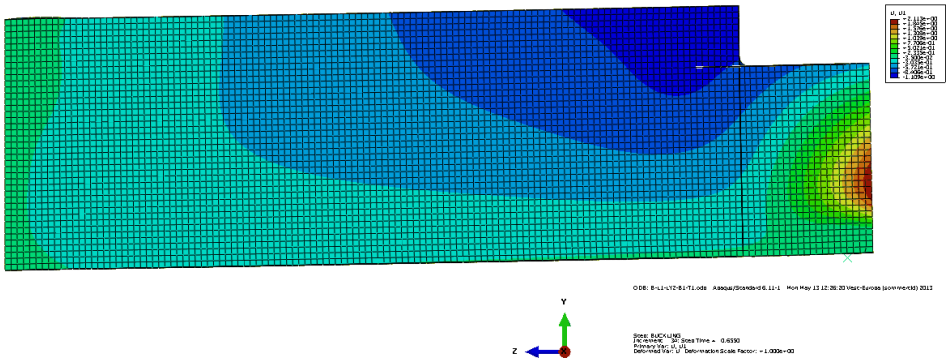

Mises stress distribution at $U2 = 30$ **mm**

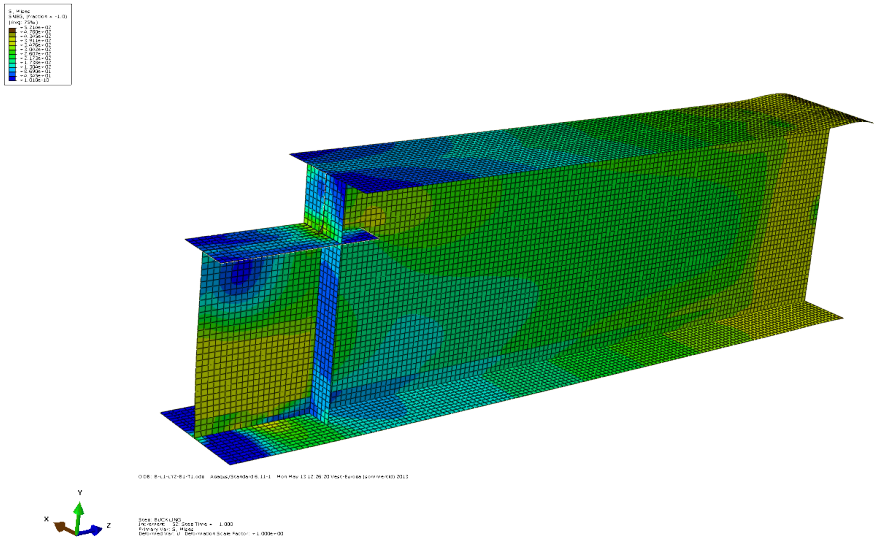

150-70-H+V2-400-7.1

$F_{max} = 253.27$ **kN**
$U2_{max} = 19.07$ **mm**

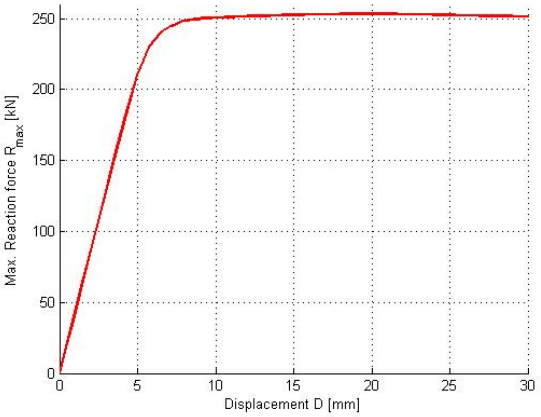

Lateral displacement at max. applied load

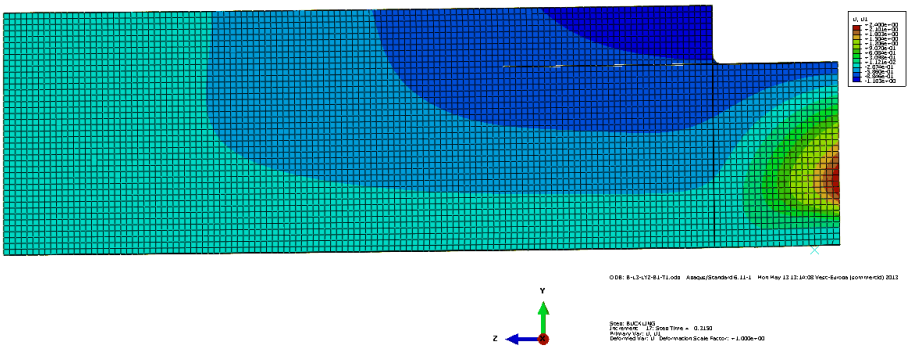

Mises stress distribution at $U2 = 30$ mm

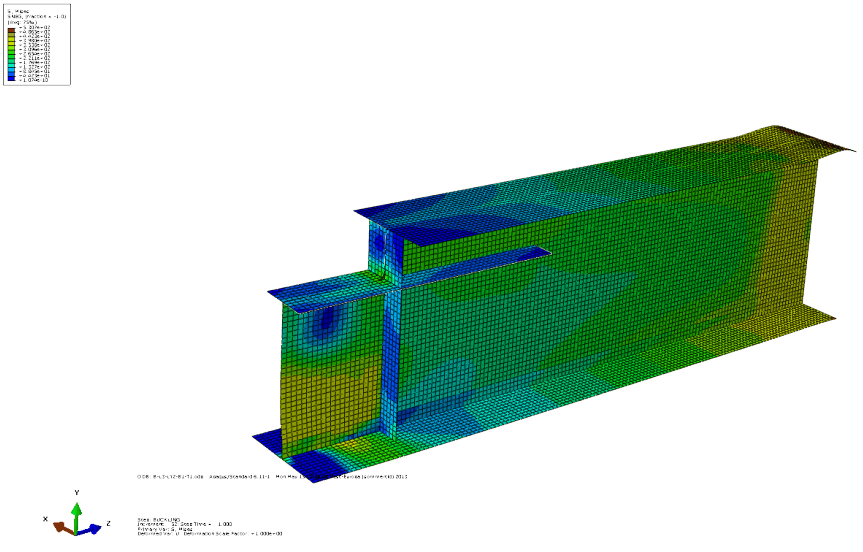

150-70-H+V2-800-7.1

$F_{max} = 253.27$ **kN**
$U2_{max} = 19.80$ **mm**

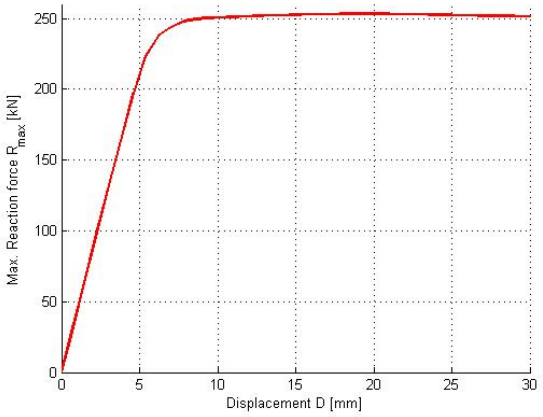

Lateral displacement at max. applied load

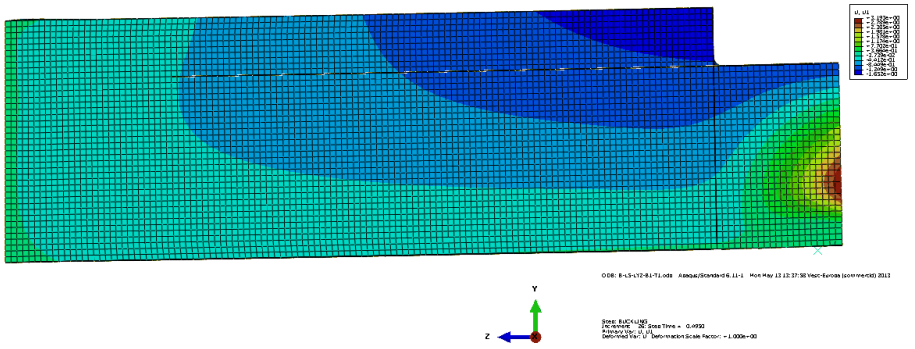

Mises stress distribution at $U2 = 30$ mm

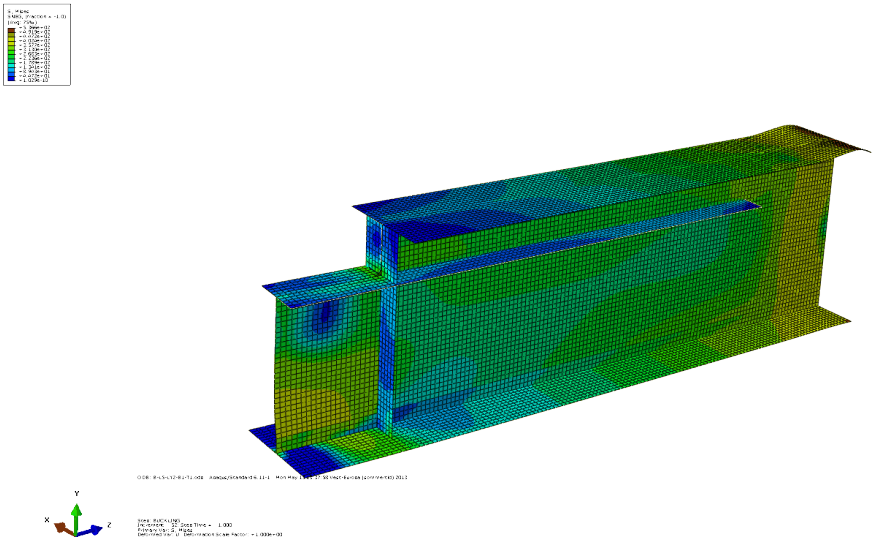

200-110-H+V2-200-7.1

$F_{max} = 252.89$ **kN**
$U2_{max} = 21.00$ **mm**

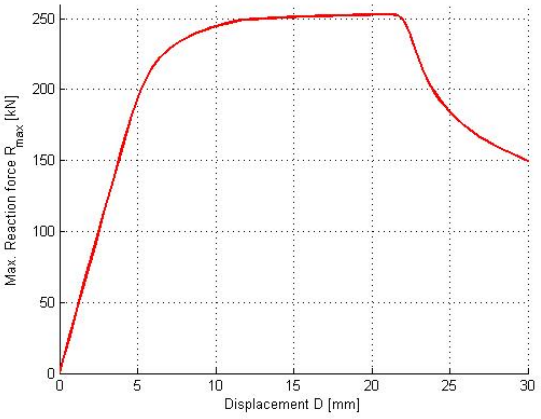

Lateral displacement at max. applied load

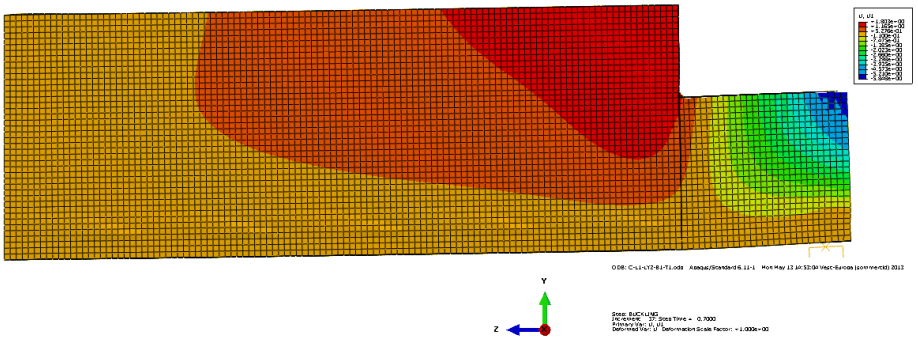

Mises stress distribution at $U2 = 30$ mm

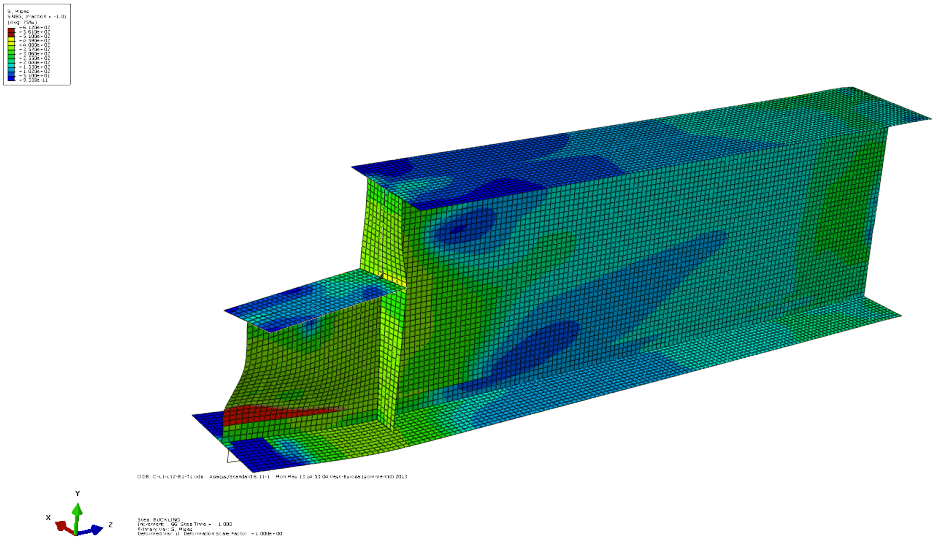

200-110-H+V2-400-7.1

$F_{max} = 252.83$ **kN**
$U2_{max} = 20.13$ **mm**

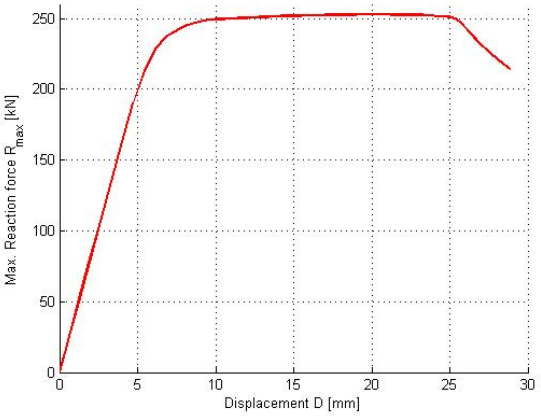

Lateral displacement at max. applied load

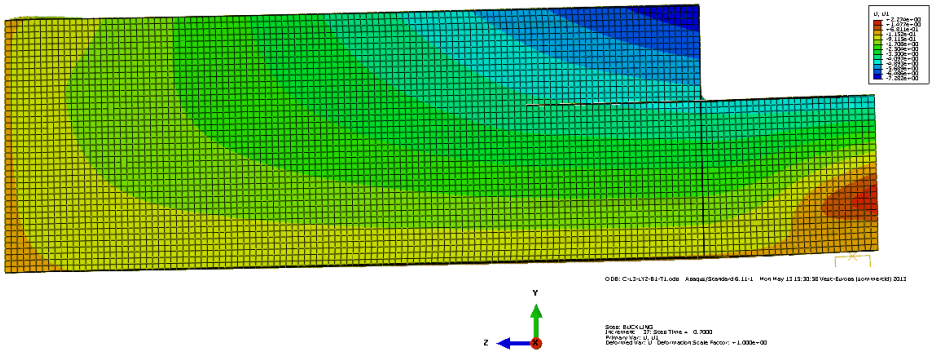

Mises stress distribution at $U2 = 30$ mm

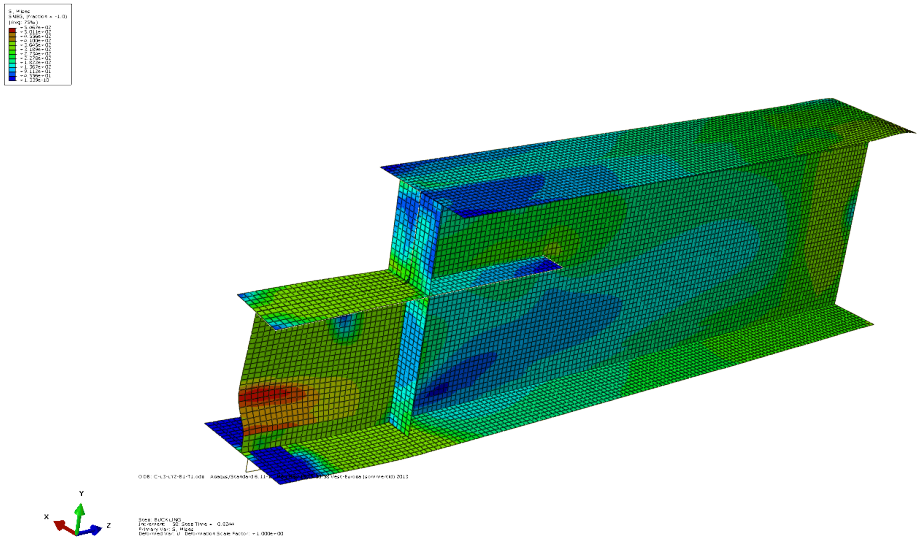

200-110-H+V2-800-7.1

$F_{max} = 252.29$ **kN**
$U2_{max} = 20.85$ **mm**

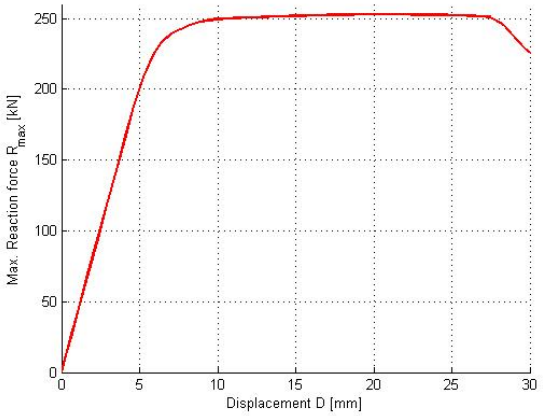

Lateral displacement at max. applied load

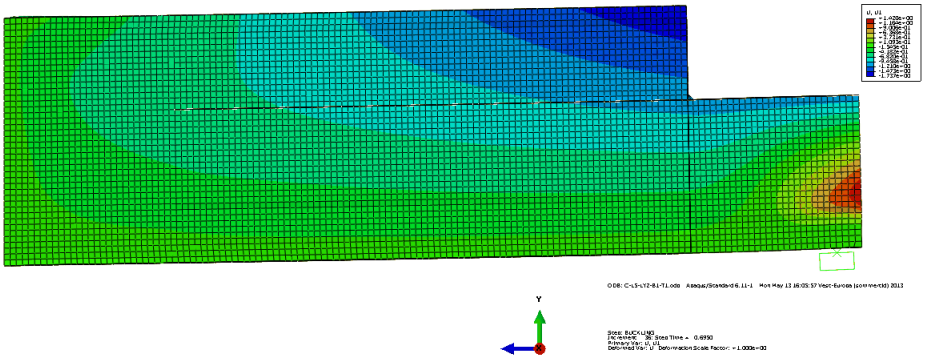

Mises stress distribution at $U2 = 30$ mm

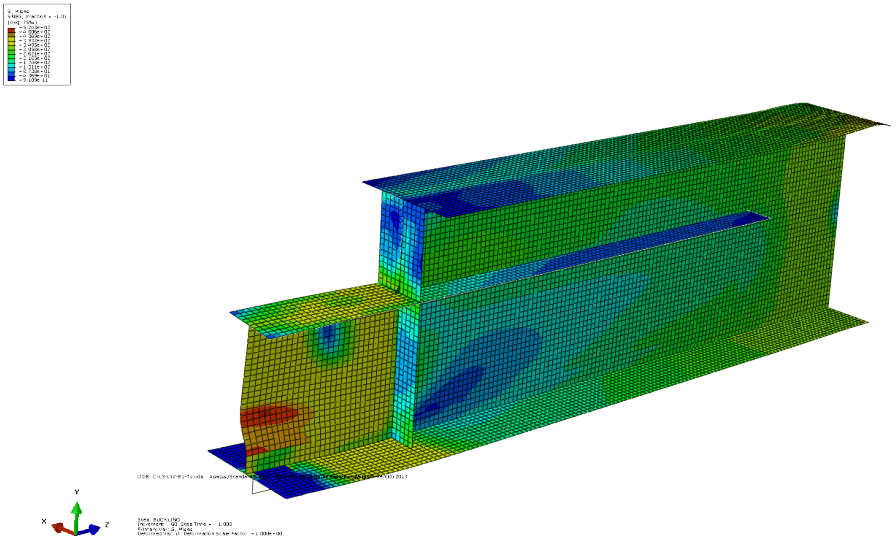

100-50-H+V1+V2-200-7.1

$F_{max} = 250.58$ **kN**
$U2_{max} = 12.60$ **mm**

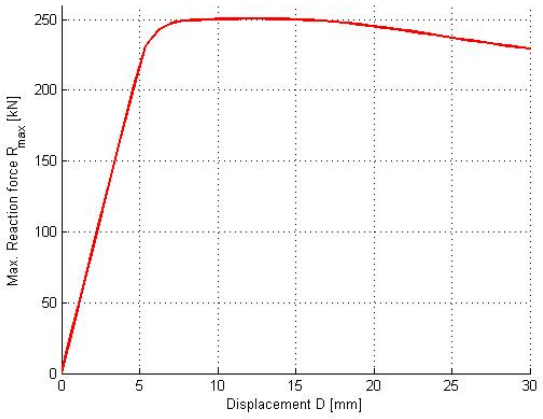

Lateral displacement at max. applied load

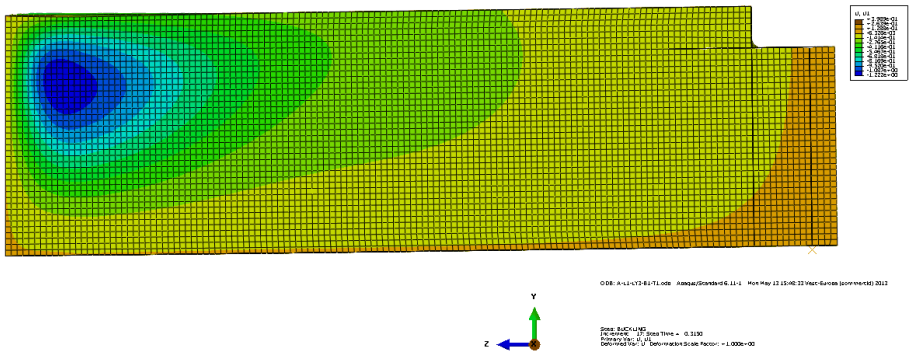

Mises stress distribution at $U2 = 30$ mm

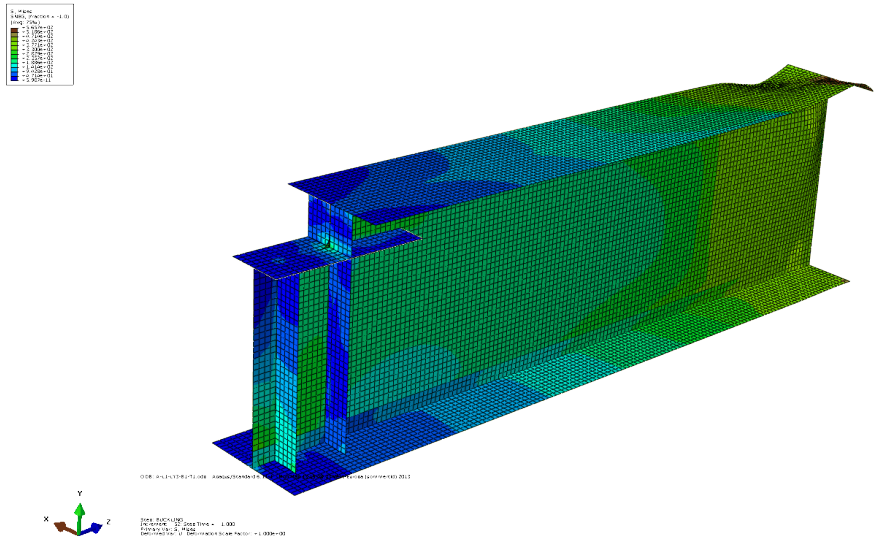

100-50-H+V1+V2-400-7.1

$F_{max} = 250.63$ **kN**
$U2_{max} = 12.45$ **mm**

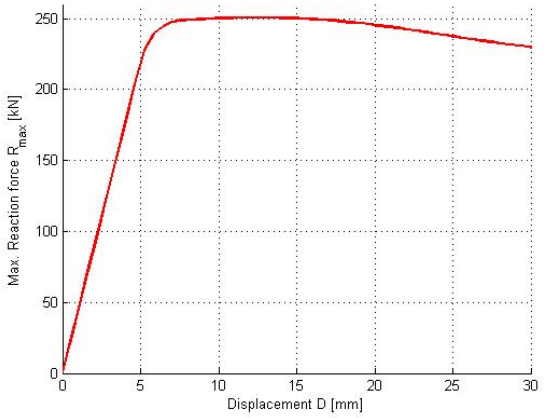

Lateral displacement at max. applied load

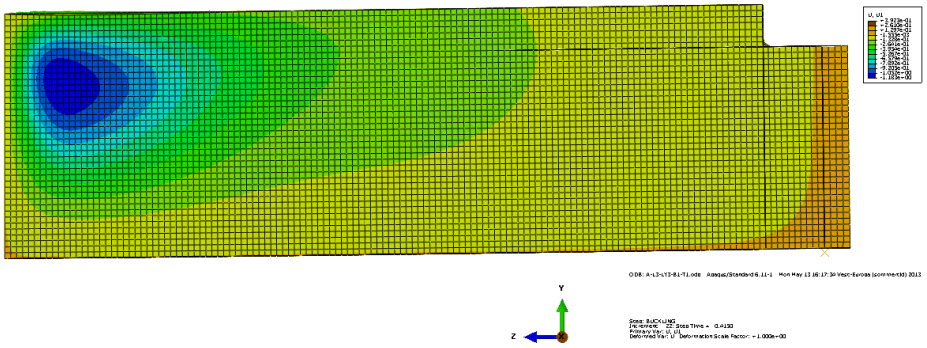

Mises stress distribution at $U2 = 30$ mm

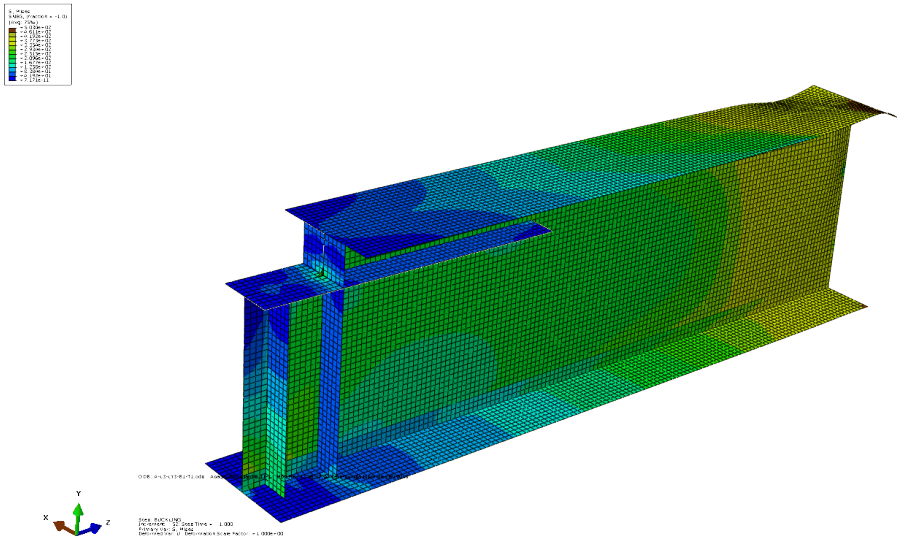

100-50-H+V1+V2-800-7.1

$F_{max} = 253.32$ **kN**
$U2_{max} = 18.45$ **mm**

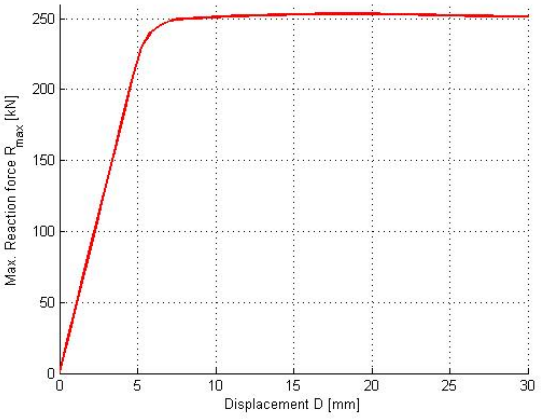

Lateral displacement at max. applied load

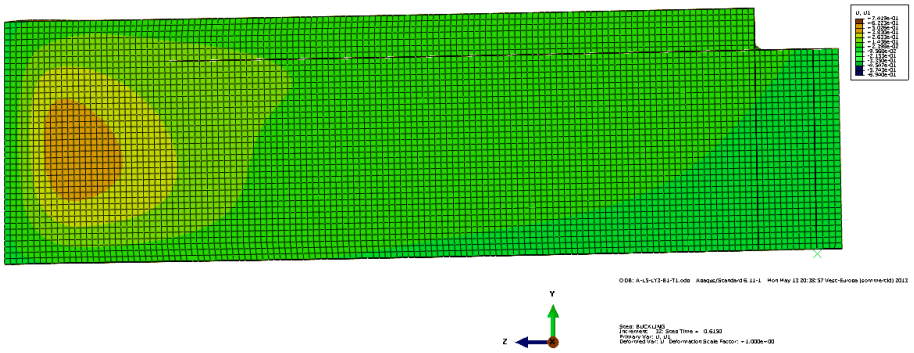

Mises stress distribution at $U2 = 30$ **mm**

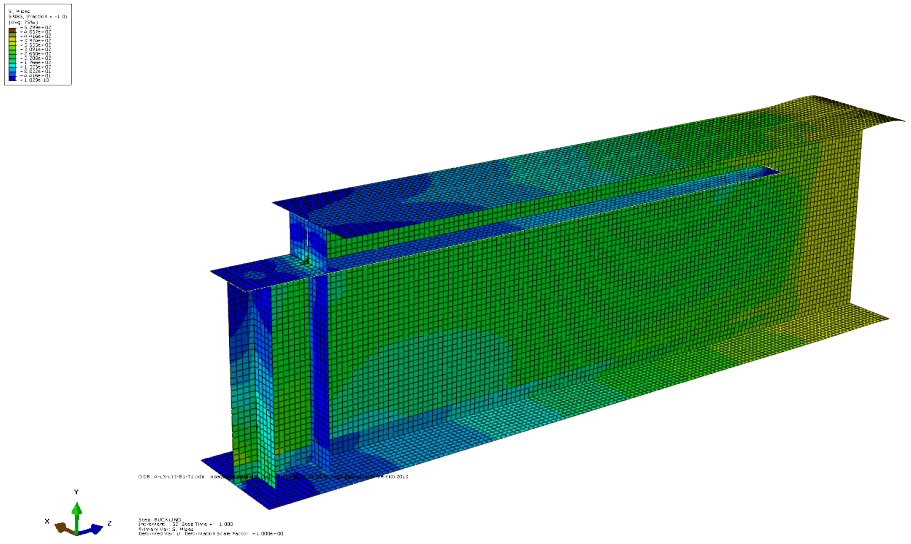

150-70-H+V1+V2-200-7.1

$F_{max} = 252.20$ **kN**
$U2_{max} = 15.00$ **mm**

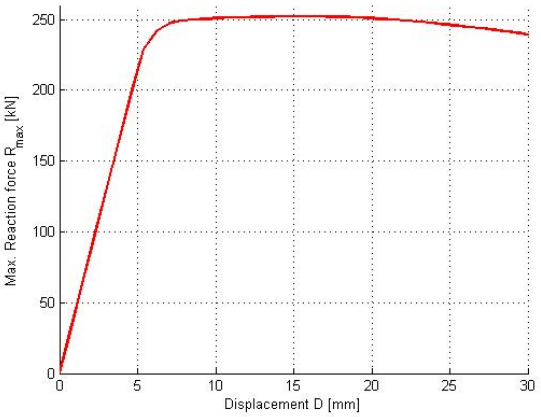

Lateral displacement at max. applied load

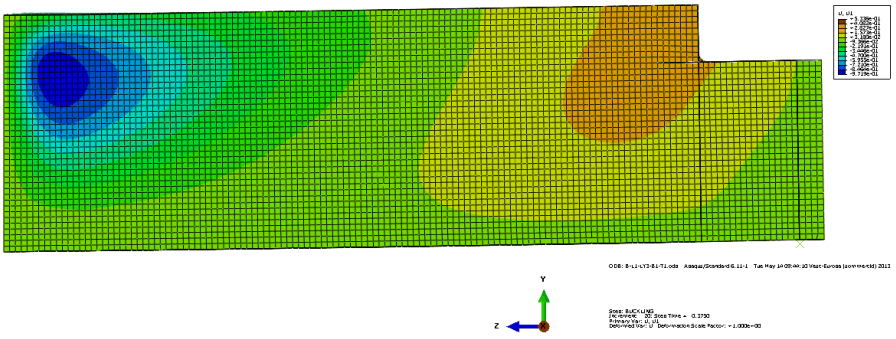

Mises stress distribution at $U2 = 30$ **mm**

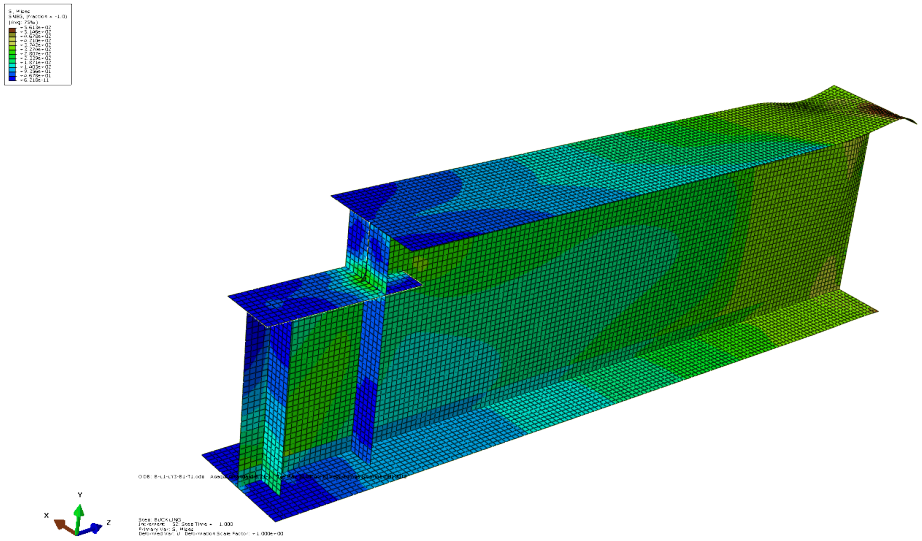

150-70-H+V1+V2-400-7.1

$F_{max} = 250.58$ **kN**
$U2_{max} = 12.60$ **mm**

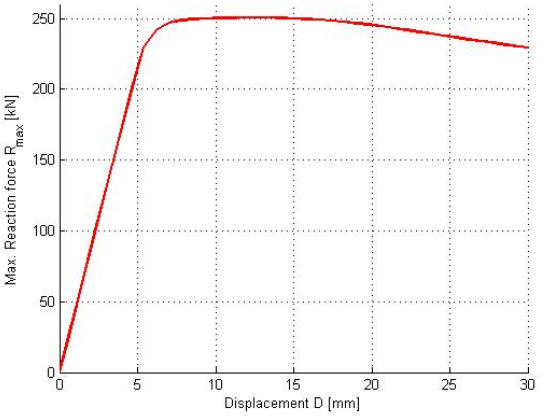

Lateral displacement at max. applied load

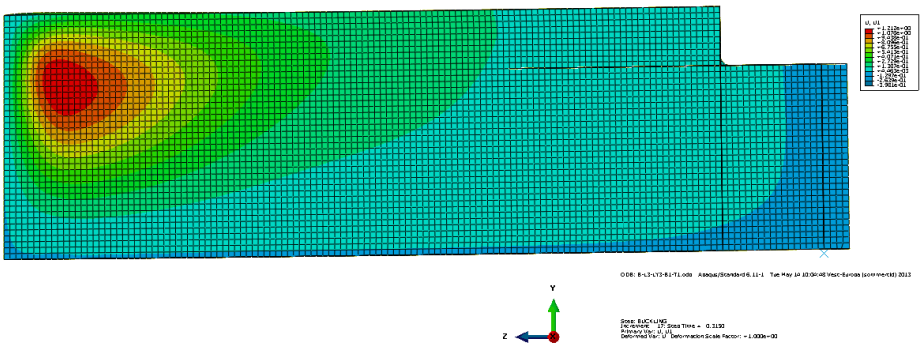

Mises stress distribution at $U2 = 30$ mm

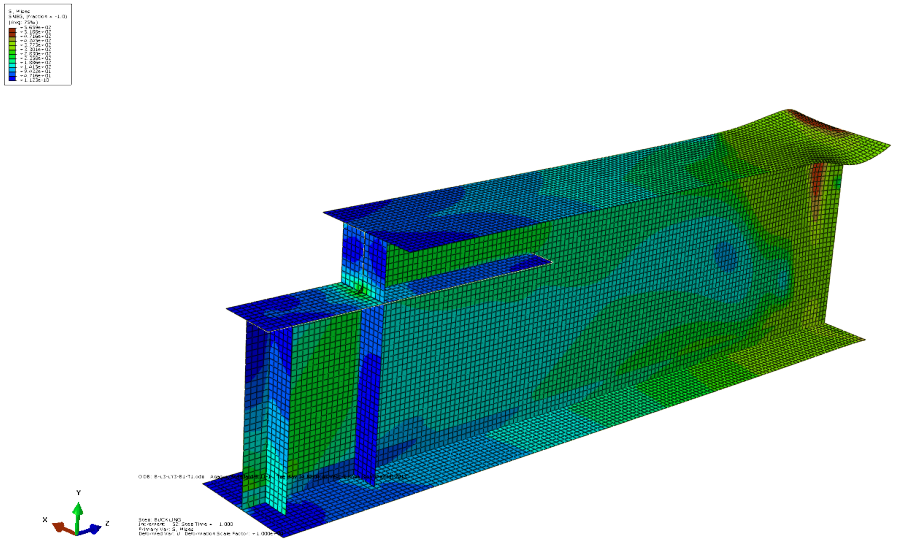

150-70-H+V1+V2-800-7.1

$F_{max} = 253.49$ **kN**
$U2_{max} = 18.20$ **mm**

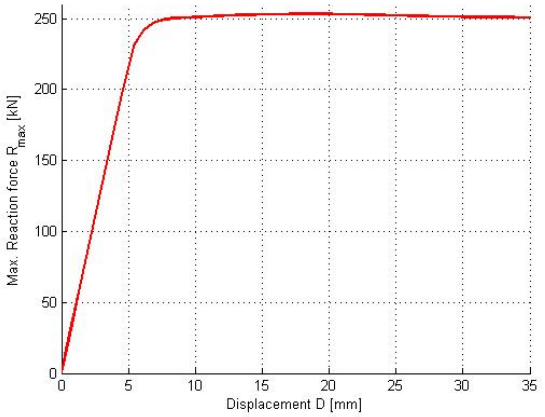

Lateral displacement at max. applied load

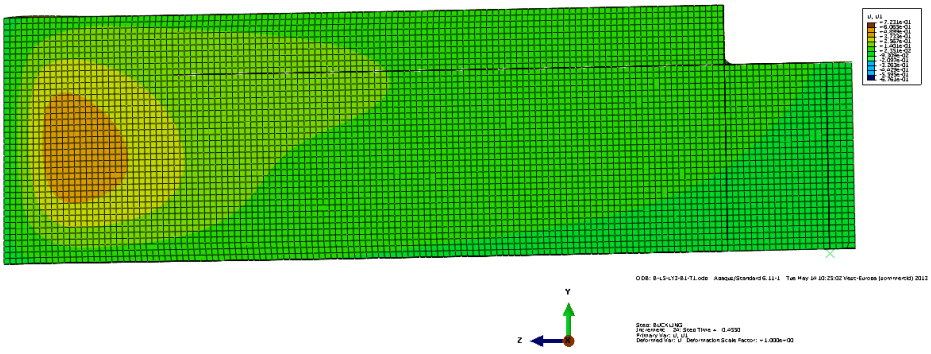

Mises stress distribution at $U2 = 35$ mm

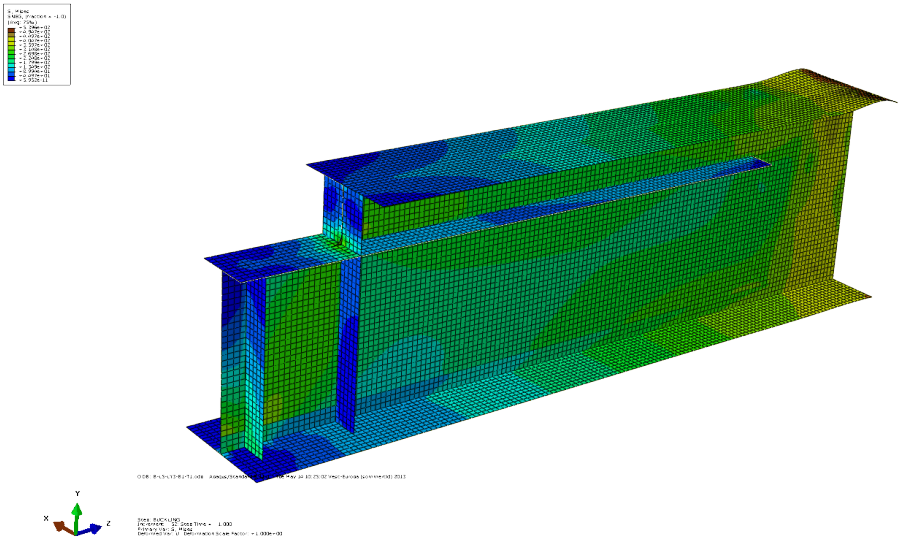

200-110-H+V1+V2-200-7.1

$F_{max} = 251.60$ **kN**
$U2_{max} = 15.93$ **mm**

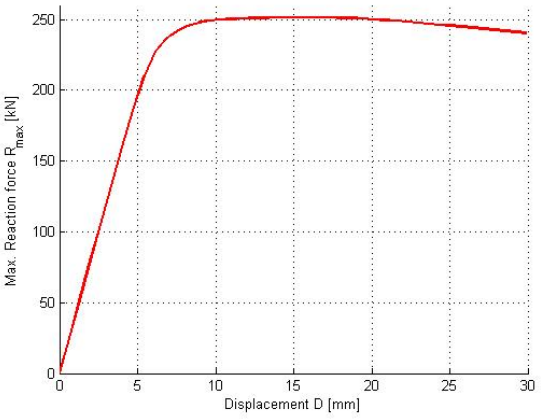

Lateral displacement at max. applied load

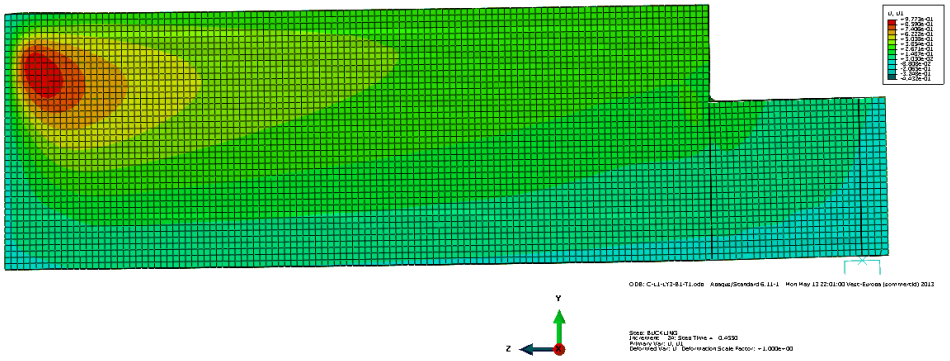

Mises stress distribution at $U2 = 30$ mm

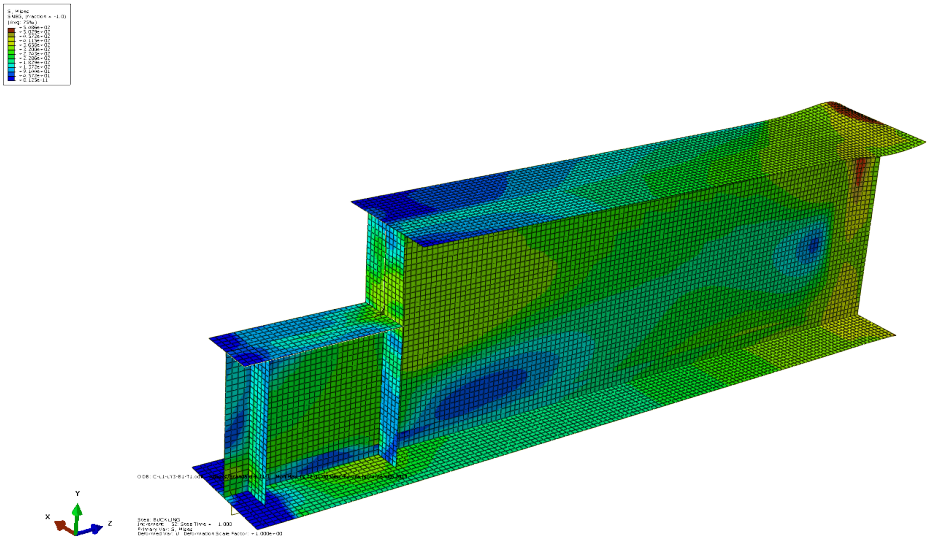

200-110-H+V1+V2-400-7.1

$F_{max} = 253.00$ **kN**
$U2_{max} = 18.73$ **mm**

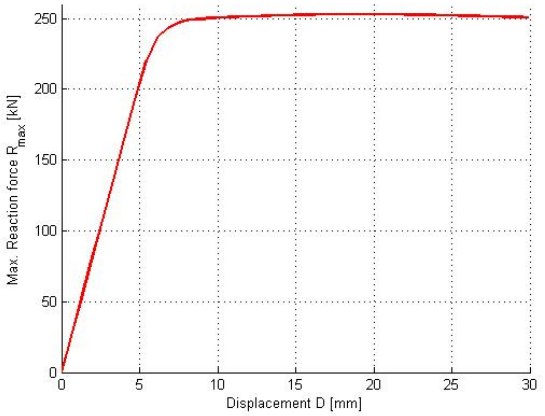

Lateral displacement at max. applied load

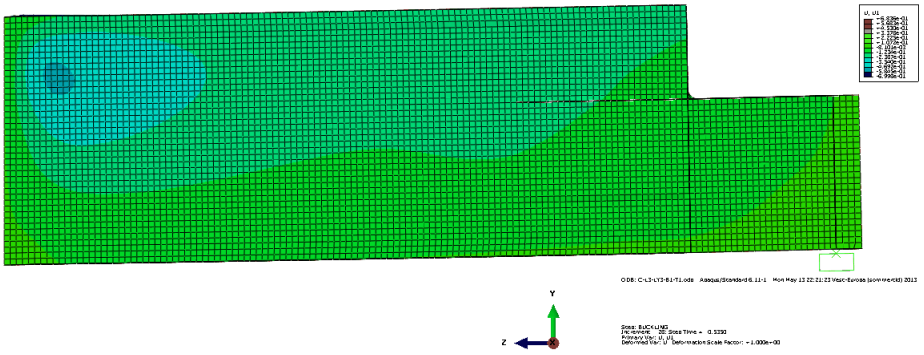

Mises stress distribution at $U2 = 30$ mm

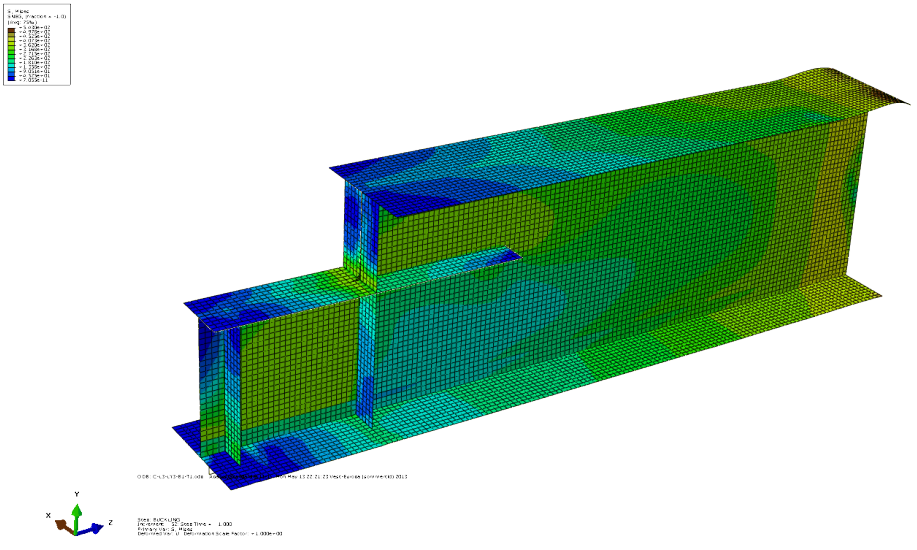

200-110-H+V1+V2-800-7.1

$F_{max} = 253.26$ **kN**
$U2_{max} = 19.00$ **mm**

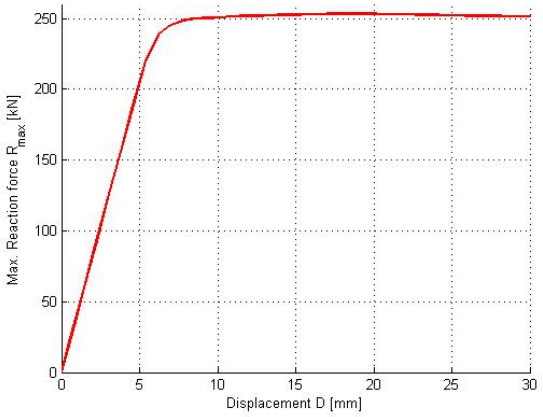

Lateral displacement at max. applied load

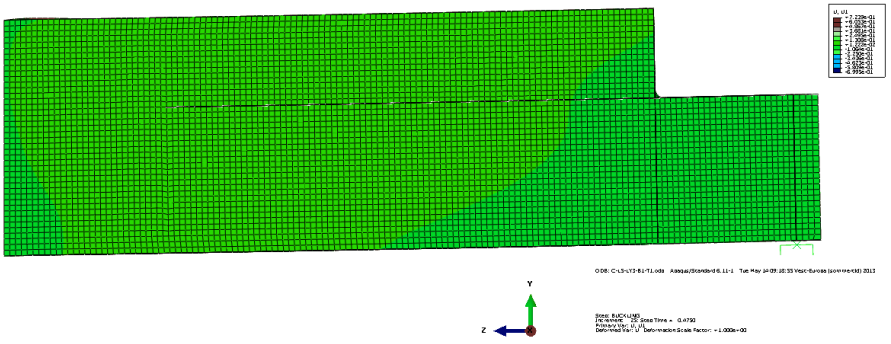

Mises stress distribution at $U2 = 30$ mm

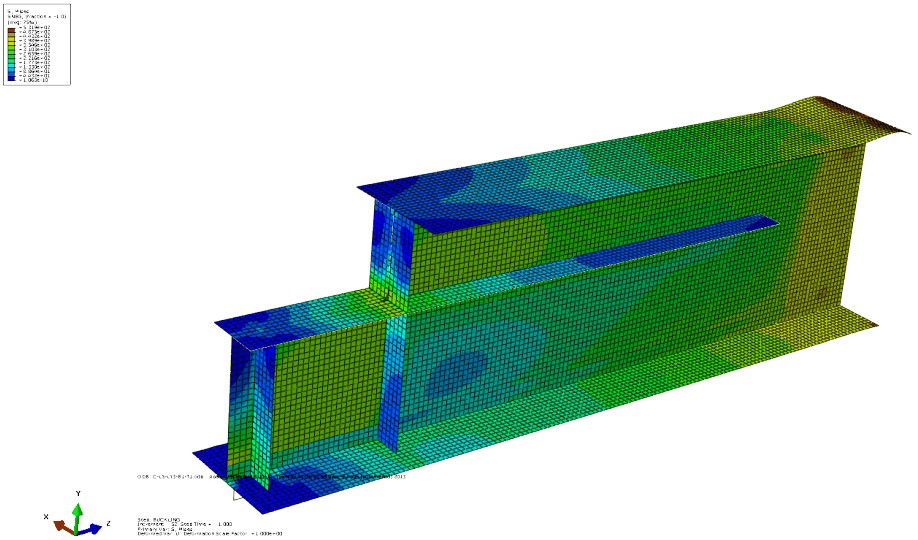

Bibliography

[1] P.K. Larsen. *Dimensjonering av stålkonstruksjoner, 2th Ed.* Tapir, 2010.

[2] Michael CH Yam, Angus CC Lam, Feng Wei, and KF Chung. The local web buckling strength of stiffened coped steel i-beams. *International Journal of Steel Structures*, 7(2): 129–138, 2007.

[3] P.Ø. Bonkerud. Kapasitet til bjelkeender med utkapp, 2007.

[4] Mathiesen KM. *Lecture notes: TKT4197 Nonlinear Finite Element Analysis.* NTNU, Department of Structural Engineering, 2012.

[5] R.D. Cook. *Concepts and Applications of Finite Element, 4th Ed.* Wiley India Pvt. Limited, 2007.

[6] Johan Maljaars, JWB Stark, HMGM Steenbergen, and R Abspoel. Development and validation of a numerical model for buckling of coped beams. *Journal of Constructional Steel Research*, 61(11):1576–1593, 2005.

[7] Jung-June Cheng, JA Yura, and CP Johnson. *Design and behavior of coped beams.* PhD thesis, 1984.

[8] Michael CH Yam, Hongwei Ma, Angus CC Lam, and KF Chung. Experimental study of the strength and behaviour of reinforced coped beams. *Journal of Constructional Steel Research*, 67(11):1749–1759, 2011.

[9] Michael CH Yam and KF Chung. A numerical study of the strength and behaviour of reinforced coped beams. *Journal of Constructional Steel Research*, 80:224–234, 2013.

[10] K. Gallaher Carlsen. Behaviour of beam connection - coped beam, 2008.

[11] S Timoshenko and S Woinowsky-Krieger. *Theory of Plates and Shells.* McGraw-Hill, New York, 1959.

[12] *NS-EN 1993-1-1. Eurocode 3: Prosjektering av stålkonstruksjoner. Del 1-5:Plater påkjent i plateplanet.* Standard Norge, 2012.

[13] Ove Lagerqvist. *Patch Loading: Resistance of Steel Girders Subjected to Concentrated Forces*. PhD thesis, 1994.

[14] J. Cheng and J. Yura. Local web buckling of coped beams. *Journal of Structural Engineering*, 112(10):2314–2331, 1986.

[15] M. Yam, A. Lam, V. Iu, and J. Cheng. Local web buckling strength of coped steel i beams. *Journal of Structural Engineering*, 129(1):3–11, 2003.

[16] K. Pettersen and S. Røe. End patch loading, 1999.

[17] P.K. Tryland T. Aalberg A., Larsen. Design of coped beam ends for concentrated load, 1999.

[18] DS Simulia. Abaqus 6.11 theory manual. *Providence, RI, USA: DS SIMULIA Corp*, 2011.

[19] OS Hopperstad and T Børvik. *Lecture notes: TKT4135 Mechanichs of Materials*. NTNU, Department of Structural Engineering, 2012.

[20] Aalberg A Larsen PK, Clausen AH. *Stålkonstruksjoner profiler og formler, 3rd Ed.* Tapir Akademiske Forlag, 2003.

[21] *Manual of steel construction. Load and resistance factor design, 2nd Edition.* American Institute of Steel Construction, Chicago, 1999.

[22] *NS-EN 1993-1-1. Eurocode 3: Prosjektering av stålkonstruksjoner. Del 1-1: Allmenne regler og regler for bygninger.* Standard Norge, 2008.

[23] Ine ABAQUS. Abaqus analysis user's manual, version 6.7. *Vol.* , 2007.

[24] KH Holthe. *Lecture notes: TKT4192: Finite Element Methods in Strength Analysis*. NTNU, Department of Structural Engineering, 2011.

[25] Karlsson Sorensen Hibbitt. Abaqus/standard user's manual, version 6.11. *Vol.* , 2011.